PAPER • OPEN ACCESS

A self-consistent multi-component model of plasma turbulence and kinetic neutral dynamics for the simulation of the tokamak boundary

To cite this article: A. Coroado and P. Ricci 2022 *Nucl. Fusion* **62** 036015

OPEN ACCESS
IOP Publishing | International Atomic Energy Agency Nuclear Fusion
Nucl. Fusion **62** (2022) 036015 (37pp) https://doi.org/10.1088/1741-4326/ac47b8

A self-consistent multi-component model of plasma turbulence and kinetic neutral dynamics for the simulation of the tokamak boundary

A. Coroado* **and P. Ricci**

École Polytechnique Fédérale de Lausanne (EPFL), Swiss Plasma Center (SPC), CH-1015 Lausanne, Switzerland

E-mail: andre.caladocoroado@epfl.ch

Received 21 July 2021, revised 9 December 2021
Accepted for publication 4 January 2022
Published 29 March 2022

Abstract

A self-consistent model is presented for the simulation of a multi-component plasma in the tokamak boundary. A deuterium plasma is considered, with the plasma species that include electrons, deuterium atomic ions and deuterium molecular ions, while the deuterium atoms and molecules constitute the neutral species. The plasma and neutral models are coupled via a number of collisional interactions, which include dissociation, ionization, charge-exchange and recombination processes. The derivation of the three-fluid drift-reduced Braginskii equations used to describe the turbulent plasma dynamics is presented, including its boundary conditions. The kinetic advection equations for the neutral species are also derived, and their numerical implementation discussed. The first results of multi-component plasma simulations carried out by using the global Braginskii solver (GBS) code are then presented and analyzed, being compared with results obtained with the single-component plasma model.

Keywords: plasma physics, tokamak boundary, neutral–plasma interaction, molecular dynamics, multi-component plasma, controlled fusion, kinetic neutrals

(Some figures may appear in colour only in the online journal)

1. Introduction

The boundary of a tokamak plays a crucial role in determining the overall performance of the device, as it sets the confinement of particles and heat, determines the heat exhaust to the vessel walls and controls the impurity level in the core [1]. The boundary is also the region where the plasma is fueled and helium ashes generated by fusion reactions are removed.

The tokamak boundary is characterized by the presence of several ion and neutral species that interact through a complex set of collisional processes [1, 2]. In particular, neutral atoms and molecules are relevant in the boundary as they result from processes such as the plasma recycling at the vessel walls and gas puffs. Recycling occurs because ions and electrons, transported along the magnetic-field lines by the parallel flow or across them by turbulent motion, eventually end at the vessel, where they recombine and re-enter the plasma as neutral particles, either being reflected, in which case they keep the energy of the original ion or, following an absorption process, being reemitted at the wall temperature. In case of absorption, a significant fraction of the atoms may associate to form molecules before being reemitted back to the plasma [3]. The exact probability of reflection or reemission, as well as the probability that atoms associate into molecules, depends on the physical properties of the limiter or divertor plate material [4]. At the same time, external injection of neutral molecules can

* Author to whom any correspondence should be addressed.

be used to fuel the plasma, reduce the heat load on the vessel wall (e.g. by reducing the temperature of the plasma and hence inducing volumetric recombination processes), or diagnose the plasma.

The neutral atoms and molecules interact with the plasma in the tokamak boundary. Indeed, neutral atoms and molecules can be ionized, thus generating atomic and molecular ions, leading to a multi-component plasma. Molecular species also undergo dissociative processes that break them into monoatomic species. Recombination, charge-exchange, elastic and inelastic collisions are also at play. These collisional interactions convert neutral particles into ions and electrons and vice versa, affect the temperature of the plasma species because of the energy required to trigger ionization and dissociation processes and modify the plasma velocity. As a result, since the dynamics of the plasma in the boundary are strongly influenced by its interaction with neutral species, it is important that simulations of the plasma dynamics in the tokamak boundary take into account its multi-component nature and the interactions between the different species to provide reliable quantitative predictions.

The description of a multi-component plasma is usually addressed by means of a fluid-diffusive model, which typically considers a version of the Braginskii fluid equations for the plasma species simplified by modelling cross-field transport through empirical anomalous transport coefficients. This approach is used by codes such as B2 [5, 6], EDGE2D [7], EMC3 [8], SOLEDGE-2D [9] and TECXY [10]. Sometimes, neutral particle species are also modelled using a diffusive fluid approach [11], for example in the UEDGE code [12]. However, the fluid closure typically used in fluid models is no longer valid when the neutral mean free path is large, i.e. of the order of the plasma gradient scale length, which is often the case in the tokamak boundary. For this reason, neutrals are more commonly modelled by using a kinetic description valid for all ranges of mean free path. These models, typically based on Monte Carlo methods for the numerical solution, are implemented in the DEGAS2 [4], EIRENE [13], GTNEUT [14] and NEUT2D [15] codes. As a matter of fact, heat exhaust studies strongly rely on integrated neutral–plasma simulations of the tokamak boundary, which are most often based upon the coupling of the aforementioned fluid-diffusive models for the multi-component plasma and Monte Carlo-based models for the several neutral species, such as B2-EIRENE [13], EDGE2D-EIRENE [16], EMC3-EIRENE [17] and SOLPS [18].

In order to shed light on perpendicular transport processes, simulations of plasma turbulence in the tokamak boundary have been carried out since a decade by using fluid and gyrofluid models, implemented in codes such as BOUT++ [19] (and its module Hermes [20]), FELTOR [21], GBS [22, 23], GDB [24], GRILLIX [25], HESEL [26] and TOKAM3X [27]. Kinetic models, implemented in other codes such as Gkeyll [28] and XGC1 [29, 30], have also been used. These simulations have allowed remarkable progress in the understanding of the mechanisms underlying turbulence and cross-field transport in a single-ion species boundary plasma. On the other hand, multi-component plasma simulations that include turbulent transport processes are still in their early days. Recent progress was made thanks to the synergy between the SOLEDGE2D [31] and TOKAM3X [27] codes. Based on the EIRENE Monte Carlo code for the kinetic simulation of the neutral species, multi-component plasma simulations are now enabled by the SOLEDGE3X code. The investigations carried out with SOLEDGE3X focused on the study of the dynamics of carbon impurities in the tokamak boundary [32]. Progress was also made by coupling the two-dimensional fluid code HESEL [26] with a one-dimensional fluid-diffusive model for the neutral particles, which accounts for both atomic and molecular species. The resulting nHESEL [26, 33, 34] code thus allows for the simulation of a single-ion plasma including the interactions with three neutral species: cold hydrogen molecules puffed into the system, warm atoms resulting from the dissociation of the hydrogen molecules and hot hydrogen atoms generated by charge-exchange processes. Such a model was used to study the plasma fueling in the presence of gas puffs and the formation of a density shoulder in the tokamak boundary at a high gas puffing rate. In addition to nHESEL simulations, we also highlight the results presented in references [35, 36], which report on a two-dimensional model for the simulation of the neutral–plasma interaction, that include the molecular dynamics. These studies highlight the impact of neutral dynamics on reducing turbulence in the tokamak boundary.

In the present work, we describe the development and numerical implementation in the GBS code of a multi-component model that addresses the turbulent multi-ion species plasma dynamics through a set of fluid drift-reduced Braginskii equations, while each multiple neutral species are simulated by solving a kinetic equation. This work generalizes the implementation of the neutral–plasma interaction in GBS described in reference [37] for single-component plasmas. Single-component GBS simulations were used to study the electron temperature drop along the magnetic field [38] and to determine the influence of neutrals on gas puff imaging (GPI) diagnostics [39]. The model has been improved recently through the implementation of mass-conservation by taking toroidal geometry consistently into account and by making use of particle-conserving boundary conditions to properly describe the recycling processes [40].

While the methodology presented in this work has the potential to include an arbitrary number of particle species and the corresponding complex scenarios, we consider a deuterium plasma, composed of five different particle species: three charged particle species, namely electrons (e^-), monoatomic deuterium ions (D^+) and diatomic deuterium ions (D_2^+), and two neutral species, namely deuterium atoms (D) and molecules (D_2). The modifications required in order to address more complex multi-component plasmas are also discussed throughout the derivation of the model.

The model constitutes the first implementation of a kinetic multi-species model that avoids the uncertainty from the Monte Carlo method, which has a deterministic component, inversely proportional to the number of particles considered, and a statistical component, inversely proportional to the square root of the product of the number of particles and the

number of iterations, as discussed in reference [41] (the effect of Monte Carlo noise on the simulation results and strategies for its reduction are discussed in detail in references [41, 42]). Instead, in the model presented in this paper, the neutral kinetic equation, valid for any neutral mean free path, is solved by discretizing the kinetic equation integrated along the neutral path. The model has the potential to provide the fundamental elements necessary for the description and understanding of the key mechanisms taking place in the boundary, such as the fueling or GPI, where molecular species play an important role.

The results of the first simulation carried out with the multi-component model are also described in the present work, shedding some light on the processes underlying plasma fueling. In particular, for the limited configuration and sheath limited regime considered, we show that molecular dissociation processes have an impact on the location of the ionization source and plasma profiles, with respect to single-component simulations.

The outline for the present paper is as follows. After the introduction, the collisional processes at play within the multi-component deuterium plasma model now implemented in GBS is presented in section 2. In section 3, we guide the reader through the derivation of the set of drift-reduced Braginskii equations used to describe a multi-component plasma, extending the approach previously followed by the single-component version of GBS. In section 4, we present the boundary conditions we apply at the tokamak wall. The kinetic model for the neutral species is discussed in section 5, where the numerical approach is also described, based on discretizing the kinetic equation integrated along the neutral path, in a generalization of the approach developed in reference [37] for a single neutral species model. Finally, in section 6 we present and discuss the preliminary results of the first multi-component plasma GBS simulations, analyzing the impact of the molecules on the plasma dynamics, also presenting comparison to results from previous single-ion plasma simulations of GBS. The summary follows. In appendix A, we derive the average energy of the reaction products and the average electron energy loss for the dissociative processes considered in the model. Appendix B presents the derivation of the friction and thermal force terms in the velocity and temperature equations used for the multi-component plasma description, following the Zhdanov closure [43] and considering the approach described in reference [32]. Appendix C features the list of kernel functions used to express the system of equations solved for the neutral species, while appendix D presents the neutral system of equations in the matrix form implemented in GBS.

2. Collisional processes in multi-component deuterium plasmas

In the present paper we aim at describing an experimentally relevant multi-component deuterium plasma. Similarly to the works in references [11, 44, 45], the plasma we consider is composed of the e, D^+ and D_2^+ species and we consider the D and D_2 neutral species. The D_2 molecules are present as the result of the association of atoms at the vessel walls and external injection. The D_2 molecules can be ionized, thus giving rise to D_2^+ ions, while dissociative processes are responsible for generating mono-atomic ions, D^+, and neutrals, D, the later being possibly further ionized into D^+. In general, the presence of D_2^{2+} ions is negligible in deuterium plasmas. Additionally, in the typical conditions of the tokamak boundary considered here, also the concentration of species that might be present in a deuterium plasma, such as the D^- and D_3^+ ions, is negligible [11, 46, 47]. Considering five different species contrasts with the three species model used in the previous GBS simulations of a single-ion species plasma [37], where only mono-atomic deuterium ions and neutrals are evolved. We highlight that, by introducing the tools necessary to deal with the fundamental processes at play in multi-component plasmas, the present model can be further extended to describe more complex scenarios that include a larger number of plasma and neutral species.

The charged particle and neutral species are coupled by means of collisional processes, which include ionization, recombination, charge-exchange and dissociation processes, as well as electron–neutral elastic collisions. We note that elastic collisions between ions and neutrals are included in charge-exchange processes. We also remark these processes appear both in the neutral and plasma species model as particle and heat sources or sinks, as well as friction terms.

We henceforth list the collisional processes considered in our multi-component model, as well as their respective reaction rates, in table 1. We remark that we neglect the distinction between fundamental and excited states for atoms, molecules and ions. In particular, we use the total cross section for each process considering the sum over the accessible electronic states of the reactants and products, following [46, 47]. Based on momentum and energy considerations, we also compute the values of the velocity and energy of the collision products. Since these also depend on the electronic states of the reactants and products, we perform an average over the states relevant to a given reaction, taking into account the cross section of each state.

We denote with v_e, v_{D^+} and $v_{D_2^+}$ the modulus of the electron, D^+ and D_2^+ velocities, while n_e, n_{D^+} and $n_{D_2^+}$ represent their densities. The cross sections $\sigma_{iz,D}$ and σ_{iz,D_2} refer to the collisions leading to the ionization of D and D_2 respectively, σ_{rec,D^+} and σ_{rec,D_2^+} are the cross sections for recombination of D^+ and D_2^+ with electrons, σ_{e-D} and σ_{e-D_2} stand for the cross sections of elastic collisions between electrons and D and D_2 respectively, σ_{diss,D_2} and σ_{diss,D_2^+} represent the dissociation cross sections of D_2 and D_2^+, $\sigma_{diss-iz,D_2}$ and $\sigma_{diss-iz,D_2^+}$ are the cross sections for dissociative ionization of D_2 and D_2^+, $\sigma_{diss-rec,D_2^+}$ is the cross section of dissociative recombination of D_2^+ ions and, finally, σ_{cx,D^+}, σ_{cx,D_2^+}, $\sigma_{cx,D-D_2^+}$ and σ_{cx,D_2-D^+} represent the cross sections for D–D^+, D_2–D_2^+, D–D_2^+ and D_2–D^+ charge-exchange interactions.

By considering Krook collision operators, the collision frequencies for ionization, recombination, elastic collisions and dissociative processes are computed as the average over the

Table 1. Collisional processes considered and their respective reaction rates.

Collisional process	Equation	Reaction frequency
Ionization of D	$e^- + D \rightarrow 2e^- + D^+$	$\nu_{iz,D} = n_e \langle v_e \sigma_{iz,D}(v_e) \rangle$
Recombination of D^+ and e^-	$e^- + D^+ \rightarrow D$	$\nu_{rec,D^+} = n_e \langle v_e \sigma_{rec,D^+}(v_e) \rangle$
e^-–D elastic collisions	$e^- + D \rightarrow e^- + D$	$\nu_{e-D} = n_e \langle v_e \sigma_{e-D}(v_e) \rangle$
Ionization of D_2	$e^- + D_2 \rightarrow 2e^- + D_2^+$	$\nu_{iz,D_2} = n_e \langle v_e \sigma_{iz,D_2}(v_e) \rangle$
Recombination of D_2^+ and e^-	$e^- + D_2^+ \rightarrow D_2$	$\nu_{rec,D_2^+} = n_e \left\langle v_e \sigma_{rec,D_2^+}(v_e) \right\rangle$
e^-–D_2 elastic collisions	$e^- + D_2 \rightarrow e^- + D_2$	$\nu_{e-D_2} = n_e \langle v_e \sigma_{e-D_2}(v_e) \rangle$
Dissociation of D_2	$e^- + D_2 \rightarrow e^- + D + D$	$\nu_{diss,D_2} = n_e \langle v_e \sigma_{diss,D_2}(v_e) \rangle$
Dissociative ionization of D_2	$e^- + D_2 \rightarrow 2e^- + D + D^+$	$\nu_{diss-iz,D_2} = n_e \langle v_e \sigma_{diss-iz,D_2}(v_e) \rangle$
Dissociation of D_2^+	$e^- + D_2^+ \rightarrow e^- + D + D^+$	$\nu_{diss,D_2^+} = n_e \left\langle v_e \sigma_{diss,D_2^+}(v_e) \right\rangle$
Dissociative ionization of D_2^+	$e^- + D_2^+ \rightarrow 2e^- + 2D^+$	$\nu_{diss-iz,D_2^+} = n_e \left\langle v_e \sigma_{diss-iz,D_2^+}(v_e) \right\rangle$
Dissociative recombination of D_2^+	$e^- + D_2^+ \rightarrow 2D$	$\nu_{diss-rec,D_2^+} = n_e \left\langle v_e \sigma_{diss-rec,D_2^+}(v_e) \right\rangle$
Charge-exchange of D^+, D	$D^+ + D \rightarrow D + D^+$	$\nu_{cx,D} = n_{D^+} \langle v_{D^+} \sigma_{cx,D^+}(v_{D^+}) \rangle$
Charge-exchange of D_2^+, D_2	$D_2^+ + D_2 \rightarrow D_2 + D_2^+$	$\nu_{cx,D_2} = n_{D_2^+} \left\langle v_{D_2^+} \sigma_{cx,D_2^+}(v_{D_2^+}) \right\rangle$
Charge-exchange of D_2^+, D	$D_2^+ + D \rightarrow D_2 + D^+$	$\nu_{cx,D-D_2^+} = n_{D_2^+} \left\langle v_{D_2^+} \sigma_{cx,D-D_2^+}(v_{D_2^+}) \right\rangle$
Charge-exchange of D_2, D^+	$D_2 + D^+ \rightarrow D_2^+ + D$	$\nu_{cx,D_2-D^+} = n_{D^+} \left\langle v_{D^+} \sigma_{cx,D_2-D^+}(v_{D^+}) \right\rangle$

electron velocity distribution function, neglecting therefore the velocity of the colliding massive particle (D, D_2, D^+ or D_2^+) when computing the relative velocity between the electron and the other particle. In fact, electrons have significantly larger thermal velocity than ions or neutrals. As for the charge-exchange interactions between D^+ ions and the neutral species D and D_2, since the dependence of the cross section upon the ion–neutral relative velocity is weak [1], we neglect the velocity of the neutral particles (D or D_2) when evaluating the relative velocity of the colliding particles (we note that the velocity of a neutral particle is typically smaller than the velocity of the ions). Thus, we compute the reaction rates σ_{cx,D^+} and σ_{cx,D_2-D^+} by averaging over the distribution function of the D^+ species, which we assume to be a Maxwellian with temperature T_{D^+}. Following the same approach when computing the cross section of charge-exchange interactions between D_2^+ ions and the D_2 and D neutrals, we average the cross sections σ_{cx,D_2^+} and $\sigma_{cx,D-D_2^+}$ over the D_2^+ distribution function, assumed to be a Maxwellian of temperature $T_{D_2^+}$.

We highlight that the values of the $\langle v\sigma \rangle$ product for most of the reactions considered in table 1 are obtained from the AMJUEL [46] and HYDEL [47] databases (precise references for each cross section are listed in table 1 of [45]). While these databases list the cross sections for ordinary hydrogen plasmas, we assume here that they apply also to deuterium. More precisely, the cross section for the e^-–D elastic collisions is obtained from [48] (page 40, table 2), while for the e^-–D_2 elastic collision we use [49] (page 917, table 13). The cross section for the D_2–D_2^+ charge-exchange reaction is taken from the HYDEL database (H.4, reaction 4.3.1), while for the D–D_2^+ charge-exchange we use the cross section values in the ALADDIN database [50], which are obtained from [51, 52]. For all the other reactions, we use the cross sections from the AMJUEL database [46]. The $\langle v\sigma \rangle$ product for the collisional processes considered in this work is plotted as a function of the temperature in figure 1. We highlight that electron–ion recombination processes are only important at very low temperatures, typically associated with detachment regimes in diverted configurations, which lie beyond the scope of the present work. While we include recombination terms in the formal derivation of the model for future reference, these terms are not included in the numerical simulations presented here and are excluded from figure 1.

Having listed the collisional processes, we now focus on the velocity and energy of their products. For charge-exchange interactions of the kind $A + B^+ \rightarrow A^+ + B$, we assume that, while A and B^+ exchange an electron, their velocities are not affected and energy is conserved. As a consequence, the ion A^+ is released from the charge-exchange collision with the velocity of A, and B is released with the velocity of B^+. For the $e^- + D \rightarrow e^- + D$ elastic collisions, given the large electron to deuterium mass ratio, we consider that the D velocity is not affected by the collision, while the electron is emitted isotropically in the reference frame of the massive particle according to a Maxwellian distribution function, $\Phi_{e[\mathbf{v}_D, T_{e,e-D}]} = \left[m_e/(2\pi T_{e,e-D})\right]^{3/2} \exp\left[-m_e(\mathbf{v} - \mathbf{v}_D)^2/(2T_{e,e-D})\right]$, centered at the velocity of the incoming D particle, $\mathbf{v}_D = \int \mathbf{v} f_D \, d\mathbf{v} / \int f_D \, d\mathbf{v}$. The temperature $T_{e,e-D}$ is established by energy conservation considerations. Precisely, we observe that the average energy of the incoming electrons consists of the sum of the kinetic energy associated with the electron fluid velocity, $\mathbf{v}_e$, and the thermal contribution, given by $(3/2)T_e$. On the other hand, the energy of the outcoming electrons has a contribution given by the collective re-emission velocity, $\mathbf{v}_D$, and a thermal contribution, $T_{e,e-D}$. It follows that $T_{e,e-D}$ satisfies the following balance, $3T_e/2 + m_e v_e^2/2 = T_{e,e-D} + m_e v_D^2/2$. The elastic collisions between electrons and D_2 can be described similarly. The re-emitted electrons have a distribution $\Phi_{e\left[\mathbf{v}_{D_2}, T_{e,e-D_2}\right]}$, with $T_{e,e-D_2}$ obtained from an analogous conservation law, $3T_e/2 + m_e v_e^2/2 = T_{e,e-D_2} + m_e v_{D_2}^2/2$.

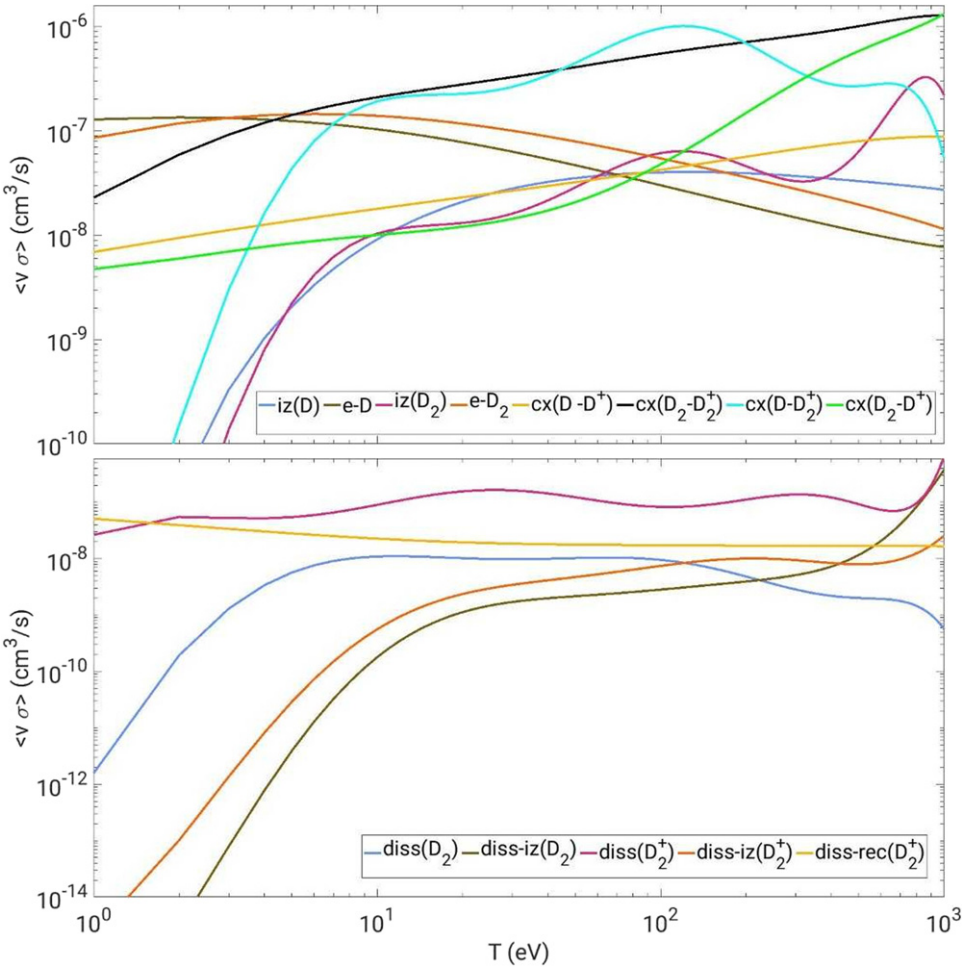

Figure 1. $\langle v\sigma \rangle$ product for the collisional processes considered in this work. Ionization processes, elastic collisions and charge-exchange processes are displayed on the top panel, dissociative reactions on the bottom panel. The $\langle v\sigma \rangle$ product is plotted as a function of the temperature of the colliding particle.

We now consider the electrons generated by ionization of D. We assume that they are described by the Maxwellian distribution function $\Phi_{e[\mathbf{v}_D, T_{e,iz(D)}]}$ centered at the fluid velocity of the D atom $\mathbf{v}_D$ with $T_{e,iz(D)}$ that takes into account the ionization energy loss, $\langle E_{iz} \rangle$, whose value is presented in table 2. More precisely, $T_{e,iz(D)}$ satisfies the energy conservation law, $3T_e/2 + m_e v_e^2/2 = 2\left[T_{e,iz(D)} + m_e v_D^2/2\right] + \langle E_{iz,D} \rangle$, as the reaction gives rise to two electrons with the same properties. The same approach is followed for the ionization of D_2, with the two released electrons being described by a Maxwellian $\Phi_{e\left[\mathbf{v}_{D_2}, T_{e,iz(D)_2}\right]}$ centered at the velocity of the D_2 molecules, $\mathbf{v}_{D_2}$, and with temperature $T_{e,iz(D)_2}$ obtained from $3T_e/2 + m_e v_e^2/2 = 2\left[T_{e,iz(D_2)} + m_e v_{D_2}^2/2\right] + \langle E_{iz,D_2} \rangle$, with $\langle E_{iz,D_2} \rangle$ the average energy loss due to ionization of D_2 (see table 2). We highlight that we neglect multi-step ionization processes when computing the cross section for ionization of D and D_2, and we do the same for all other electron impact-induced reactions, such as the dissociative processes considered here.

We apply the procedure used for ionization processes to describe the properties of the electrons resulting from dissociative processes, with the electron generated by dissociation of D_2 being described by the Maxwellian $\Phi_{e\left[\mathbf{v}_{D_2}, T_{e,diss(D)_2}\right]}$ centered around $\mathbf{v}_{D_2}$ and with temperature $T_{e,diss(D)_2}$ obtained from $3T_e/2 + m_e v_e^2/2 = T_{e,diss(D_2)} + m_e v_{D_2}^2/2 + \langle E_{diss,D_2} \rangle$. We remark that $\langle E_{diss,D_2} \rangle$ is the electron average energy loss due to Franck–Condon dissociation of D_2 molecules. In this process, the incoming electron excites the molecule, which later dissociates into a D atom and a D^+ ion. Since the excitation energy is larger than the dissociation energy of D_2 molecules, the remaining energy is converted into kinetic energy of the resulting atoms. The Franck–Condon model and the calculation of the average energy loss and reaction products energy is discussed in detail in appendix A, for all dissociative processes.

Regarding dissociation of D_2^+, the resulting electron is similarly modelled by a Maxwellian $\Phi_{e\left[\mathbf{v}_{D_2}^+, T_{e,diss(D)_2^+}\right]}$ centered at the velocity of the D_2^+ ion and with temperature $T_{e,diss(D)_2^+}$ given by energy conservation, $3T_e/2 + m_e v_e^2/2 = T_{e,diss(D_2^+)} + m_e v_{D_2^+}^2/2 + \left\langle E_{diss,D_2^+} \right\rangle$. On the other hand, dissociative ionization of D_2 generates two electrons, whose Maxwellian distribution function, $\Phi_{e\left[\mathbf{v}_{D_2}, T_{e,diss-iz(D)_2}\right]}$, is centered around the D_2 velocity, $\mathbf{v}_{D_2}$, and characterized by a temperature $T_{e,diss-iz(D_2)}$, obtained from $3T_e/2 + m_e v_e^2/2 =$

Table 2. Average electron energy loss and average energy of reaction products for the ionization and dissociative processes included in the model.

Collisional process	Electron energy loss	Reaction product temperature
Ionization of D	$\langle E_{\mathrm{iz,D}}\rangle = 13.60$ eV	—
Ionization of D_2	$\langle E_{\mathrm{iz,D_2}}\rangle = 15.43$ eV	—
Dissociation of D_2	$\langle E_{\mathrm{diss,D_2}}\rangle \simeq 14.3$ eV	$T_{\mathrm{D,diss(D_2)}} \simeq 1.95$ eV
Dissociative-ionization of D_2 ($E_e < 26$ eV)	$E_{\mathrm{diss-iz,D_2}} = 18.25$ eV	$T_{\mathrm{D,diss-iz(D_2)}} \simeq 0.25$ eV
Dissociative-ionization of D_2 ($E_e > 26$ eV)	$E_{\mathrm{diss-iz,D_2}} = 33.6$ eV	$T_{\mathrm{D,diss-iz(D_2)}} \simeq 7.8$ eV
Dissociation of D_2^+	$\left\langle E_{\mathrm{diss,D_2^+}}\right\rangle \simeq 13.7$ eV	$T_{\mathrm{D,diss}\left(\mathrm{D_2^+}\right)} \simeq 3.0$ eV
Dissociative-ionization of D_2^+	$\left\langle E_{\mathrm{diss-iz,D_2^+}}\right\rangle \simeq 15.5$ eV	$T_{\mathrm{D,diss-iz}\left(\mathrm{D_2^+}\right)} \simeq 0.4$ eV
Dissociative-recombination of D_2^+	—	$T_{\mathrm{D,diss-rec}\left(\mathrm{D_2^+}\right)} \simeq 11.7$ eV

$2\left[T_{\mathrm{e,diss-iz(D_2)}} + m_e v_{\mathrm{D_2}}^2/2\right] + \langle E_{\mathrm{diss-iz,D_2}}\rangle$. Similarly, the electrons generated by dissociative ionization of D_2^+ are assumed to follow a Maxwellian $\Phi_{\mathrm{e}\left[\mathbf{v}_{\mathrm{D_2^+}}, T_{\mathrm{e,diss-iz(D)_2^+}}\right]}$ centered at $\mathbf{v}_{\mathrm{D_2^+}}$ and with temperature $T_{\mathrm{e,diss-iz(D_2^+)}}$ obtained from the corresponding energy conservation law, $3T_e/2 + m_e v_e^2/2 = 2\left[T_{\mathrm{e,diss-iz(D_2^+)}} + m_e v_{\mathrm{D_2^+}}^2/2\right] + \left\langle E_{\mathrm{diss-iz,D_2^+}}\right\rangle$.

The evaluation of the temperature of the D atoms and D^+ ions released from dissociative reactions are based on modelling these reactions as Franck–Condon dissociation processes. These temperatures are summarized in table 2 and rely on data from [47]. The detailed calculations are presented in the appendix A. We also remark that these particles are emitted isotropically in the frame of the center of mass of the incoming D_2 or D_2^+ particle. Thus, the D atoms generated in dissociation of D_2 molecules, for instance, are assumed to have a Maxwellian distribution $\Phi_{\mathrm{D}\left[\mathbf{v}_{\mathrm{D_2}}, T_{\mathrm{D,diss(D_2)}}\right]}$. Analogously, we describe the neutral D atoms and D^+ ions generated by dissociative-ionization of D_2 molecules by the Maxwellian distributions $\Phi_{\mathrm{D}\left[\mathbf{v}_{\mathrm{D_2}}, T_{\mathrm{D,diss-iz}\left(\mathrm{D_2}\right)}\right]}$ and $\Phi_{\mathrm{D^+}\left[\mathbf{v}_{\mathrm{D_2}}, T_{\mathrm{D,diss-iz}\left(\mathrm{D_2}\right)}\right]}$ respectively, with the temperature $T_{\mathrm{D,diss-iz(D_2)}}$ listed in table 2 and evaluated in appendix A. Similarly, $\Phi_{\mathrm{D}\left[\mathbf{v}_{\mathrm{D_2^+}}, T_{\mathrm{D,diss}\left(\mathrm{D_2^+}\right)}\right]}$ and $\Phi_{\mathrm{D^+}\left[\mathbf{v}_{\mathrm{D_2^+}}, T_{\mathrm{D,diss}\left(\mathrm{D_2^+}\right)}\right]}$ are the Maxwellian distributions of D atoms and D^+ ions generated by dissociation of D_2^+ ions, where $\mathbf{v}_{\mathrm{D_2^+}}$ is the fluid velocity of the D_2^+ ion population that includes the leading order components (see section 3). Finally, dissociative-ionization of D_2^+ generates D^+ ions that are described by a Maxwellian distribution $\Phi_{\mathrm{D^+}\left[\mathbf{v}_{\mathrm{D_2^+}}, T_{\mathrm{D,diss-iz}\left(\mathrm{D_2^+}\right)}\right]}$. To conclude, we note that the D atoms and D^+ generated by dissociative-recombination of D_2^+ are described by the Maxwellian distributions $\Phi_{\mathrm{D}\left[\mathbf{v}_{\mathrm{D_2^+}}, T_{\mathrm{D,diss-rec}\left(\mathrm{D_2^+}\right)}\right]}$ and $\Phi_{\mathrm{D^+}\left[\mathbf{v}_{\mathrm{D_2^+}}, T_{\mathrm{D,diss-rec}\left(\mathrm{D_2^+}\right)}\right]}$ respectively, with $T_{\mathrm{D,diss-rec(D_2^+)}}$ the average thermal energy of the reaction products.

3. The three-fluid drift-reduced Braginskii equations

The kinetic equations for e^-, D^+ and D_2^+, which include the terms associated with the neutral–plasma interactions, are the starting point for the derivation of the Braginskii set of equations, used here to model the plasma dynamics. These equations generalise the ones considered in the single-ion species model described in references [23, 37], by adding the new collisional neutral–plasma interaction terms listed in table 1, as well as an equation for the description of molecular ions, D_2^+. The kinetic equations are

$$\begin{aligned}
&\frac{\partial f_e}{\partial t} + \mathbf{v}\cdot\frac{\partial f_e}{\partial \mathbf{x}} + \mathbf{a}\cdot\frac{f_e}{\partial \mathbf{v}} \\
&\quad = \nu_{\mathrm{iz,D}} n_{\mathrm{D}}\left[2\Phi_{\mathrm{e}\left[\mathbf{v}_{\mathrm{D}}, T_{\mathrm{e,iz(D)}}\right]} - \frac{f_e}{n_e}\right] \\
&\qquad + \nu_{\mathrm{e-D}} n_{\mathrm{D}}\left[\Phi_{\mathrm{e}\left[\mathbf{v}_{\mathrm{D}}, T_{\mathrm{e},en(D)}\right]} - \frac{f_e}{n_e}\right] - \nu_{\mathrm{rec,D^+}}\frac{n_{\mathrm{D^+}}}{n_e} f_e \\
&\qquad + \nu_{\mathrm{iz,D_2}} n_{\mathrm{D_2}}\left[2\Phi_{\mathrm{e}\left[\mathbf{v}_{\mathrm{D_2}}, T_{\mathrm{e,iz(D_2)}}\right]} - \frac{f_e}{n_e}\right] \\
&\qquad + \nu_{\mathrm{e-D_2}} n_{\mathrm{D_2}}\left[\Phi_{\mathrm{e}\left[\mathbf{v}_{\mathrm{D_2}}, T_{\mathrm{e},en(D_2)}\right]} - \frac{f_e}{n_e}\right] - \nu_{\mathrm{rec,D_2^+}}\frac{n_{\mathrm{D_2^+}}}{n_e} f_e \\
&\qquad + \nu_{\mathrm{diss,D_2}} n_{\mathrm{D_2}}\left[\Phi_{\mathrm{e}\left[\mathbf{v}_{\mathrm{D_2}}, T_{\mathrm{e,diss(D_2)}}\right]} - \frac{f_e}{n_e}\right] \\
&\qquad + \nu_{\mathrm{diss-iz,D_2}} n_{\mathrm{D_2}}\left[2\Phi_{\mathrm{e}\left[\mathbf{v}_{\mathrm{D_2}}, T_{\mathrm{e,diss-iz(D_2)}}\right]} - \frac{f_e}{n_e}\right] \\
&\qquad + \nu_{\mathrm{diss-iz,D_2^+}} n_{\mathrm{D_2^+}}\left[2\Phi_{\mathrm{e}\left[\mathbf{v}_{\mathrm{D_2^+}}, T_{\mathrm{e,diss-iz(D_2^+)}}\right]} - \frac{f_e}{n_e}\right] \\
&\qquad + \nu_{\mathrm{diss,D_2^+}} n_{\mathrm{D_2^+}}\left[\Phi_{\mathrm{e}\left[\mathbf{v}_{\mathrm{D_2^+}}, T_{\mathrm{e,diss(D_2^+)}}\right]} - \frac{f_e}{n_e}\right] \\
&\qquad - \nu_{\mathrm{diss-rec,D_2^+}} n_{\mathrm{D_2^+}}\frac{f_e}{n_e} + C(f_e),
\end{aligned} \tag{1}$$

$$\frac{\partial f_{\mathrm{D}^+}}{\partial t} + \mathbf{v}\cdot\frac{\partial f_{\mathrm{D}^+}}{\partial \mathbf{x}} + \mathbf{a}\cdot\frac{f_{\mathrm{D}^+}}{\partial \mathbf{v}} = \nu_{\mathrm{iz,D}} f_{\mathrm{D}} - \nu_{\mathrm{rec,D}^+} f_{\mathrm{D}^+} - \nu_{\mathrm{cx,D}}\left(\frac{n_{\mathrm{D}}}{n_{\mathrm{D}^+}} f_{\mathrm{D}^+} - f_{\mathrm{D}}\right) + \nu_{\mathrm{cx,D-D_2^+}} f_{\mathrm{D}} - \nu_{\mathrm{cx,D_2-D^+}}\frac{n_{\mathrm{D_2}}}{n_{\mathrm{D}^+}} f_{\mathrm{D}^+} + \nu_{\mathrm{diss-iz,D_2}} f_{\mathrm{D_2}} + 2\nu_{\mathrm{diss-iz,D_2^+}} f_{\mathrm{D_2^+}} + \nu_{\mathrm{diss,D_2^+}} f_{\mathrm{D_2^+}} + C(f_{\mathrm{D}^+}), \quad (2)$$

and

$$\frac{\partial f_{\mathrm{D_2^+}}}{\partial t} + \mathbf{v}\cdot\frac{\partial f_{\mathrm{D_2^+}}}{\partial \mathbf{x}} + \mathbf{a}\cdot\frac{f_{\mathrm{D_2^+}}}{\partial \mathbf{v}} = \nu_{\mathrm{iz,D_2}} f_{\mathrm{D_2}} - \nu_{\mathrm{rec,D_2^+}} f_{\mathrm{D_2^+}} - \nu_{\mathrm{cx,D_2}}\left(\frac{n_{\mathrm{D_2}}}{n_{\mathrm{D_2^+}}} f_{\mathrm{D_2^+}} - f_{\mathrm{D_2}}\right) - \nu_{\mathrm{cx,D_2-D^+}} f_{\mathrm{D_2}} - \nu_{\mathrm{cx,D-D_2^+}}\frac{n_{\mathrm{D}}}{n_{\mathrm{D_2^+}}} f_{\mathrm{D_2^+}} - \left(\nu_{\mathrm{diss-iz,D_2^+}} + \nu_{\mathrm{diss,D_2^+}} + \nu_{\mathrm{diss-rec,D_2^+}}\right) f_{\mathrm{D_2^+}} + C(f_{\mathrm{D_2^+}}). \quad (3)$$

In equations (1)–(3), $\mathbf{v}$ is the particle velocity, $\mathbf{a}$ is the particle acceleration due to the Lorentz force, $\partial/\partial\mathbf{x}$ is the gradient in real space and $\partial/\partial\mathbf{v}$ in the velocity space. The $C(f_{\mathrm{e}})$, $C(f_{\mathrm{D}^+})$ and $C(f_{\mathrm{D_2^+}})$ terms represent Coulomb collisions between charged particles affecting the e, D^+ and $\mathrm{D_2^+}$ distribution functions, respectively.

The Braginskii equations for the three-species plasma (e^-, D^+ and $\mathrm{D_2^+}$) are then obtained by taking the first three moments of the kinetic equations for each species in the limit $\Omega_{\mathrm{cD}^+}\tau_{\mathrm{D}^+} \gg 1$, with $\Omega_{\mathrm{cD}^+} = eB/m_{\mathrm{D}^+}$ the cyclotron frequency (m_{D^+} denotes the D^+ ion mass and e is the elementary charge) and τ_{D^+} the characteristic Coulomb collision time for D^+ ions. The Braginskii equations, including the neutral–plasma interaction terms, can be derived by following the steps presented in reference [53], and take the following form

$$\frac{\partial n_{\mathrm{e}}}{\partial t} + \nabla\cdot(n_{\mathrm{e}}\mathbf{v}_{\mathrm{e}}) = n_{\mathrm{D}}\nu_{\mathrm{iz,D}} - n_{\mathrm{D}^+}\nu_{\mathrm{rec,D}^+} + n_{\mathrm{D_2}}\nu_{\mathrm{iz,D_2}} - n_{\mathrm{D_2^+}}\nu_{\mathrm{rec,D_2^+}} + n_{\mathrm{D_2}}\nu_{\mathrm{diss-iz,D_2}} + n_{\mathrm{D_2^+}}\nu_{\mathrm{diss-iz,D_2^+}} - n_{\mathrm{D_2^+}}\nu_{\mathrm{diss-rec,D_2^+}}, \quad (4)$$

$$\frac{\partial n_{\mathrm{D}^+}}{\partial t} + \nabla\cdot\left(n_{\mathrm{D}^+}\mathbf{v}_{\mathrm{D}^+}\right) = n_{\mathrm{D}}\nu_{\mathrm{iz,D}} - n_{\mathrm{D}^+}\nu_{\mathrm{rec,D}^+} + n_{\mathrm{D}}\nu_{\mathrm{cx,D-D_2^+}} - n_{\mathrm{D_2}}\nu_{\mathrm{cx,D_2-D^+}} + n_{\mathrm{D_2}}\nu_{\mathrm{diss-iz,D_2}} + n_{\mathrm{D_2^+}}\left(2\nu_{\mathrm{diss-iz,D_2^+}} + \nu_{\mathrm{diss,D_2^+}}\right), \quad (5)$$

$$\frac{\partial n_{\mathrm{D_2^+}}}{\partial t} + \nabla\cdot\left(n_{\mathrm{D_2^+}}\mathbf{v}_{\mathrm{D_2^+}}\right) = n_{\mathrm{D_2}}\nu_{\mathrm{iz,D_2}} - n_{\mathrm{D_2^+}}\nu_{\mathrm{rec,D_2^+}} + n_{\mathrm{D_2}}\nu_{\mathrm{cx,D_2-D^+}} - n_{\mathrm{D}}\nu_{\mathrm{cx,D-D_2^+}} - n_{\mathrm{D_2^+}}\left(\nu_{\mathrm{diss-iz,D_2^+}} + \nu_{\mathrm{diss,D_2^+}} + \nu_{\mathrm{diss-rec,D_2^+}}\right), \quad (6)$$

$$m_{\mathrm{e}}n_{\mathrm{e}}\frac{\mathrm{d}_{\mathrm{e}}v_{\mathrm{e}\alpha}}{\mathrm{d}t} = -\frac{\partial p_{\mathrm{e}}}{\partial x_\alpha} - \frac{\partial \Pi_{\mathrm{e}\alpha\beta}}{\partial x_\beta} - en_{\mathrm{e}}\left[E_\alpha + (\mathbf{v}_{\mathrm{e}}\times\mathbf{B})_\alpha\right] + R_{\mathrm{e}\alpha} + m_{\mathrm{e}}\left[n_{\mathrm{D}}\left(2\nu_{\mathrm{iz,D}} + \nu_{\mathrm{e-D}}\right)\left(v_{\mathrm{D}\alpha} - v_{\mathrm{e}\alpha}\right) + n_{\mathrm{D_2}}\left(2\nu_{\mathrm{iz,D_2}} + \nu_{\mathrm{e-D_2}}\right)\left(v_{\mathrm{D_2}\alpha} - v_{\mathrm{e}\alpha}\right) + 2n_{\mathrm{D_2}}\nu_{\mathrm{diss-iz,D_2}}\left(v_{\mathrm{D_2}\alpha} - v_{\mathrm{e}\alpha}\right) + 2\nu_{\mathrm{diss-iz,D_2^+}}n_{\mathrm{D_2^+}}\left(v_{\mathrm{D_2^+}\alpha} - v_{\mathrm{e}\alpha}\right) + n_{\mathrm{D_2^+}}\nu_{\mathrm{diss,D_2^+}}\left(v_{\mathrm{D_2^+}\alpha} - v_{\mathrm{e}\alpha}\right) + n_{\mathrm{D_2}}\nu_{\mathrm{diss,D_2}}\left(v_{\mathrm{D_2}\alpha} - v_{\mathrm{e}\alpha}\right)\right], \quad (7)$$

$$m_{\mathrm{D}}n_{\mathrm{D}^+}\frac{\mathrm{d}_{\mathrm{D}^+}v_{\mathrm{D}^+\alpha}}{\mathrm{d}t} = -\frac{\partial p_{\mathrm{D}^+}}{\partial x_\alpha} - \frac{\partial \Pi_{\mathrm{D}^+\alpha\beta}}{\partial x_\beta} + en_{\mathrm{D}^+}\left[E_\alpha + \left(\mathbf{v}_{\mathrm{D}^+}\times\mathbf{B}\right)_\alpha\right] + R_{\mathrm{D}^+\alpha} + m_{\mathrm{D}}\left[n_{\mathrm{D}}(\nu_{\mathrm{iz,D}} + \nu_{\mathrm{cx,D}} + \nu_{\mathrm{cx,D-D_2^+}})(v_{\mathrm{D}\alpha} - v_{\mathrm{D}^+\alpha}) + n_{\mathrm{D_2}}\nu_{\mathrm{diss-iz,D_2}}(v_{\mathrm{D_2}\alpha} - v_{\mathrm{D}^+\alpha}) + n_{\mathrm{D_2^+}}\left(2\nu_{\mathrm{diss-iz,D_2^+}} + \nu_{\mathrm{diss,D_2^+}}\right)(v_{\mathrm{D_2^+}\alpha} - v_{\mathrm{D}^+\alpha})\right], \quad (8)$$

$$m_{\mathrm{D_2}}n_{\mathrm{D_2^+}}\frac{\mathrm{d}_{\mathrm{D_2^+}}v_{\mathrm{D_2^+}\alpha}}{\mathrm{d}t} = -\frac{\partial p_{\mathrm{D_2^+}}}{\partial x_\alpha} - \frac{\partial \Pi_{\mathrm{D}^+\alpha\beta}}{\partial x_\beta} + en_{\mathrm{D_2^+}}\left[E_\alpha + \left(\mathbf{v}_{\mathrm{D_2^+}}\times\mathbf{B}\right)_\alpha\right] + R_{\mathrm{D_2^+}\alpha} + m_{\mathrm{D_2}}n_{\mathrm{D_2}}(\nu_{\mathrm{iz,D_2}} + \nu_{\mathrm{cx,D_2}} + \nu_{\mathrm{cx,D_2-D^+}}) \times (v_{\mathrm{D_2}\alpha} - v_{\mathrm{D_2^+}\alpha}), \quad (9)$$

$$\frac{3}{2}n_{\mathrm{e}}\frac{\mathrm{d}_{\mathrm{e}}T_{\mathrm{e}}}{\mathrm{d}t} + p_{\mathrm{e}}\nabla\cdot\mathbf{v}_{\mathrm{e}} = -\nabla\cdot\mathbf{q}_{\mathrm{e}} - \Pi_{\mathrm{e}\alpha\beta}\frac{\partial v_{\mathrm{e}\beta}}{\partial x_\alpha} + Q_{\mathrm{e}} + n_{\mathrm{D}}\nu_{\mathrm{iz,D}}\left[-E_{\mathrm{iz,D}} - \frac{3}{2}T_{\mathrm{e}} + \frac{3}{2}m_{\mathrm{e}}\mathbf{v}_{\mathrm{e}}\cdot\left(\mathbf{v}_{\mathrm{e}} - \frac{4}{3}\mathbf{v}_{\mathrm{D}}\right)\right] - n_{\mathrm{D}}\nu_{\mathrm{e-D}}m_{\mathrm{e}}\mathbf{v}_{\mathrm{e}}\cdot(\mathbf{v}_{\mathrm{D}} - \mathbf{v}_{\mathrm{e}})$$

$$
\begin{aligned}
&+ n_{\mathrm{D}_2}\nu_{\mathrm{iz,D}_2}\left[-E_{\mathrm{iz,D}_2} - \frac{3}{2}T_\mathrm{e} + \frac{3}{2}m_\mathrm{e}\mathbf{v}_\mathrm{e}\cdot\left(\mathbf{v}_\mathrm{e} - \frac{4}{3}\mathbf{v}_{\mathrm{D}_2}\right)\right]\\
&- n_{\mathrm{D}_2}\nu_{\mathrm{e-D}_2}m_\mathrm{e}\mathbf{v}_\mathrm{e}\cdot(\mathbf{v}_{\mathrm{D}_2} - \mathbf{v}_\mathrm{e})\\
&+ n_{\mathrm{D}_2}\nu_{\mathrm{diss,D}_2}\left[-E_{\mathrm{diss,D}_2} + m_\mathrm{e}\mathbf{v}_\mathrm{e}\cdot\left(\mathbf{v}_\mathrm{e} - \mathbf{v}_{\mathrm{D}_2}\right)\right]\\
&+ n_{\mathrm{D}_2}\nu_{\mathrm{diss-iz,D}_2}\left[-E_{\mathrm{diss-iz,D}_2} - \frac{3}{2}T_\mathrm{e}\right.\\
&\left.+ \frac{3}{2}m_\mathrm{e}\mathbf{v}_\mathrm{e}\cdot\left(\mathbf{v}_\mathrm{e} - \frac{4}{3}\mathbf{v}_{\mathrm{D}_2}\right)\right]\\
&+ n_{\mathrm{D}_2^+}\nu_{\mathrm{diss,D}_2^+}\left[-E_{\mathrm{diss,D}_2^+} + m_\mathrm{e}\mathbf{v}_\mathrm{e}\cdot\left(\mathbf{v}_\mathrm{e} - \mathbf{v}_{\mathrm{D}_2^+}\right)\right]\\
&+ n_{\mathrm{D}_2^+}\nu_{\mathrm{diss-iz,D}_2^+}\left[-E_{\mathrm{diss-iz,D}_2^+} - \frac{3}{2}T_\mathrm{e}\right.\\
&\left.+ \frac{3}{2}m_\mathrm{e}\mathbf{v}_\mathrm{e}\cdot\left(\mathbf{v}_\mathrm{e} - \frac{4}{3}\mathbf{v}_{\mathrm{D}_2^+}\right)\right], \qquad (10)
\end{aligned}
$$

$$
\begin{aligned}
&\frac{3}{2}n_{\mathrm{D}^+}\frac{\mathrm{d}_{\mathrm{D}^+}T_{\mathrm{D}^+}}{\mathrm{d}t} + p_{\mathrm{D}^+}\nabla\cdot\mathbf{v}_{\mathrm{D}^+}\\
&\quad= -\nabla\cdot\mathbf{q}_{\mathrm{D}^+} - \Pi_{\mathrm{D}^+\alpha\beta}\frac{\partial v_{\mathrm{D}^+\beta}}{\partial x_\alpha} + Q_{\mathrm{D}^+}\\
&\qquad+ n_\mathrm{D}(\nu_{\mathrm{iz,D}} + \nu_{\mathrm{cx,D}} + \nu_{\mathrm{cx,D-D}_2^+})\\
&\qquad\times\left[\frac{3}{2}\left(T_\mathrm{D} - T_{\mathrm{D}^+}\right) + \frac{m_{\mathrm{D}^+}}{2}\left(\mathbf{v}_D - \mathbf{v}_{\mathrm{D}^+}\right)^2\right]\\
&\qquad+ n_{\mathrm{D}_2}\nu_{\mathrm{diss-iz,D}_2}\left[\frac{3}{2}\left(T_{\mathrm{D}^+,\mathrm{diss-iz(D}_2)} - T_{\mathrm{D}^+}\right)\right.\\
&\qquad\left.+ \frac{m_{\mathrm{D}^+}}{2}\left(\mathbf{v}_{\mathrm{D}_2} - \mathbf{v}_{\mathrm{D}^+}\right)^2\right]\\
&\qquad+ 2n_{\mathrm{D}_2^+}\nu_{\mathrm{diss-iz,D}_2^+}\left[\frac{3}{2}\left(T_{\mathrm{D}^+,\mathrm{diss-iz}\left(\mathrm{D}_2^+\right)} - T_{\mathrm{D}^+}\right)\right.\\
&\qquad\left.+ \frac{m_{\mathrm{D}^+}}{2}\left(\mathbf{v}_{\mathrm{D}_2^+} - \mathbf{v}_{\mathrm{D}^+}\right)^2\right]\\
&\qquad+ n_{\mathrm{D}_2^+}\nu_{\mathrm{diss,D}_2^+}\left[\frac{3}{2}\left(T_{\mathrm{D}^+,\mathrm{diss}\left(\mathrm{D}_2^+\right)} - T_{\mathrm{D}^+}\right)\right.\\
&\qquad\left.+ \frac{m_{\mathrm{D}^+}}{2}\left(\mathbf{v}_{\mathrm{D}_2^+} - \mathbf{v}_{\mathrm{D}^+}\right)^2\right], \qquad (11)
\end{aligned}
$$

$$
\begin{aligned}
&\frac{3}{2}n_{\mathrm{D}_2^+}\frac{\mathrm{d}_{\mathrm{D}_2^+}T_{\mathrm{D}_2^+}}{\mathrm{d}t} + p_{\mathrm{D}_2^+}\nabla\cdot\mathbf{v}_{\mathrm{D}_2^+}\\
&\quad= -\nabla\cdot\mathbf{q}_{\mathrm{D}_2^+} - \Pi_{\mathrm{D}_2^+\alpha\beta}\frac{\partial v_{\mathrm{D}_2^+\beta}}{\partial x_\alpha} + Q_{\mathrm{D}_2^+}\\
&\qquad+ n_{\mathrm{D}_2}(\nu_{\mathrm{cx,D}_2} + \nu_{\mathrm{iz,D}_2} + \nu_{\mathrm{cx,D}_2\mathrm{-D}^+}) \qquad (12)\\
&\qquad\times\left[\frac{3}{2}\left(T_{\mathrm{D}_2^+} - T_{\mathrm{D}_2^+}\right) + \frac{m_{\mathrm{D}_2^+}}{2}(\mathbf{v}_{\mathrm{D}_2} - \mathbf{v}_{\mathrm{D}_2^+})^2\right],
\end{aligned}
$$

where $\Pi_{\mathrm{e}\alpha\beta}$ is the component of the stress tensor along the α and β directions, $\mathbf{R}_\mathrm{e}$ is the friction force acting on the electrons, $\mathbf{q}_\mathrm{e}$ is the electron heat flux density, Q_e is the electron heat generated by Coulomb collisions, $\mathrm{d}_\mathrm{e}/\mathrm{d}t = \partial/\partial t + (\mathbf{v}_\mathrm{e}\cdot\nabla)$ is the electron advective derivative and $\mathbf{v}_\mathrm{e} = \mathbf{v}_{\perp\mathrm{e}} + \mathbf{v}_{\parallel\mathrm{e}}$ is the electron velocity, that includes the components perpendicular and parallel to the magnetic field. The equivalent notation is used for the D^+ and D_2^+ species.

The drift-limit of the Braginskii equations is finally derived by applying the $\mathrm{d}/\mathrm{d}t \ll \Omega_{\mathrm{cD}^+}$ ordering, valid in typical conditions of the tokamak boundary. Only leading order components in $(1/\Omega_{\mathrm{cD}^+})\mathrm{d}/\mathrm{d}t$ are retained in the electron perpendicular velocity, i.e. $\mathbf{v}_{\perp\mathrm{e}} = \mathbf{v}_{\perp\mathrm{e}0} = \mathbf{v}_{E\times B} + \mathbf{v}_\mathrm{de}$, with $\mathbf{v}_{E\times B} = (\mathbf{E}\times\mathbf{B})/B^2$ the $E\times B$ drift and $\mathbf{v}_\mathrm{de} = (\mathbf{B}\times\nabla p_\mathrm{e})/(en_\mathrm{e}B^2)$ the electron diamagnetic drift, thus neglecting electron inertia. Similarly, the D^+ perpendicular velocity is decomposed as $\mathbf{v}_{\perp\mathrm{D}^+} = \mathbf{v}_{\perp\mathrm{D}^+0} + \mathbf{v}_{\mathrm{pol,D}^+} + \mathbf{v}_{\mathrm{fric,D}^+}$, where the leading order perpendicular velocity,

$$
\mathbf{v}_{\perp\mathrm{D}^+0} = \mathbf{v}_{E\times B} + \mathbf{v}_{\mathrm{dD}^+}, \qquad (13)
$$

is the sum of the $E\times B$ drift and the diamagnetic drift, $\mathbf{v}_{\mathrm{dD}^+} = (\mathbf{B}\times\nabla p_{\mathrm{D}^+})/(en_{\mathrm{D}^+}B^2)$. The polarization drift,

$$
\begin{aligned}
\mathbf{v}_{\mathrm{pol,D}^+} &= -\frac{1}{n_{\mathrm{D}^+}\Omega_{\mathrm{cD}^+}}\frac{\mathrm{d}_{\mathrm{D}^+}}{\mathrm{d}t}\left(\frac{n_{\mathrm{D}^+}}{B}\nabla_\perp\phi + \frac{1}{B}\nabla_\perp p_{\mathrm{D}^+}\right)\\
&\quad+ \frac{1}{m_{\mathrm{D}^+}n_{\mathrm{D}^+}\Omega_{\mathrm{cD}^+}}\mathbf{b}\times\left[G_{\mathrm{D}^+}\mathbf{k} - \frac{\nabla G_{\mathrm{D}^+}}{3}\right], \qquad (14)
\end{aligned}
$$

is of higher order than $\mathbf{v}_{\perp\mathrm{D}^+0}$ in the $\mathrm{d}/\mathrm{d}t \ll \Omega_{\mathrm{cD}^+}$ expansion, as shown in reference [53]. Similarly, the drift arising from friction between D^+ ions and other species,

$$
\begin{aligned}
\mathbf{v}_{\mathrm{fric,D}^+} &= \frac{n_\mathrm{D}}{n_{\mathrm{D}^+}}\frac{\nu_{\mathrm{cx,D}} + \nu_{\mathrm{iz,D}} + \nu_{\mathrm{cx,D-D}_2^+}}{\Omega_{\mathrm{cD}^+}}\left(\mathbf{v}_{\perp\mathrm{D}} - \mathbf{v}_{\perp\mathrm{D}^+0}\right)\\
&\quad\times\mathbf{b} + \frac{n_{\mathrm{D}_2}}{n_{\mathrm{D}^+}}\frac{\nu_{\mathrm{iz-diss,D}_2}}{\Omega_{\mathrm{cD}^+}}\left(\mathbf{v}_{\perp\mathrm{D}_2} - \mathbf{v}_{\perp\mathrm{D}^+0}\right)\times\mathbf{b}\\
&\quad+ \frac{n_{\mathrm{D}_2^+}}{n_{\mathrm{D}^+}}\frac{2\nu_{\mathrm{diss-iz,D}_2^+} + \nu_{\mathrm{diss,D}_2^+}}{\Omega_{\mathrm{cD}^+}}\left(\mathbf{v}_{\perp\mathrm{D}_2^+0} - \mathbf{v}_{\perp\mathrm{D}^+0}\right)\\
&\quad\times\mathbf{b}, \qquad (15)
\end{aligned}
$$

is also of higher order in $(1/\Omega_{\mathrm{cD}^+})\mathrm{d}/\mathrm{d}t$. This term includes contributions from collisions of D^+ with D, D_2 and D_2^+ particles. Assuming $v_\mathrm{D} \lesssim v_{\mathrm{D}^+}$, $v_{\mathrm{D}_2} \lesssim v_{\mathrm{D}^+}$ and $v_{\mathrm{D}_2^+} \lesssim v_{\mathrm{D}^+}$, and noticing that $\nu/\Omega_{\mathrm{cD}^+} \ll 1$, one obtains $v_{\mathrm{fric,D}^+} \sim (\nu/\Omega_{\mathrm{cD}^+})v_{\mathrm{D}^+} \ll v_{\mathrm{D}^+}$. For this reason, $\mathbf{v}_{\mathrm{D}^+}$ and $\mathbf{v}_{\mathrm{D}^+}$ are approximated with their leading order components, i.e. $\mathbf{v}_{\perp\mathrm{D}^+} \simeq \mathbf{v}_{\perp\mathrm{D}^+0}$ and $\mathbf{v}_{\perp\mathrm{D}_2^+} \simeq \mathbf{v}_{\perp\mathrm{D}_2^+0}$, in equation (15). In equations (14) and (15) we introduce the gyroviscous term for D^+ ions $G_{\mathrm{D}^+} = -\eta_{0\mathrm{D}^+}\left[2\nabla_\parallel v_{\parallel\mathrm{D}^+} + C(\phi)/B + C(p_{\mathrm{D}^+})/(Z_{\mathrm{D}^+}n_{\mathrm{D}^+}B)\right]$, the D^+ viscosity $\eta_{0\mathrm{D}^+}$, the magnetic field curvature vector $\mathbf{k} = (\mathbf{b}\cdot\nabla)\,\mathbf{b}$, the gradient along the magnetic field $\nabla_\parallel = \mathbf{b}\cdot\nabla$, the gradient perpendicular to the magnetic field $\nabla_\perp = \nabla - \mathbf{b}\nabla_\parallel$, and the magnetic field unit vector $\mathbf{b} = \mathbf{B}/B$.

For the derivation of the drift-limit of the D_2^+ velocity, we follow a similar approach, as the $\mathrm{d}/\mathrm{d}t \ll \Omega_{\mathrm{cD}_2^+}$ ordering is also valid in typical tokamak boundary conditions. The D_2^+ ions perpendicular velocity is thus given by $\mathbf{v}_{\perp\mathrm{D}_2^+} = \mathbf{v}_{\perp\mathrm{D}_2^+0} +$

$\mathbf{v}_{\mathrm{pol},\mathrm{D}_2^+} + \mathbf{v}_{\mathrm{fric},\mathrm{D}_2^+}$, with

$$\mathbf{v}_{\perp \mathrm{D}_2^+ 0} = \mathbf{v}_{E\times B} + \mathbf{v}_{\mathrm{dD}_2^+} \tag{16}$$

the leading order component, with $\mathbf{v}_{\mathrm{dD}_2^+} = (\mathbf{B}\times\nabla p_{\mathrm{D}_2^+})/(en_{\mathrm{D}_2^+}B^2)$. The velocity $\mathbf{v}_{\mathrm{pol},\mathrm{D}_2^+}$ denotes the polarization drift and $\mathbf{v}_{\mathrm{fric},\mathrm{D}_2^+}$ stands for the drift velocity arising from friction between D_2^+ ions and other species. Their expressions are given by

$$\mathbf{v}_{\mathrm{pol},\mathrm{D}_2^+} = -\frac{1}{n_{\mathrm{D}_2^+}\Omega_{\mathrm{cD}_2^+}}\frac{\mathrm{d}_{\mathrm{D}_2^+}}{\mathrm{d}t}\left(\frac{n_{\mathrm{D}_2^+}}{B}\nabla_\perp\phi + \frac{1}{B}\nabla_\perp p_{\mathrm{D}_2^+}\right) + \frac{1}{m_{\mathrm{D}_2^+}n_{\mathrm{D}_2^+}\Omega_{\mathrm{cD}_2^+}}\mathbf{b}\times\left[G_{\mathrm{D}_2^+}\mathbf{k} - \frac{\nabla G_{\mathrm{D}_2^+}}{3}\right], \tag{17}$$

and

$$\mathbf{v}_{\mathrm{fric},\mathrm{D}_2^+} = \frac{n_{\mathrm{D}_2}}{n_{\mathrm{D}_2^+}}\frac{\nu_{\mathrm{iz},\mathrm{D}_2} + \nu_{\mathrm{cx},\mathrm{D}_2} + \nu_{\mathrm{cx},\mathrm{D}_2-\mathrm{D}^+}}{\Omega_{\mathrm{cD}_2^+}} \times\left(\mathbf{v}_{\perp\mathrm{D}_2} - \mathbf{v}_{\perp\mathrm{D}_2^+0}\right)\times\mathbf{b}, \tag{18}$$

with $G_{\mathrm{D}_2^+} = -\eta_{0\mathrm{D}_2^+}\left[2\nabla_\parallel v_{\parallel\mathrm{D}_2^+} + C(\phi)/B + C(p_{\mathrm{D}_2^+})/(n_{\mathrm{D}_2^+}B)\right]$ the D_2^+ gyroviscous term and $\eta_{0\mathrm{D}_2^+}$ the related viscosity. The approximation $\mathbf{v}_{\perp\mathrm{D}_2^+} \simeq \mathbf{v}_{\perp\mathrm{D}_2^+0}$ is used in equation (18).

To obtain an expression for the parallel friction forces and parallel heat fluxes and close the Braginskii equations, we use the collisional closure proposed by Zhdanov in reference [43], leveraging the formulation presented in references [32, 54], more suitable for numerical implementation. The application of this procedure to the particular case of the multispecies plasma considered here is described in appendix B, where we take advantage of the fact that the D_2^+ density is considerably smaller than the D^+ density, i.e. $n_{\mathrm{D}_2^+}/n_{\mathrm{D}^+} \ll 1$, for typical tokamak boundary conditions, which leads to $n_\mathrm{e} \simeq n_{\mathrm{D}^+}$ because of quasi-neutrality. On the other hand, the contributions from the perpendicular heat flux arising from $\nabla\cdot\mathbf{q}_\mathrm{e}$ and $\nabla\cdot\mathbf{q}_{\mathrm{D}^+}$ in the T_e and T_{D^+} equations, respectively, can be evaluated as in the single-ion species model [22, 23], in particular following the derivation presented in reference [53]. This approach can be generalised to evaluate the term arising from the perpendicular component of $\nabla\cdot\mathbf{q}_{\mathrm{D}_2^+}$ in the $T_{\mathrm{D}_2^+}$ equation. We remark that the collisional heat exchange in equations (10)–(12), denoted by Q_e, Q_{D^+} and $Q_{\mathrm{D}_2^+}$, are negligible compared to the other terms in the temperature equations and therefore are not considered in the present work, similarly to the approach followed in previous versions of GBS [22, 23, 55]. Thus, the drift-reduced Braginskii system of equations is composed of the continuity equation for the electron species, the continuity equation for the D_2^+ species, the vorticity equations that ensures quasi-neutrality, $n_\mathrm{e} = n_{\mathrm{D}^+} + n_{\mathrm{D}_2^+}$, and the equations for the parallel velocities and temperature of all species. They take the form

$$\begin{aligned}\frac{\partial n_\mathrm{e}}{\partial t} =& -\frac{\rho_*^{-1}}{B}[\phi, n_\mathrm{e}] + \frac{2}{B}\left[C(p_\mathrm{e}) - n_\mathrm{e}C(\phi)\right] \\ &- \nabla\cdot(n_\mathrm{e}v_{\parallel\mathrm{e}}\mathbf{b}) + D_{n_\mathrm{e}}\nabla_\perp^2 n_\mathrm{e} + S_{n_\mathrm{e}} \\ &+ n_\mathrm{D}\nu_{\mathrm{iz},\mathrm{D}} - n_{\mathrm{D}^+}\nu_{\mathrm{rec},\mathrm{D}^+} + n_{\mathrm{D}_2}\nu_{\mathrm{iz},\mathrm{D}_2} - n_{\mathrm{D}_2^+}\nu_{\mathrm{rec},\mathrm{D}_2^+} \\ &+ n_{\mathrm{D}_2}\nu_{\mathrm{diss-iz},\mathrm{D}_2} + n_{\mathrm{D}_2^+}\nu_{\mathrm{diss-iz},\mathrm{D}_2^+} - n_{\mathrm{D}_2^+}\nu_{\mathrm{diss-rec},\mathrm{D}_2^+},\end{aligned} \tag{19}$$

$$\begin{aligned}\frac{\partial n_{\mathrm{D}_2^+}}{\partial t} =& -\frac{\rho_*^{-1}}{B}[\phi, n_{\mathrm{D}_2^+}] - \nabla\cdot(n_{\mathrm{D}_2^+}v_{\parallel\mathrm{D}_2^+}\mathbf{b}) \\ &- \frac{2}{B}\left[n_{\mathrm{D}_2^+}C(T_{\mathrm{D}_2^+}) + T_{\mathrm{D}_2^+}C(n_{\mathrm{D}_2^+}) + n_{\mathrm{D}_2^+}C(\phi)\right] \\ &+ D_{n_{\mathrm{D}_2^+}}\nabla_\perp^2 n_{\mathrm{D}_2^+} + S_{n_{\mathrm{D}_2^+}} + n_{\mathrm{D}_2}\nu_{\mathrm{iz},\mathrm{D}_2} - n_{\mathrm{D}_2^+}\nu_{\mathrm{rec},\mathrm{D}_2^+} \\ &+ n_{\mathrm{D}_2}\nu_{\mathrm{cx},\mathrm{D}_2-\mathrm{D}^+} - n_\mathrm{D}\nu_{\mathrm{cx},\mathrm{D}-\mathrm{D}_2^+} \\ &- n_{\mathrm{D}_2^+}\left(\nu_{\mathrm{diss-iz},\mathrm{D}_2^+} + \nu_{\mathrm{diss},\mathrm{D}_2^+} + \nu_{\mathrm{diss-rec},\mathrm{D}_2^+}\right),\end{aligned} \tag{20}$$

$$\begin{aligned}\frac{\partial\Omega}{\partial t} =& -\nabla\cdot\left[\frac{\rho_*^{-1}}{B}\left(\left[\phi, B\boldsymbol{\Omega}_{\mathrm{D}^+}\right] + 2\left[\phi, B\boldsymbol{\omega}_{\mathrm{D}_2^+}\right]\right)\right] \\ &- \nabla\cdot\left[\frac{v_{\parallel\mathrm{D}^+}}{B}\nabla_\parallel\left(B\boldsymbol{\Omega}_{\mathrm{D}^+}\right) + \frac{v_{\parallel\mathrm{D}_2^+}}{B}\nabla_\parallel\left(B\boldsymbol{\omega}_{\mathrm{D}_2^+}\right)\right] \\ &+ \frac{2}{B}\left[n_\mathrm{e}C(T_\mathrm{e}) + T_\mathrm{e}C(n_\mathrm{e}) + n_{\mathrm{D}^+}C(T_{\mathrm{D}^+})\right. \\ &\left. + T_{\mathrm{D}^+}C(n_{\mathrm{D}^+}) + n_{\mathrm{D}_2^+}C(T_{\mathrm{D}_2^+}) + T_{\mathrm{D}_2^+}C(n_{\mathrm{D}_2^+})\right] \\ &+ \nabla\cdot\left(j_\parallel\mathbf{b}\right) + \left[\nabla G_{\mathrm{D}^+}\cdot\left(\frac{\boldsymbol{b}\times\boldsymbol{k}}{B}\right)\right. \\ &\left. + G_{\mathrm{D}^+}\nabla\cdot\left(\frac{\boldsymbol{b}\times\boldsymbol{k}}{B}\right) - \frac{2}{3B}C\left(G_{\mathrm{D}^+}\right)\right] \\ &+ \left[\nabla G_{\mathrm{D}_2^+}\cdot\left(\frac{\boldsymbol{b}\times\boldsymbol{k}}{B}\right) + G_{\mathrm{D}_2^+}\nabla\cdot\left(\frac{\boldsymbol{b}\times\boldsymbol{k}}{B}\right)\right. \\ &\left. - \frac{2}{3B}C\left(G_{\mathrm{D}_2^+}\right)\right] + \eta_{0\Omega}\nabla_\parallel^2\Omega + D_{\perp\Omega}\nabla_\perp^2\Omega \\ &- \nabla\cdot\left[\frac{2n_{\mathrm{D}_2}}{n_{\mathrm{D}_2^+}}\left(\nu_{\mathrm{cx},\mathrm{D}_2} + \nu_{\mathrm{iz},\mathrm{D}_2} + \nu_{\mathrm{cx},\mathrm{D}_2-\mathrm{D}^+}\right)\boldsymbol{\omega}_{\mathrm{D}_2^+}\right] \\ &- \nabla\cdot\left[\frac{n_\mathrm{D}}{n_{\mathrm{D}^+}}\left(\nu_{\mathrm{cx},\mathrm{D}} + \nu_{\mathrm{iz},\mathrm{D}} + \nu_{\mathrm{cx},\mathrm{D}-\mathrm{D}_2^+}\right)\boldsymbol{\omega}_{\mathrm{D}^+}\right] \\ &- \nabla\cdot\left[\frac{n_{\mathrm{D}_2}}{n_{\mathrm{D}^+}}\nu_{\mathrm{diss-iz},\mathrm{D}_2}\boldsymbol{\omega}_{\mathrm{D}^+}\right] \\ &+ \nabla\cdot\left[\frac{n_{\mathrm{D}_2^+}}{n_{\mathrm{D}^+}}\left(2\nu_{\mathrm{diss-iz},\mathrm{D}_2^+} + \nu_{\mathrm{di},\mathrm{D}_2^+}\right)\left(\boldsymbol{\omega}_{\mathrm{D}_2^+} - \boldsymbol{\omega}_{\mathrm{D}^+}\right)\right],\end{aligned} \tag{21}$$

$$\begin{aligned}\frac{\partial v_{\parallel\mathrm{e}}}{\partial t} =& -\frac{\rho_*^{-1}}{B}[\phi, v_{\parallel\mathrm{e}}] - v_{\parallel\mathrm{e}}\nabla_\parallel v_{\parallel\mathrm{e}} \\ &+ \frac{m_\mathrm{D}}{m_\mathrm{e}}\left[\nabla_\parallel\phi - \frac{\nabla_\parallel p_\mathrm{e}}{n_\mathrm{e}} - \frac{2}{3n_\mathrm{e}}\nabla_\parallel G_\mathrm{e} - 0.71\nabla_\parallel T_\mathrm{e}\right] \\ &- \frac{m_\mathrm{D}}{m_\mathrm{e}}\nu\left(v_{\parallel\mathrm{e}} - v_{\parallel\mathrm{D}^+}\right) + D_{v_{\parallel\mathrm{e}}}\nabla_\perp^2 v_{\parallel\mathrm{e}}\end{aligned}$$

$$+\frac{1}{n_{\mathrm{e}}}\Big[n_{\mathrm{D}}\left(2\nu_{\mathrm{iz,D}}+\nu_{\mathrm{e-D}}\right)\left(v_{\parallel\mathrm{D}}-v_{\parallel\mathrm{e}}\right)+n_{\mathrm{D}_2}\left(2\nu_{\mathrm{iz,D_2}}+\nu_{\mathrm{e-D_2}}\right)\left(v_{\parallel\mathrm{D_2}}-v_{\parallel\mathrm{e}}\right)+n_{\mathrm{D}_2}\left(2\nu_{\mathrm{diss-iz,D_2}}+\nu_{\mathrm{diss,D_2}}\right)\left(v_{\parallel\mathrm{D_2}}-v_{\parallel\mathrm{e}}\right)+n_{\mathrm{D}_2^+}\left(2\nu_{\mathrm{diss-iz,D}_2^+}+\nu_{\mathrm{diss,D}_2^+}\right)\left(v_{\parallel\mathrm{D}_2^+}-v_{\parallel\mathrm{e}}\right)\Big], \tag{22}$$

$$\frac{\partial v_{\parallel\mathrm{D}^+}}{\partial t}=-\frac{\rho_*^{-1}}{B}[\phi,v_{\parallel\mathrm{D}^+}]-v_{\parallel\mathrm{D}^+}\nabla_\parallel v_{\parallel\mathrm{D}^+}-\nabla_\parallel\phi-\frac{\nabla_\parallel p_{\mathrm{D}}^+}{n_{\mathrm{D}^+}}-\frac{2}{3n_{\mathrm{D}^+}}\nabla_\parallel G_{\mathrm{D}^+}+0.71\frac{n_{\mathrm{e}}}{n_{\mathrm{D}^+}}\nabla_\parallel T_{\mathrm{e}}-\nu\frac{n_{\mathrm{e}}}{n_{\mathrm{D}^+}}\left(v_{\parallel\mathrm{D}^+}-v_{\parallel\mathrm{e}}\right)+D_{v_{\parallel\mathrm{D}^+}}\nabla_\perp^2 v_{\parallel\mathrm{D}^+}+\frac{1}{n_{\mathrm{D}^+}}\Big[n_{\mathrm{D}}(\nu_{\mathrm{iz,D}}+\nu_{\mathrm{cx,D}}+\nu_{\mathrm{cx,D-D}_2^+})\times(v_{\parallel\mathrm{D}}-v_{\parallel\mathrm{D}^+})+n_{\mathrm{D}_2^+}\nu_{\mathrm{diss-iz,D_2}}(v_{\parallel\mathrm{D_2}}-v_{\parallel\mathrm{D}^+})+n_{\mathrm{D}_2^+}\left(2\nu_{\mathrm{diss-iz,D}_2^+}+\nu_{\mathrm{diss,D}_2^+}\right)(v_{\parallel\mathrm{D}_2^+}-v_{\parallel\mathrm{D}^+})\Big], \tag{23}$$

$$\frac{\partial v_{\parallel\mathrm{D}_2^+}}{\partial t}=-\frac{\rho_*^{-1}}{B}[\phi,v_{\parallel\mathrm{D}_2^+}]-v_{\parallel\mathrm{D}_2^+}\nabla_\parallel v_{\parallel\mathrm{D}_2^+}+\frac{1}{2}\left[-\nabla_\parallel\phi-\frac{\nabla p_{\mathrm{D}_2^+}}{n_{\mathrm{D}_2^+}}-\frac{2}{3n_{\mathrm{D}_2^+}}\nabla_\parallel G_{\mathrm{D}_2^+}\right]+D_{v_{\parallel\mathrm{D}_2^+}}\nabla_\perp^2 v_{\parallel\mathrm{D}_2^+}+\frac{n_{\mathrm{D_2}}}{n_{\mathrm{D}_2^+}}\left(\nu_{\mathrm{iz,D_2}}+\nu_{\mathrm{cx,D_2}}+\nu_{\mathrm{cx,D_2-D^+}}\right)(v_{\parallel\mathrm{D_2}}-v_{\parallel\mathrm{D}_2^+}), \tag{24}$$

$$\frac{\partial T_{\mathrm{e}}}{\partial t}=-\frac{\rho_*^{-1}}{B}[\phi,T_{\mathrm{e}}]-v_{\parallel\mathrm{e}}\nabla_\parallel T_{\mathrm{e}}+\frac{4T_{\mathrm{e}}}{3B}\left[\frac{C(p_{\mathrm{e}})}{n_{\mathrm{e}}}+\frac{5}{2}C(T_{\mathrm{e}})-C(\phi)\right]-\frac{2T_{\mathrm{e}}}{3}\nabla\cdot\left(v_{\parallel\mathrm{e}}\mathbf{b}\right)+\frac{2}{3n_{\mathrm{e}}}\frac{1.62}{\nu}\left[n_{\mathrm{e}}T_{\mathrm{e}}\left(\nabla_\parallel T_{\mathrm{e}}\right)\nabla\cdot\mathbf{b}+\nabla_\parallel\left(n_{\mathrm{e}}T_{\mathrm{e}}\nabla_\parallel T_{\mathrm{e}}\right)\right]-\frac{2}{3}0.71T_{\mathrm{e}}\nabla\cdot(v_{\parallel\mathrm{e}}-v_{\parallel\mathrm{D}^+})\mathbf{b}-\frac{2}{3}0.71\times\left(\frac{T_{\mathrm{e}}}{n_{\mathrm{e}}}\nabla_\parallel n_{\mathrm{e}}+\nabla_\parallel T_{\mathrm{e}}\right)\left(v_{\parallel\mathrm{e}}-v_{\parallel\mathrm{D}^+}\right)+x_{\perp\mathrm{e}}\nabla_\perp^2 T_{\mathrm{e}}+\nabla_\parallel\left(x_{\parallel\mathrm{e}}\nabla_\parallel T_{\mathrm{e}}\right)+S_{T_{\mathrm{e}}}+\frac{n_{\mathrm{D}}}{n_{\mathrm{e}}}\nu_{\mathrm{iz,D}}\left[-\frac{2}{3}E_{\mathrm{iz,D}}-T_{\mathrm{e}}+\frac{m_{\mathrm{e}}}{m_{\mathrm{D}}}v_{\parallel\mathrm{e}}\left(v_{\parallel\mathrm{e}}-\frac{4}{3}v_{\parallel\mathrm{D}}\right)\right]-\frac{n_{\mathrm{D}}}{n_{\mathrm{e}}}\nu_{\mathrm{e-D}}\frac{m_{\mathrm{e}}}{m_{\mathrm{D}}}\frac{2}{3}v_{\parallel\mathrm{e}}(v_{\parallel\mathrm{D}}-v_{\parallel\mathrm{e}})+\frac{n_{\mathrm{D_2}}}{n_{\mathrm{e}}}\nu_{\mathrm{iz,D_2}}\times\left[-\frac{2}{3}E_{\mathrm{iz,D_2}}-T_{\mathrm{e}}+\frac{m_{\mathrm{e}}}{m_{\mathrm{D}}}v_{\parallel\mathrm{e}}\left(v_{\parallel\mathrm{e}}-\frac{4}{3}v_{\parallel\mathrm{D_2}}\right)\right]-\frac{n_{\mathrm{D_2}}}{n_{\mathrm{e}}}\nu_{\mathrm{e-D_2}}\frac{m_{\mathrm{e}}}{m_{\mathrm{D}}}\frac{2}{3}v_{\parallel\mathrm{e}}(v_{\parallel\mathrm{D_2}}-v_{\parallel\mathrm{e}})+\frac{n_{\mathrm{D_2}}}{n_{\mathrm{e}}}\nu_{\mathrm{diss,D_2}}\times\left[-\frac{2}{3}E_{\mathrm{diss,D_2}}+\frac{2}{3}\frac{m_{\mathrm{e}}}{m_{\mathrm{D}}}v_{\parallel\mathrm{e}}\left(v_{\parallel\mathrm{e}}-v_{\parallel\mathrm{D_2}}\right)\right]+\frac{n_{\mathrm{D_2}}}{n_{\mathrm{e}}}\nu_{\mathrm{diss-iz,D_2}}\left[-\frac{2}{3}E_{\mathrm{diss-iz,D_2}}-T_{\mathrm{e}}+\frac{m_{\mathrm{e}}}{m_{\mathrm{D}}}v_{\parallel\mathrm{e}}\left(v_{\parallel\mathrm{e}}-\frac{4}{3}v_{\parallel\mathrm{D_2}}\right)\right]+\frac{n_{\mathrm{D}_2^+}}{n_{\mathrm{e}}}\nu_{\mathrm{diss,D}_2^+}\times\left[-\frac{2}{3}E_{\mathrm{diss,D}_2^+}+\frac{2}{3}\frac{m_{\mathrm{e}}}{m_{\mathrm{D}}}v_{\parallel\mathrm{e}}\left(v_{\parallel\mathrm{e}}-v_{\parallel\mathrm{D}_2^+}\right)\right]+\frac{n_{\mathrm{D}_2^+}}{n_{\mathrm{e}}}\nu_{\mathrm{diss-iz,D}_2^+}\left[-\frac{2}{3}E_{\mathrm{diss-iz,D}_2^+}-T_{\mathrm{e}}+\frac{m_{\mathrm{e}}}{m_{\mathrm{D}}}v_{\parallel\mathrm{e}}\left(v_{\parallel\mathrm{e}}-\frac{4}{3}v_{\parallel\mathrm{D}_2^+}\right)\right], \tag{25}$$

$$\frac{\partial T_{\mathrm{D}^+}}{\partial t}=-\frac{\rho_*^{-1}}{B}[\phi,T_{\mathrm{D}^+}]-v_{\parallel\mathrm{D}^+}\nabla_\parallel T_{\mathrm{D}^+}+\frac{4}{3}\frac{T_{\mathrm{D}^+}}{B}\left[-C(\phi)+\frac{C(p_{\mathrm{e}}+p_{\mathrm{D}_2^+})}{n_{\mathrm{D}^+}}\right]-\frac{2T_{\mathrm{D}^+}}{3n_{\mathrm{D}^+}}\Big[n_{\mathrm{e}}\nabla\cdot\left(v_{\parallel\mathrm{e}}\mathbf{b}\right)-n_{\mathrm{D}_2^+}\nabla\cdot\left(v_{\parallel\mathrm{D}_2^+}\mathbf{b}\right)+v_{\parallel\mathrm{e}}\nabla_\parallel n_{\mathrm{e}}-v_{\parallel\mathrm{D}_2^+}\nabla_\parallel n_{\mathrm{D}_2^+}-v_{\parallel\mathrm{D}^+}\nabla_\parallel n_{\mathrm{D}^+}\Big]-\frac{10}{3}\frac{T_{\mathrm{D}^+}}{B}C(T_{\mathrm{D}^+})+\frac{2}{3n_{\mathrm{D}^+}}\frac{2.32}{\sqrt{2}\nu}\sqrt{\frac{m_{\mathrm{e}}}{m_{\mathrm{D}}}}\nabla\times\left(n_{\mathrm{e}}T_{\mathrm{D}^+}\nabla_\parallel T_{\mathrm{D}^+}\right)\mathbf{b}+x_{\perp\mathrm{D}^+}\nabla_\perp^2 T_{\mathrm{D}^+}+\nabla_\parallel\left(x_{\parallel\mathrm{D}^+}\nabla_\parallel T_{\mathrm{D}^+}\right)+S_{T_{\mathrm{D}^+}}+\frac{1}{n_{\mathrm{D}^+}}\Big\{n_{\mathrm{D}}\left(\nu_{\mathrm{iz,D}}+\nu_{\mathrm{cx,D}}+\nu_{\mathrm{cx,D-D}_2^+}\right)\times\left[T_{\mathrm{D}}-T_{\mathrm{D}^+}+\frac{1}{3}\left(v_{\parallel\mathrm{D}}-v_{\parallel\mathrm{D}^+}\right)^2\right]+n_{\mathrm{D_2}}\nu_{\mathrm{diss-iz,D_2}}\times\left[T_{\mathrm{D}^+,\mathrm{diss-iz(D_2)}}-T_{\mathrm{D}^+}+\frac{1}{3}\left(v_{\parallel\mathrm{D_2}}-v_{\parallel\mathrm{D}^+}\right)^2\right]+2n_{\mathrm{D}_2^+}\nu_{\mathrm{diss-iz,D}_2^+}\left[T_{\mathrm{D}^+,\mathrm{diss-iz}\left(\mathrm{D}_2^+\right)}-T_{\mathrm{D}^+}+\frac{1}{3}\left(v_{\parallel\mathrm{D}_2^+}-v_{\parallel\mathrm{D}^+}\right)^2\right]+n_{\mathrm{D}_2^+}\nu_{\mathrm{diss,D}_2^+}\times\left[T_{\mathrm{D}^+,\mathrm{diss}\left(\mathrm{D}_2^+\right)}-T_{\mathrm{D}^+}+\frac{1}{3}\left(v_{\parallel\mathrm{D}_2^+}-v_{\parallel\mathrm{D}^+}\right)^2\right]\Big\} \tag{26}$$

and

$$\frac{\partial T_{\mathrm{D}_2^+}}{\partial t}=-\frac{\rho_*^{-1}}{B}[\phi,T_{\mathrm{D}_2^+}]-v_{\parallel\mathrm{D}_2^+}\nabla_\parallel T_{\mathrm{D}_2^+}-\frac{4}{3}\frac{T_{\mathrm{D}_2^+}}{B}\left[C(\phi)+\frac{C(p_{\mathrm{D}_2^+})}{n_{\mathrm{D}_2^+}}\right]-\frac{10}{3}\frac{T_{\mathrm{D}_2^+}}{B}C(T_{\mathrm{D}_2^+})$$

$$
\begin{aligned}
&- \frac{2T_{\mathrm{D}_2^+}}{3}\nabla\cdot\left(v_{\parallel\mathrm{D}_2^+}\mathbf{b}\right) + \frac{2}{3n_{\mathrm{D}_2^+}}\frac{0.92}{\sqrt{2}\nu}\sqrt{\frac{m_\mathrm{e}}{m_\mathrm{D}}}\nabla \\
&\times\left(n_\mathrm{e}T_{\mathrm{D}^+}\nabla_\parallel T_{\mathrm{D}^+}\right)\mathbf{b} + x_{\perp\mathrm{D}_2^+}\nabla_\perp^2 T_{\mathrm{D}_2^+} \\
&+ \nabla_\parallel\left(x_{\parallel\mathrm{D}_2^+}\nabla_\parallel T_{\mathrm{D}_2^+}\right) + S_{T_{\mathrm{D}_2^+}} \\
&+ \frac{n_{\mathrm{D}_2}}{n_{\mathrm{D}_2^+}}(\nu_{\mathrm{cx},\mathrm{D}_2} + \nu_{\mathrm{iz},\mathrm{D}_2} + \nu_{\mathrm{cx},\mathrm{D}_2-\mathrm{D}^+}) \\
&\times\left[T_{\mathrm{D}_2^+} - T_{\mathrm{D}_2^+} + \frac{2}{3}(v_{\parallel\mathrm{D}_2} - v_{\parallel\mathrm{D}_2^+})^2\right]. \qquad (27)
\end{aligned}
$$

In equations (19)–(27) we introduce $[A,B] = \mathbf{b}\cdot(\nabla A\times\nabla B)$, $C(A) = (B/2)\left[\nabla\times(\mathbf{b}/B)\right]\cdot\nabla A$ and the plasma vorticity $\Omega = \Omega_{\mathrm{D}^+} + 2\Omega_{\mathrm{D}_2^+}$, with the D^+ contribution given by $\Omega_{\mathrm{D}^+} = \nabla\cdot\boldsymbol{\omega}_{\mathrm{D}^+} = \nabla\cdot\left[\left(n_{\mathrm{D}^+}/B^2\right)\nabla_\perp\phi + \left(1/B^2\right)\nabla_\perp p_{\mathrm{D}^+}\right]$ and an analogous D_2^+ contribution, $\Omega_{\mathrm{D}_2^+}$. The system is thus closed by the generalized Poisson equation, which is obtained by inverting the definition of the plasma vorticity, Ω, yielding

$$
\begin{aligned}
&\nabla_\perp\cdot\left[\frac{n_{\mathrm{D}^+} + 2n_{\mathrm{D}_2^+}}{B^2}\nabla_\perp\phi\right] \\
&\qquad = \Omega - \nabla_\perp\cdot\left[\frac{1}{B^2}\nabla_\perp\left(p_{\mathrm{D}^+} + 2p_{\mathrm{D}_2^+}\right)\right]. \qquad (28)
\end{aligned}
$$

We remark that the electron gyroviscous term in equation (22) is defined similarly to the ion gyroviscous terms, $G_\mathrm{e} = -\eta_{0\mathrm{e}}\left[2\nabla_\parallel v_{\parallel\mathrm{e}} + C(\phi)/B - C(p_\mathrm{e})/(n_\mathrm{e}B)\right]$.
Equation (21) is written avoiding the Boussinesq approximation and taking into account all components of the velocity of the ion species D^+ and D_2^+, including the higher order polarization and friction contributions. On the other hand, in order to express the advective derivative for the ion species, $\mathrm{d}_{\mathrm{D}^+}/\mathrm{d}t$ and $\mathrm{d}_{\mathrm{D}_2^+}/\mathrm{d}t$, we only consider the leading order components of the perpendicular velocity, $v_{\perp\mathrm{D}^+0}$ and $v_{\perp\mathrm{D}_2^+0}$, therefore neglecting $\mathbf{v}_\mathrm{pol}$ and $\mathbf{v}_\mathrm{fric}$. Similarly, we neglect the friction and polarization drifts in the continuity equation for D_2^+. We also remark that the terms of higher order in $1/\Omega_{\mathrm{cD}_2^+}\mathrm{d}/\mathrm{d}t$ in the perpendicular velocity of D_2^+ ions are neglected when writing $\nabla\cdot\mathbf{v}_{\mathrm{D}_2^+}$ in the temperature equations, equations (26) and (27), which is a necessary assumption in order to avoid explicit time derivatives arising from the polarization drift velocity, $\mathbf{v}_{\mathrm{pol},\mathrm{D}_2^+}$. Nevertheless, all terms are considered in the divergence of the perpendicular velocity of D^+ ions in equation (26), as we make use of $\nabla\cdot\mathbf{j} = 0$ to write $\nabla\cdot\mathbf{v}_{\mathrm{D}^+}$ in terms of $\nabla\cdot\mathbf{v}_\mathrm{e}$ and $\nabla\cdot\mathbf{v}_{\mathrm{D}_2^+}$. Finally, when taking the divergence of these terms, we make use of $\nabla\cdot\mathbf{v}_\mathrm{D} \ll \nabla\cdot\mathbf{v}_{\mathrm{D}^+}$ to neglect the contribution of the velocity of D atoms, which is valid since $\rho_{\mathrm{s},\mathrm{D}^+} \ll \lambda_{\mathrm{mfp,D}}$ (with $\rho_{\mathrm{s},\mathrm{D}^+} = c_{\mathrm{s},\mathrm{D}^+}/\Omega_{\mathrm{c},\mathrm{D}^+}$ the sound Larmor radius of D^+ ions, $c_{\mathrm{s},\mathrm{D}^+} = \sqrt{T_\mathrm{e}/m_{\mathrm{D}^+}}$ the D^+ ions sound speed and $\lambda_{\mathrm{mfp,D}}$ the mean free path of a D atoms). This relation can be generalized to the other neutral and ion species, namely D_2 molecules and D_2^+ ions. Thus we neglect the contribution of the divergence of neutral particle velocities when compared to the divergence of ion velocities. We highlight that the diffusion terms considered in equations (19)–(27) are introduced to improve the numerical stability of GBS implementation. Finally, we note that S_{n_e}, $S_{n_{\mathrm{D}^+}}$, S_{T_e}, $S_{T_{\mathrm{D}^+}}$ and $S_{T_{\mathrm{D}_2^+}}$ in equations (19)–(27) represent the density and temperature source terms for the different plasma species at the edge–core interface, which mimic the plasma and energy outflow from the core into the simulation domain. These sources are thus responsible for setting realistic boundary conditions for the plasma at the edge–core interface.

We highlight that neglecting the polarization drift of the D_2^+ species is reasonable in the scenario considered here, where D_2^+ density is considerably smaller than the D^+ density. If multiple ion species with similar densities are considered, e.g. in the simulation of a D–T plasma, the polarization drift of all species has to be taken into account, which can be done by using a different time integration scheme with respect to the one used in GBS [22, 23]. At the same time, a D–T plasma leads to more complex expressions for the parallel heat flux and friction force terms, due to the constraints provided by the Zhdanov closure. A multispecies model for the 2D simulation of a D–T plasma is presented in detail in reference [56].

We note that dimensionless units are used in equations (19)–(27) and in the rest of the paper. The densities, n_e, n_{D^+} and $n_{\mathrm{D}_2^+}$, are normalized to the reference value n_0, while temperatures, T_e, T_{D^+} and $T_{\mathrm{D}_2^+}$, are normalized to the respective reference values, $T_{\mathrm{e}0}$, T_{D^+0} and $T_{\mathrm{D}_2^+0} = T_{\mathrm{D}^+0}$, which are related by the dimensionless quantity $\tau = T_{\mathrm{D}^+0}/T_{\mathrm{e}0}$. Conversely, lengths parallel to the magnetic field are normalized to the tokamak major radius, R_0, lengths perpendicular to the magnetic field are normalized to the ion sound Larmor radius, $\rho_{\mathrm{s}0} = c_{\mathrm{s}0}/\Omega_{\mathrm{cD}^+0}$, where $c_{\mathrm{s}0} = T_{\mathrm{e}0}/m_{\mathrm{D}^+}$ is the normalized D^+ ion sound speed and $\Omega_{\mathrm{cD}^+0} = eB_0/m_{\mathrm{D}^+}$ is the D^+ ion cyclotron frequency at the magnetic axis, and time is normalized to $R_0/c_{\mathrm{s}0}$. All other normalizations follow, namely the parallel velocities, $v_{\parallel\mathrm{e}}$, $v_{\parallel\mathrm{D}^+}$ and $v_{\parallel\mathrm{D}_2^+}$, are normalized to $c_{\mathrm{s}0}$, the plasma vorticity Ω is normalized to $n_0T_{\mathrm{e}0}/(\rho_{\mathrm{s}0}^2B_0^2)$, perpendicular diffusion coefficients $D_\perp$ and conductivities $\chi_\perp$ are normalized to $c_{\mathrm{s}0}\rho_{\mathrm{s}0}^2/R_0$, while the parallel diffusion coefficients $D_\parallel$ and conductivities $\chi_\parallel$ are normalized to $c_{\mathrm{s}0}R_0$. Normalized quantities are used in the rest of the paper, except when explicitly mentioned. The parameter $\rho_\star = \rho_{\mathrm{s}0}/R_0$ is the ratio between the D^+ ion sound Larmor radius and the tokamak major radius R_0. We also note that ν is the dimensionless resistivity given by $\nu = (e^2n_{\mathrm{e}0}R_0)/(m_\mathrm{D}c_{\mathrm{s}0}\sigma_\parallel)$, with the parallel conductivity defined in terms of the electron characteristic time τ_e as $\sigma_\parallel = e^2n_\mathrm{e}\tau_\mathrm{e}/(0.51m_\mathrm{e})$.

We conclude with a few final remarks on equations (19)–(27). We first note that the parallel conductivity appearing in the temperature equations for electrons is expressed in the form $\chi_{\parallel,\mathrm{e}} = \chi_{\parallel0,\mathrm{e}}T_\mathrm{e}^{5/2}$, where we retain the Spitzer temperature dependence while we neglect the weaker space and time variation of the $2/(3n_\mathrm{e})$ factor, similarly to the approach followed in the single-component plasma model previously implemented in GBS ([22, 23]). A similar approach is followed for $\chi_{\parallel,\mathrm{D}^+}$ and $\chi_{\parallel,\mathrm{D}_2^+}$. This is not expected

to impact the simulation results in the sheath-limited regime, where conductivity-related contributions are small. Finally, we point that, since the D_2^+ density may drop to a very low value, numerical issues may arise in the equations for $v_{\parallel D_2^+}$ and $T_{D_2^+}$ due to terms featuring a $1/n_{D_2^+}$ dependence. For a robust numerical approach, we evolve the parallel flux and pressure of the D_2^+ ion species, $\Gamma_{\parallel D_2^+} = n_{D_2^+} v_{\parallel D_2^+}$ and $p_{D_2^+} = n_{D_2^+} T_{D_2^+}$, instead of $v_{\parallel D_2^+}$ and $T_{D_2^+}$. The equations for the time evolution of $\Gamma_{\parallel D_2^+}$ and $p_{D_2^+}$ are

$$\frac{\partial \Gamma_{\parallel D_2^+}}{\partial t} = \frac{\partial n_{D_2^+}}{\partial t} v_{\parallel D_2^+} + n_{D_2^+} \frac{\partial v_{\parallel D_2^+}}{\partial t}, \tag{29}$$

and

$$\frac{\partial p_{D_2^+}}{\partial t} = \frac{\partial n_{D_2^+}}{\partial t} T_{D_2^+} + n_{D_2^+} \frac{\partial T_{D_2^+}}{\partial t}, \tag{30}$$

with $\partial_t n_{D_2^+}$, $\partial_t v_{\parallel D_2^+}$ and $\partial_t T_{D_2^+}$ given, respectively, by equations (20), (24) and (27). We focus on the parallel flux, $\Gamma_{\parallel D_2^+}$, and pressure, $p_{D_2^+}$, when presenting the simulation results.

4. Boundary conditions

The boundary conditions implemented in the previous GBS models for single-ion species plasma are extended in the present work to include the molecular ion species D_2^+. In the case considered here, of a plasma with a toroidal limiter, the domain boundary includes the limiter plates, the outer wall and the interface with the core, where the low plasma collisionality with a long mean free path along the magnetic field direction questions the application of a fluid model.

We first consider the boundary conditions at the limiter plates, where most of the plasma ends by flowing along the magnetic field lines. Those are the most important boundary conditions to impact the simulation dynamics. The boundary conditions are imposed at the interface between the collisional pre-sheath (CP) and the magnetic pre-sheath (MP), derived from the Bohm–Chodura boundary conditions, following the approach described in reference [57] in the cold ion limit and generalized in reference [58] to account for finite ion temperature. Here, we further extend this procedure to the case of a multi-ion species plasma. For this purpose, we use the (y, x, z) coordinates, with z the direction of the magnetic field, x the direction perpendicular to the magnetic field and parallel to the limiter surface, and y the direction perpendicular to both x and z (here all spatial coordinates are normalized to ρ_{s0}, while the other quantities are normalized as in equations (19)–(27)). We also introduce $s = y\cos\alpha + z\sin\alpha$, the coordinate perpendicular to the limiter plate, with α the angle between the magnetic field line and the plane of the limiter.

As a first step in the derivation of the boundary conditions, we note that the steady-state dynamics of the multispecies plasma in the CP is described by means of the continuity equation for the D^+ and D_2^+ species (quasi-neutrality provides the electron density) and the parallel momentum equations for e^-, D^+ and D_2^+. In steady state, these can be written as

$$\nabla \cdot (n_{D^+} \mathbf{v}_{D^+}) = S_{p,D^+}, \tag{31}$$

$$\nabla \cdot (n_{D_2^+} \mathbf{v}_{D_2^+}) = S_{p,D_2^+}, \tag{32}$$

$$n_e(\mathbf{v}_e \cdot \nabla)\mathbf{v}_e = -\mu(n_e \mathbf{E} + n_e \mathbf{v}_{D^+}) \times \mathbf{B} + \nabla p_e + \mathbf{S}_{m,e}, \tag{33}$$

$$n_{D^+}\left(\mathbf{v}_{D^+} \cdot \nabla \mathbf{v}_{D^+}\right) = \left(n_{D^+}\mathbf{E} + n_{D^+}\mathbf{v}_{D^+}\right) \times \mathbf{B} - \nabla p_{D^+} + \mathbf{S}_{m,D^+} \tag{34}$$

and

$$n_{D_2^+}\left(\mathbf{v}_{D_2^+} \cdot \nabla \mathbf{v}_{D_2^+}\right) = \left(n_{D_2^+}\mathbf{E} + n_{D_2^+}\mathbf{v}_{D_2^+}\right) \times \mathbf{B} - \nabla p_{D_2^+} + \mathbf{S}_{m,D_2^+}, \tag{35}$$

with $\mu = m_e/m_{D^+}$, S_{p,D^+} and S_{p,D_2^+} the particle sources for D^+ and D_2^+, and $\mathbf{S}_{m,e}$, $\mathbf{S}_{m,D^+}$ and $\mathbf{S}_{m,D_2^+}$ the momentum sources for e^-, D^+ and D_2^+.

From equations (31)–(35) and following the approach described in reference [58], a system of five equations for $\partial_s n_{D^+}$, $\partial_s n_{D_2^+}$, $\partial_s v_{\parallel D^+}$ and $\partial_s v_{\parallel D_2^+}$, $\partial_s \phi$ is hence obtained for the interface between the CP and the MP border, considering the $\mu \ll 1$ limit and isothermal ions and electrons. For this purpose, at the MP entrance, gradients along the x direction are assumed weaker than gradients along s by a factor $\epsilon = \rho_{s0}/L_{n_e} \simeq \rho_{s0}/L_{T_e} \simeq \rho_{s0}/L_\phi \ll 1$, with L_{n_e}, L_{T_e} and L_ϕ respectively the scale lengths of n_e, T_e and ϕ along the x direction. In addition, finite Larmor radius (FLR) effects are neglected and, to express the y and x components of the velocity of each ion species, D^+ and D_2^+, we consider only the leading order terms in $(1/\Omega_{cD^+})\mathrm{d}/\mathrm{d}t$ (see equations (13) and (16)). This yields

$$v_{y,D^+} = v_{y,E\times B} + v_{y,dD^+}, \tag{36}$$

$$v_{x,D^+} = v_{x,E\times B} + v_{x,dD^+}, \tag{37}$$

$$v_{y,D_2^+} = v_{y,E\times B} + v_{y,dD_2^+} \tag{38}$$

and

$$v_{x,D_2^+} = v_{x,E\times B} + v_{x,dD_2^+}, \tag{39}$$

where $v_{y,E\times B}$ and $v_{x,E\times B}$ are respectively the y and x components of the $E \times B$ drift velocity, v_{y,dD^+} and v_{x,dD^+} are the y and x components of the D^+ diamagnetic velocity and v_{y,dD_2^+} and v_{x,dD_2^+} are the y and x components of the D_2^+ diamagnetic velocity. Finally, we define the velocity of the D^+ ions along the s direction as $v_{s,D^+} = v_{\parallel D^+}\sin\alpha + v_{y,D^+}\cos\alpha$. We also introduce the velocity of the D^+ ions along the s direction that excludes the diamagnetic contribution, that is $v'_{s,D^+} = v_{s,D^+} - v_{y,dD^+}\cos\alpha$ and $v'_{s,D_2^+} = v_{s,D_2^+} - v_{y,dD_2^+}\cos\alpha$ for the D_2^+ ions. The system in equations (31)–(35) yields

$$v_{s,D^+}\partial_s n_{D^+} + n_{D^+}\sin\alpha\,\partial_s v_{\parallel D^+} - \partial_x n_{D^+}\cos\alpha\,\partial_s\phi = S_{p,D^+}, \tag{40}$$

$$v_{s,D_2^+}\partial_s n_{D_2^+} + n_{D_2^+}\sin\alpha\,\partial_s v_{\parallel D_2^+} - \partial_x n_{D_2^+}\cos\alpha\,\partial_s\phi = S_{p,D_2^+}, \tag{41}$$

$$n_{\mathrm{D}^+} v_{s,\mathrm{D}^+} \partial_s v_{\parallel \mathrm{D}^+} + n_{\mathrm{D}^+} (\sin\alpha - \partial_x v_{\parallel \mathrm{D}^+} \cos\alpha) \partial_s \phi + T_{\mathrm{D}^+} \sin\alpha \partial_s n_{\mathrm{D}^+} = S_{\parallel \mathrm{m},\mathrm{D}^+}, \tag{42}$$

$$n_{\mathrm{D}_2^+} v_{s,\mathrm{D}_2^+} \partial_s v_{\parallel \mathrm{D}_2^+} + n_{\mathrm{D}_2^+} (\sin\alpha - \partial_x v_{\parallel \mathrm{D}_2^+} \cos\alpha) \partial_s \phi + T_{\mathrm{D}_2^+} \sin\alpha \partial_s n_{\mathrm{D}_2^+} = S_{\parallel \mathrm{m},\mathrm{D}_2^+} \tag{43}$$

and

$$\mu \sin\alpha T_\mathrm{e} \partial_s n_\mathrm{e} - \mu \sin\alpha n_\mathrm{e} \partial_s \phi = S_{\parallel \mathrm{m,e}}, \tag{44}$$

where $S_{\parallel \mathrm{m},\mathrm{D}^+} = \mathbf{S}_{\mathrm{m},\mathrm{D}^+} \cdot \mathbf{b}$, $\mathbf{S}_{\parallel \mathrm{m},\mathrm{D}_2^+} = \mathbf{S}_{\mathrm{m},\mathrm{D}_2^+} \cdot \mathbf{b}$ and $\mathbf{S}_{\parallel \mathrm{m,e}} = \mathbf{S}_{\mathrm{m,e}} \cdot \mathbf{b}$. We then make use of the quasi-neutrality condition, $n_\mathrm{e} = n_{\mathrm{D}^+} + n_{\mathrm{D}_2^+}$, to obtain a system of five linear equations that we express in matrix form as $M\mathbf{x} = \mathbf{S}$, with

$$\mathbf{M} = \begin{pmatrix} v'_{s,\mathrm{D}^+} & n_{\mathrm{D}^+} \sin\alpha & 0 & 0 & -\cos\alpha \partial_x n_{\mathrm{D}^+} \\ T_{\mathrm{D}^+} \sin\alpha & n_{\mathrm{D}^+} v'_{s,\mathrm{D}^+} & 0 & 0 & n_{\mathrm{D}^+}(\sin\alpha - \partial_x v_{\parallel \mathrm{D}^+} \cos\alpha) \\ 0 & 0 & v'_{s,\mathrm{D}_2^+} & n_{\mathrm{D}_2^+} \sin\alpha & -\cos\alpha \partial_x n_{\mathrm{D}_2^+} \\ 0 & 0 & T_{\mathrm{D}_2^+} \sin\alpha & n_{\mathrm{D}_2^+} v'_{s,\mathrm{D}_2^+} & n_{\mathrm{D}_2^+}(\sin\alpha - \partial_x v_{\parallel \mathrm{D}_2^+} \cos\alpha) \\ \mu \sin\alpha T_\mathrm{e} & 0 & \mu \sin\alpha T_\mathrm{e} & 0 & -\mu(n_{\mathrm{D}^+} + n_{\mathrm{D}_2^+}) \sin\alpha \end{pmatrix}, \tag{45}$$

$$\mathbf{x} = \begin{pmatrix} \partial_s n_{\mathrm{D}^+} \\ \partial_s n_{\mathrm{D}_2^+} \\ \partial_s v_{\parallel \mathrm{D}^+} \\ \partial_s v_{\parallel \mathrm{D}_2^+} \\ \partial_s \phi \end{pmatrix} \tag{46}$$

and

$$\mathbf{S} = \begin{pmatrix} S_{\mathrm{p},\mathrm{D}^+} \\ S_{\mathrm{p},\mathrm{D}_2^+} \\ S_{\parallel \mathrm{m},\mathrm{D}^+} \\ S_{\parallel \mathrm{m},\mathrm{D}_2^+} \\ S_{\parallel \mathrm{m,e}} \end{pmatrix}. \tag{47}$$

Following [57, 58], we observe that, while the source terms are important in the CP, they are small at the MP entrance with respect to the gradient terms. This allows one to assume $|\Sigma_j M_{ij} X_j| \gg |S_i|$ at the MP entrance. Thus, the linear system $M\mathbf{x} = \mathbf{S}$ reduces to $M\mathbf{x} = 0$ at the MP entrance. We solve $\det(M) = 0$ with respect to $v'_{s\mathrm{D}^+}$ to obtain the non-trivial solution at the MP entrance. For this purpose, following [59], the parallel velocity of the D_2^+ ion species, $v_{\parallel \mathrm{D}_2^+}$, is related to $v_{\parallel \mathrm{D}^+}$,

$$v_{\parallel \mathrm{D}_2^+} = \sqrt{\frac{m_{\mathrm{D}^+}}{m_{\mathrm{D}_2^+}}} v_{\parallel \mathrm{D}^+} = \frac{v_{\parallel \mathrm{D}^+}}{\sqrt{2}}. \tag{48}$$

In addition, we assume $n_{\mathrm{D}_2^+}/n_\mathrm{e} \ll 1$ (and therefore $n_{\mathrm{D}^+} \simeq n_\mathrm{e}$) and keep only zero order terms in ϵ, neglecting therefore all derivatives along the x direction. The condition $\det(M) = 0$ then yields

$$v'_{s\mathrm{D}^+} = \pm\sqrt{T_\mathrm{e} F_\mathrm{T}} \sin\alpha \tag{49}$$

where the $\pm$ signs refer to the magnetic field lines entering/leaving the vessel and we have defined $F_\mathrm{T} = 1 + \tau T_{\mathrm{D}^+}/T_\mathrm{e}$. We now note that $v'_{s,\mathrm{D}^+} = v_{\parallel \mathrm{D}^+} \sin\alpha$, since we neglect $v_{y,E\times B} \cos\alpha = \partial_x \phi \cos\alpha$, to obtain the boundary condition for $v_{\parallel \mathrm{D}^+}$ at the limiter,

$$v_{\parallel \mathrm{D}^+} = \pm\sqrt{T_\mathrm{e} F_\mathrm{T}}. \tag{50}$$

The expressions of the boundary conditions for the other plasma quantities then follow. In fact, equation (42) can be inverted to express $\partial_s \phi$ in terms of $\partial_s v_{\parallel \mathrm{D}^+}$, which yields

$$\partial_s \phi = -\frac{v'_{s\mathrm{D}^+} \partial_s v_{\parallel \mathrm{D}^+}}{F_\mathrm{T} \sin\alpha} = \mp \frac{\sqrt{T_\mathrm{e}}}{\sqrt{F_\mathrm{T}}} \partial_s v_{\parallel \mathrm{D}^+}. \tag{51}$$

We then use equation (44) to express $\partial_s n_\mathrm{e}$ in terms of $\partial_s \phi$, that is

$$\partial_s n_\mathrm{e} = \frac{n_\mathrm{e}}{T_\mathrm{e}} \partial_s \phi = \mp \frac{n_\mathrm{e}}{\sqrt{T_\mathrm{e} F_\mathrm{T}}} \partial_s v_{\parallel \mathrm{D}^+} \tag{52}$$

and, making use of $n_{\mathrm{D}^+} = n_\mathrm{e}$, we also obtain

$$\partial_s n_{\mathrm{D}^+} = n_\mathrm{e}/T_\mathrm{e} \partial_s \phi = \mp \frac{n_\mathrm{e}}{\sqrt{T_\mathrm{e} F_\mathrm{T}}} \partial_s v_{\parallel \mathrm{D}^+}. \tag{53}$$

Regarding the density of the D_2^+ ions, we use equation (41), deriving the following boundary condition

$$\partial_s n_{\mathrm{D}_2^+} = \mp n_{\mathrm{D}_2^+} / \sqrt{T_\mathrm{e} F_\mathrm{T}} \partial_s v_{\parallel \mathrm{D}^+}. \tag{54}$$

In order to derive the boundary conditions for T_e, T_{D^+} and $T_{\mathrm{D}_2^+}$, we notice that temperature gradients along the direction perpendicular to the wall are small compared to the gradients of the other physical quantities. In fact, [57, 58] show that $\partial_s T_\mathrm{e} \sim \partial_s T_{\mathrm{D}^+} \simeq 0.1 \partial_s \phi$. In the present work, we follow this prescription and assume $\partial_s T_\mathrm{e} = \partial_s T_{\mathrm{D}^+} = \partial_s T_{\mathrm{D}_2^+} = 0.1 \partial_s \phi$ (we note that our tests show that imposing $\partial_s T_\mathrm{e} = \partial_s T_{\mathrm{D}^+} = \partial_s T_{\mathrm{D}_2^+} = 0$ does not affect the simulation results noticeably).

To obtain the boundary condition for Ω at the MP entrance, we start from its defin-

ition, $\Omega = \nabla\cdot\left[(n_{\mathrm{D}^+}/B^2)\nabla_\perp\phi + (1/B^2)\nabla_\perp p_{\mathrm{D}^+}\right] + \nabla\cdot\left[(n_{\mathrm{D}_2^+}/B^2)\nabla_\perp\phi + (1/B^2)\nabla_\perp p_{\mathrm{D}_2^+}\right]$. We write the second order derivatives in the directions perpendicular to the magnetic field retaining only derivatives along the y direction, since $\partial_x^2 \ll \partial_y^2$. Since $\partial_y B = 0$ at the limiter, the $1/B^2$ factor can be considered constant when the derivatives defining Ω are evaluated. We then write the derivatives along the y direction in terms of derivatives along s and consider $T_{\mathrm{D}_2^+} = T_{\mathrm{D}^+}$ (for simplicity). This yields

$$\Omega = -\cos\alpha\left[\partial_s(n_\mathrm{e} + n_{\mathrm{D}_2^+})\partial_s\phi + T_{\mathrm{D}^+}\partial_s^2(n_\mathrm{e} + n_{\mathrm{D}_2^+}) + (n_\mathrm{e} + n_{\mathrm{D}_2^+})\partial_s^2\phi\right]. \tag{55}$$

We now take advantage of equations (52) and (54) to express $\partial_s n_\mathrm{e}$ and $\partial_s n_{\mathrm{D}^+}$ in terms of $\partial_s\phi$ and use equation (51) to obtain the final expression of the boundary condition for Ω, that is

$$\Omega = -(n_\mathrm{e} + n_{\mathrm{D}_2^+})F_\mathrm{T}\cos^2\alpha\left[\pm\frac{\sqrt{T_\mathrm{e}}}{\sqrt{F_\mathrm{T}}}\partial_s^2 v_{\parallel\mathrm{D}^+} \mp \frac{1}{\sqrt{T_\mathrm{e}}F_T}(\partial_s v_{\parallel\mathrm{D}^+})^2\right]. \tag{56}$$

Finally, the boundary condition for the electron parallel velocity is obtained from the analysis of the electron kinetic distribution function at the MP entrance. As discussed in reference [57], this gives

$$v_{\parallel\mathrm{e}} = \sqrt{T_\mathrm{e}}\left[\pm\exp\left(\Lambda - \frac{\phi}{T_\mathrm{e}}\right)\right], \tag{57}$$

where $\Lambda = \log\left[\sqrt{(1/2\pi)(m_\mathrm{i}/m_\mathrm{e})}\right] \simeq 3$.

At the vessel outer wall and the core interface, ad hoc boundary conditions are considered, similarly to the approach used in previous models of GBS [23, 57, 58]. In fact, a set of first-principles boundary conditions is yet to be derived for such boundaries. The impact of these ad hoc boundary conditions upon the simulation results is controlled by extending radially the simulation domain towards the wall and the core. The conditions we impose include homogeneous Neumann boundary conditions to n_e, n_{D^+}, T_e, T_{D^+}, $T_{\mathrm{D}_2^+}$, $v_{\parallel\mathrm{e}}$, $v_{\parallel\mathrm{D}^+}$ and $v_{\parallel\mathrm{D}_2^+}$. Since the density of D_2^+ ions is expected to be very low at the core–edge interface (no particles outflowing from the core), we use Dirichlet boundary conditions at the core interface for $n_{\mathrm{D}_2^+}$, setting it to a residual value, while homogeneous Neumann boundary conditions are considered at the vessel outer wall. We also use Dirichlet boundary conditions for the vorticity, setting $\Omega = 0$ at both the wall and the core interface. Regarding the ϕ boundary conditions, we follow the approach presented in reference [60], where $\phi = \Lambda T_\mathrm{e}$ is considered at the vessel wall. Finally, $\phi = \phi_0$ is considered at the core interface, where ϕ_0 is a constant value chosen to prevent large gradients of ϕ.

5. The kinetic model for the neutral species and its formal solution

In order to compute the neutral distribution functions of D and D_2, f_D and f_{D_2}, we consider a set of two coupled kinetic equations, that is

$$\begin{aligned}\frac{\partial f_\mathrm{D}}{\partial t} + \mathbf{v}\cdot\frac{\partial f_\mathrm{D}}{\partial \mathbf{x}} = &-\nu_{\mathrm{iz,D}} f_\mathrm{D} - \nu_{\mathrm{cx,D}}\left(f_\mathrm{D} - \frac{n_\mathrm{D}}{n_{\mathrm{D}^+}}f_{\mathrm{D}^+}\right) \\ &+ \nu_{\mathrm{rec,D}^+} f_{\mathrm{D}^+} + \nu_{\mathrm{cx,D_2-D^+}}\left(\frac{n_{\mathrm{D}_2}}{n_{\mathrm{D}^+}}f_{\mathrm{D}^+}\right) \\ &- \nu_{\mathrm{cx,D-D_2^+}} f_\mathrm{D} + 2\nu_{\mathrm{diss,D_2}} f_{\mathrm{D}_2} \\ &+ \nu_{\mathrm{diss-iz,D_2}} f_{\mathrm{D}_2} + \nu_{\mathrm{diss,D_2^+}} f_{\mathrm{D}_2^+} \\ &+ 2\nu_{\mathrm{diss-rec,D_2^+}} f_{\mathrm{D}_2^+},\end{aligned} \tag{58}$$

and

$$\begin{aligned}\frac{\partial f_{\mathrm{D}_2}}{\partial t} + \mathbf{v}\cdot\frac{\partial f_{\mathrm{D}_2}}{\partial \mathbf{x}} = &-\nu_{\mathrm{iz,D_2}} f_{\mathrm{D}_2} - \nu_{\mathrm{cx,D_2}}\left(f_{\mathrm{D}_2} - \frac{n_{\mathrm{D}_2}}{n_{\mathrm{D}_2^+}}f_{\mathrm{D}_2^+}\right) \\ &+ \nu_{\mathrm{rec,D_2^+}} f_{\mathrm{D}_2^+} - \nu_{\mathrm{cx,D_2-D^+}} f_{\mathrm{D}_2} \\ &+ \nu_{\mathrm{cx,D-D_2^+}}\left(\frac{n_\mathrm{D}}{n_{\mathrm{D}_2^+}}f_{\mathrm{D}_2^+}\right) \\ &- \nu_{\mathrm{diss,D_2}} f_{\mathrm{D}_2} - \nu_{\mathrm{diss-iz,D_2}} f_{\mathrm{D}_2}.\end{aligned} \tag{59}$$

We highlight that collisions between neutral particles are not considered in the present model, since they are not expected to play an important role in the boundary dynamics except in detachment conditions. This comes from the fact that the densities of both neutral species, n_D and n_{D_2}, are smaller than the density of the D^+ ions by one or two orders of magnitude, except in detachment.

The formal solution of equations (58) and (59) can be obtained by using the method of characteristics, assuming that the plasma quantities are known. This yields

$$\begin{aligned}f_\mathrm{D}(\mathbf{x},\mathbf{v},t) = \int_0^{r'_\mathrm{b}} &\left[\frac{S_\mathrm{D}(\mathbf{x}',\mathbf{v},t')}{v} + \delta\left(r' - r'_\mathrm{b}\right) f_\mathrm{D}(\mathbf{x}'_\mathrm{b},\mathbf{v},t'_\mathrm{b})\right] \\ &\times \exp\left[-\frac{1}{v}\int_0^{r'}\nu_{\mathrm{eff_D}}(\mathbf{x}'',t'')\mathrm{d}r''\right]\frac{J(\mathbf{x}')}{J(\mathbf{x})}\mathrm{d}r'\end{aligned} \tag{60}$$

and

$$\begin{aligned}f_{\mathrm{D}_2}(\mathbf{x},\mathbf{v},t) = \int_0^{r'_\mathrm{b}} &\left[\frac{S_{\mathrm{D}_2}(\mathbf{x}',\mathbf{v},t')}{v} \right. \\ &\left. + \delta\left(r' - r'_\mathrm{b}\right) f_{\mathrm{D}_2}(\mathbf{x}'_\mathrm{b},\mathbf{v},t'_\mathrm{b})\right] \\ &\times \exp\left[-\frac{1}{v}\int_0^{r'}\nu_{\mathrm{eff_{D_2}}}(\mathbf{x}'',t'')\mathrm{d}r''\right]\frac{J(\mathbf{x}')}{J(\mathbf{x})}\mathrm{d}r'.\end{aligned} \tag{61}$$

The solutions presented in equations (60) and (61) show that the distribution functions of D and D_2 at position $\mathbf{x}$, velocity $\mathbf{v}$ and time t result from the neutrals generated at a location $\mathbf{x}' = \mathbf{x} - r'\boldsymbol{\Omega}$, in the plasma volume or at the boundary, and

at time $t' = t - r'/v$, with $\mathbf{\Omega} = \mathbf{v}/v$ the unit vector aligned with the neutral velocity and r' the distance measured from $\mathbf{x}'$ to $\mathbf{x}$ (the subscript 'b' denotes the intersection point between the domain boundary and the characteristic starting at $\mathbf{x}$ with direction $\mathbf{\Omega}$). Since the neutrals are solved on the (R, Z) coordinate system, with R the distance from the torus axis and Z the vertical coordinate measured from the equatorial midplane, the integral includes the Jacobian corresponding to the coordinate system $J(\mathbf{x}) = R(\mathbf{x})$. The volumetric source due to the collisional processes in equation (60) is

$$\begin{aligned} S_{\mathrm{D}}(\mathbf{x}', \mathbf{v}, t') = {} & \nu_{\mathrm{cx,D}}(\mathbf{x}', t') n_{\mathrm{D}}(\mathbf{x}', t') \Phi_{\left[\mathbf{v}_{\mathrm{D}^+}, T_{\mathrm{D}^+}\right]}(\mathbf{x}', \mathbf{v}, t') \\ & + \nu_{\mathrm{cx,D_2-D^+}}(\mathbf{x}', t') n_{\mathrm{D_2}}(\mathbf{x}', t') \\ & \times \Phi_{\left[\mathbf{v}_{\mathrm{D}^+}, T_{\mathrm{D}^+}\right]}(\mathbf{x}', \mathbf{v}, t') + \nu_{\mathrm{rec,D^+}}(\mathbf{x}', t') n_{\mathrm{D^+}} \\ & \times (\mathbf{x}', \mathbf{v}, t') \Phi_{\left[\mathbf{v}_{\mathrm{D}^+}, T_{\mathrm{D}^+}\right]}(\mathbf{x}', \mathbf{v}, t') \\ & + 2\nu_{\mathrm{diss,D_2}}(\mathbf{x}', t') n_{\mathrm{D_2}}(\mathbf{x}', t') \\ & \times \Phi_{\left[\mathbf{v}_{\mathrm{D_2}}, T_{\mathrm{D,diss(D_2)}}\right]}(\mathbf{x}', \mathbf{v}, t') \\ & + \nu_{\mathrm{diss-iz,D_2}}(\mathbf{x}', t') n_{\mathrm{D_2}}(\mathbf{x}', t') \\ & \times \Phi_{\left[\mathbf{v}_{\mathrm{D_2}}, T_{\mathrm{D,diss-iz(D_2)}}\right]}(\mathbf{x}', \mathbf{v}, t') \\ & + \nu_{\mathrm{diss,D_2^+}}(\mathbf{x}', t') n_{\mathrm{D_2^+}}(\mathbf{x}', \mathbf{v}, t') \\ & \times \Phi_{\left[\mathbf{v}_{\mathrm{D_2^+}}, T_{\mathrm{D,diss}\left(D_2^+\right)}\right]}(\mathbf{x}', \mathbf{v}, t') \\ & + 2\nu_{\mathrm{diss-rec,D_2^+}}(\mathbf{x}', t') n_{\mathrm{D_2^+}}(\mathbf{x}', \mathbf{v}, t') \\ & \times \Phi_{\left[\mathbf{v}_{\mathrm{D_2^+}}, T_{\mathrm{D,diss-rec}\left(D_2^+\right)}\right]}(\mathbf{x}', \mathbf{v}, t') \end{aligned} \tag{62}$$

since D ions can be generated in the plasma volume by D–$\mathrm{D^+}$ and $\mathrm{D_2}$–$\mathrm{D^+}$ charge-exchange interactions, recombination of $\mathrm{D^+}$ ions with electrons, dissociation of $\mathrm{D_2}$ molecules into two D atoms, dissociative ionization of $\mathrm{D_2}$ into D and $\mathrm{D^+}$, dissociation of $\mathrm{D_2^+}$ ions into D and $\mathrm{D^+}$, and dissociative recombination of $\mathrm{D_2^+}$ into two D atoms.

Similarly, $\mathrm{D_2}$ molecules can be generated in the plasma by $\mathrm{D_2}$–$\mathrm{D_2^+}$ and D–$\mathrm{D_2^+}$ charge-exchange interactions or recombination of $\mathrm{D_2^+}$ ions with electrons. Therefore, the volumetric source term in equation (61) is

$$\begin{aligned} S_{\mathrm{D_2}}(\mathbf{x}', \mathbf{v}, t') = {} & \nu_{\mathrm{cx,D_2}}(\mathbf{x}', t') n_{\mathrm{D_2}}(\mathbf{x}', t') \\ & \times \Phi_{\left[\mathbf{v}_{\mathrm{D_2^+}}, T_{\mathrm{D_2^+}}\right]}(\mathbf{x}', \mathbf{v}, t') \\ & + \nu_{\mathrm{rec,D_2^+}}(\mathbf{x}', t') n_{\mathrm{D_2^+}}(\mathbf{x}', \mathbf{v}, t') \\ & \times \Phi_{\left[\mathbf{v}_{\mathrm{D_2^+}}, T_{\mathrm{D_2^+}}\right]}(\mathbf{x}', \mathbf{v}, t') \\ & + \nu_{\mathrm{cx,D-D_2^+}}(\mathbf{x}', t') n_{\mathrm{D}}(\mathbf{x}', t') \\ & \times \Phi_{\left[\mathbf{v}_{\mathrm{D_2^+}}, T_{\mathrm{D_2^+}}\right]}(\mathbf{x}', \mathbf{v}, t'). \end{aligned} \tag{63}$$

We remark that $\Phi_{\left[\mathbf{v}_{\mathrm{D}^+}, T_{\mathrm{D}^+}\right]}(\mathbf{x}', \mathbf{v}, t') = \left[m_{\mathrm{D}^+}/(2\pi T_{\mathrm{D}^+})\right]^{3/2} \exp\left[-m_{\mathrm{D}^+}(\mathbf{v} - \mathbf{v}_{\mathrm{D}^+})^2/(2T_{\mathrm{D}^+})\right]$ is a Maxwellian distribution function describing the $\mathrm{D^+}$ ion population, centered at the ion velocity $\mathbf{v}_{\mathrm{D}^+}(\mathbf{x}', t')$, which includes only the leading order components, i.e. $\mathbf{v}_{\mathrm{D}^+} = v_{\parallel \mathrm{D}^+}\mathbf{b} + \mathbf{v}_{\perp \mathrm{D}^+ 0}$, and based on the $\mathrm{D^+}$ temperature, $\mathbf{T}_{\mathrm{D}^+}(\mathbf{x}', t')$. Similarly, $\Phi_{\left[\mathbf{v}_{\mathrm{D_2^+}}, T_{\mathrm{D_2^+}}\right]}(\mathbf{x}', \mathbf{v}, t')$ is a Maxwellian distribution that describes the $\mathrm{D_2^+}$ ions and is defined analogously. We remark that, when evaluating the average velocity of the Maxwellian distributions describing neutrals generated from $\mathrm{D_2}$ and $\mathrm{D_2^+}$, we assume that $\mathbf{v}_{\mathrm{D_2}}$ and $\mathbf{v}_{\mathrm{D_2^+}}$ can be neglected, i.e. $|\mathbf{v}_{\mathrm{D_2}}| \lesssim |\mathbf{v}_{\mathrm{D}^+}|$ and $|\mathbf{v}_{\mathrm{D_2^+}}| \lesssim |\mathbf{v}_{\mathrm{D}^+}|$. Regarding the dissociative processes, we recall that the temperature $T_{\mathrm{D,diss(D_2)}}$ is the average thermal energy of D atoms generated by dissociation of $\mathrm{D_2}$, presented in table 2 and calculated in appendix A. The energy of the neutral D atoms generated by other dissociative processes is evaluated using a similar approach.

The effective frequencies for depletion of neutral particles are given by

$$\nu_{\mathrm{eff,D}}(\mathbf{x}'', t'') = \nu_{\mathrm{iz,D}}(\mathbf{x}'', t'') + \nu_{\mathrm{cx,D}}(\mathbf{x}'', t'') + \nu_{\mathrm{cx,D-D_2^+}}(\mathbf{x}'', t'') \tag{64}$$

and

$$\begin{aligned} \nu_{\mathrm{eff,D_2}}(\mathbf{x}'', t'') = {} & \nu_{\mathrm{iz,D_2}}(\mathbf{x}'', t'') + \nu_{\mathrm{cx,D_2}}(\mathbf{x}'', t'') \\ & + \nu_{\mathrm{cx,D_2-D^+}}(\mathbf{x}'', t'') + \nu_{\mathrm{diss,D_2}}(\mathbf{x}'', t'') \\ & + \nu_{\mathrm{diss-iz,D_2}}(\mathbf{x}'', t''), \end{aligned} \tag{65}$$

since the volumetric sinks of D atoms are due to ionization or charge-exchange with $\mathrm{D^+}$ or $\mathrm{D_2^+}$, while $\mathrm{D_2}$ are depleted by ionization, charge-exchange with $\mathrm{D_2^+}$ or $\mathrm{D^+}$, dissociation or dissociative ionization.

A contribution to the neutral distribution functions in equations (60) and (61) is related to the neutral recycling at the boundary walls. Therefore, we now focus on the neutral processes that take place there. A fraction, $\alpha_{\mathrm{refl}}(\mathbf{x}'_{\mathbf{b}})$, of the $\mathrm{D_2^+}$ ions that reach the boundary walls, after recombination with electrons and formation of $\mathrm{D_2}$ neutrals is reflected back into the plasma. The remaining fraction, $1 - \alpha_{\mathrm{refl}}(\mathbf{x}'_{\mathbf{b}})$, is absorbed and reemitted at wall temperature as $\mathrm{D_2}$, also following a recombination process. Analogous considerations hold when describing $\mathrm{D_2}$ neutrals that reach the boundary. The $\mathrm{D_2}$ molecules can, in fact, be reflected or reemitted with the same probability as $\mathrm{D_2^+}$.

Regarding the atomic species, since the wall temperature is low, a fraction, β_{assoc}, of the $\mathrm{D^+}$ and D particles absorbed at the walls associate and are reemitted back into the plasma as $\mathrm{D_2}$ molecules. The $\mathrm{D^+}$ ions and D neutrals reaching the boundaries that do not associate undergo reflection and reemission processes similar to the ones described for $\mathrm{D_2^+}$ ions and $\mathrm{D_2}$ particles, the probability of reflection, $\alpha_{\mathrm{refl}}(\mathbf{x}'_{\mathbf{b}})$, being the same. As a consequence, the distribution functions at the vessel, $f_{\mathrm{D}}(\mathbf{x}'_{\mathrm{b}}, \mathbf{v}, t')$ and $f_{\mathrm{D_2}}(\mathbf{x}'_{\mathrm{b}}, \mathbf{v}, t')$, for $v_p = \mathbf{v} \cdot \hat{\mathbf{n}} > 0$ (with $\hat{\mathbf{n}}$ the unit vector normal to the boundary) yield

$$f_{\mathrm{D}}(\mathbf{x}_{\mathbf{b}}',\mathbf{v},t') = (1-\alpha_{\mathrm{refl}}(\mathbf{x}_{\mathbf{b}}'))\Gamma_{\mathrm{reem,D}}(\mathbf{x}_{\mathbf{b}}',t')\chi_{\mathrm{in,D}}(\mathbf{x}_{\mathbf{b}}',\mathbf{v}) + \alpha_{\mathrm{refl}}(\mathbf{x}_{\mathbf{b}}')\left[f_{\mathrm{out,D}}(\mathbf{x}_{\mathbf{b}}',\mathbf{v}-2\mathbf{v}_{\mathbf{p}},t') + \frac{\Gamma_{\mathrm{out,D^+}}(\mathbf{x}_{\mathbf{b}}',t')}{v_p}\Phi_{\left[\mathbf{v}_{\mathrm{refl}\left(\mathrm{D^+}\right)},T_{\mathrm{D^+}}\right]}(\mathbf{x}_{\mathbf{b}}',\mathbf{v},t')\right] \quad (66)$$

and

$$f_{\mathrm{D_2}}(\mathbf{x}_{\mathrm{b}}',\mathbf{v},t') = (1-\alpha_{\mathrm{refl}}(\mathbf{x}_{\mathbf{b}}'))\Gamma_{\mathrm{reem,D_2}}(\mathbf{x}_{\mathbf{b}}',t')\chi_{\mathrm{in,D_2}}(\mathbf{x}_{\mathbf{b}}',\mathbf{v}) + \alpha_{\mathrm{refl}}(\mathbf{x}_{\mathbf{b}}')\left[f_{\mathrm{out,D_2}}(\mathbf{x}_{\mathbf{b}}',\mathbf{v}-2\mathbf{v}_{\mathbf{p}},t') + \frac{\Gamma_{\mathrm{out,D_2^+}}(\mathbf{x}_{\mathbf{b}}',t')}{v_p}\Phi_{\left[\mathbf{v}_{\mathrm{refl}\left(\mathrm{D_2^+}\right)},T_{\mathrm{D_2^+}}\right]}(\mathbf{x}_{\mathbf{b}}',\mathbf{v},t')\right]. \quad (67)$$

We first analyze the contributions of reflected particles in equations (66) and (67). The reflected D and D_2 are described by the distribution functions $f_{\mathrm{out,D}}(\mathbf{x}_{\mathbf{b}}',\mathbf{v}-2\mathbf{v}_{\mathbf{p}},t')$ and $f_{\mathrm{out,D_2}}(\mathbf{x}_{\mathbf{b}}',\mathbf{v}-2\mathbf{v}_{\mathbf{p}},t')$, since $\mathbf{v}-2\mathbf{v}_{\mathbf{p}}$ is the velocity of the reflected neutrals as they flow towards the wall, with $\mathbf{v}_{\mathbf{p}} = v_p\hat{\mathbf{n}}$ the velocity along the direction normal to the wall surface. On the other hand, the contribution from the reflected D^+ and D_2^+ is modelled by considering the projection of the flux of outflowing D^+ and D_2^+ along the direction normal to the boundary surface, given respectively by $\Gamma_{\mathrm{out,D^+}}(\mathbf{x}_{\mathbf{b}}') = -\mathbf{\Gamma}_{\mathrm{out,D^+}}(\mathbf{x}_{\mathbf{b}}')\cdot\hat{\mathbf{n}}$ and $\Gamma_{\mathrm{out,D_2^+}}(\mathbf{x}_{\mathbf{b}}') = -\mathbf{\Gamma}_{\mathrm{out,D_2^+}}(\mathbf{x}_{\mathbf{b}}')\cdot\hat{\mathbf{n}}$. These fluxes include the contributions of the plasma parallel flow and the leading order perpendicular drifts, i.e. the $E\times B$ and diamagnetic drifts, yielding

$$\mathbf{\Gamma}_{\mathrm{out,D^+}}(\mathbf{x}_{\mathbf{b}}') = n_{\mathrm{D^+}}v_{\parallel\mathrm{D^+}}\mathbf{b} + n_{\mathrm{D^+}}\mathbf{v}_{\perp\mathrm{D^+}0} \quad (68)$$

and

$$\mathbf{\Gamma}_{\mathrm{out,D_2^+}}(\mathbf{x}_{\mathbf{b}}') = n_{\mathrm{D_2^+}}v_{\parallel\mathrm{D_2^+}}\mathbf{b} + n_{\mathrm{D_2^+}}\mathbf{v}_{\perp\mathrm{D_2^+}0}. \quad (69)$$

We assume that the velocity distribution of the D neutrals generated by reflection of D^+ ions is described by a Maxwellian centered at the velocity, $\mathbf{v}_{\mathrm{refl}(\mathrm{D^+})} = \mathbf{v}_{\mathrm{D^+}} - 2\mathbf{v}_{\mathbf{p}_{\mathrm{D^+}}}$, with $\mathbf{v}_{\mathbf{p}_{\mathrm{D^+}}} = \left(\mathbf{v}_{\mathrm{D^+}}\cdot\hat{\mathbf{n}}\right)\hat{\mathbf{n}}$, and with temperature of the incoming D^+ ions, $T_{\mathrm{D^+}}$, given by $\Phi_{\left[\mathbf{v}_{\mathrm{refl}(\mathrm{D^+})},T_{\mathrm{D^+}}\right]}(\mathbf{x}',\mathbf{v},t')$. Analogously, the D_2 neutrals generated by reflection of D_2^+ ions are described by a Maxwellian distribution of velocities, $\Phi_{\left[\mathbf{v}_{\mathrm{refl}\left(\mathrm{D_2^+}\right)},T_{\mathrm{D^+}}\right]}(\mathbf{x}',\mathbf{v},t')$, being $\mathbf{v}_{\mathrm{refl}\left(\mathrm{D_2^+}\right)} = \mathbf{v}_{\mathrm{D_2^+}} - 2\mathbf{v}_{\mathbf{p}_{\mathrm{D_2^+}}}$, with $\mathbf{v}_{\mathbf{p}_{\mathrm{D_2^+}}} = \left(\mathbf{v}_{\mathrm{D_2^+}}\cdot\hat{\mathbf{n}}\right)\hat{\mathbf{n}}$ and $T_{\mathrm{D_2^+}}$ the temperature of the incoming D_2^+ ions.

We now focus on the contributions in equations (66) and (67) accounting for reemission of neutrals from the boundary. These are written in terms of

$$\Gamma_{\mathrm{reem,D}}(\mathbf{x}_{\mathbf{b}}') = (1-\beta_{\mathrm{assoc}})\left[\Gamma_{\mathrm{out,D}}(\mathbf{x}_{\mathbf{b}}') + \Gamma_{\mathrm{out,D^+}}(\mathbf{x}_{\mathbf{b}}')\right] \quad (70)$$

and

$$\Gamma_{\mathrm{reem,D_2}}(\mathbf{x}_{\mathbf{b}}') = \Gamma_{\mathrm{out,D_2}}(\mathbf{x}_{\mathbf{b}}') + \Gamma_{\mathrm{out,D_2^+}}(\mathbf{x}_{\mathbf{b}}') + \frac{\beta_{\mathrm{assoc}}}{2}\left[\Gamma_{\mathrm{out,D}}(\mathbf{x}_{\mathbf{b}}') + \Gamma_{\mathrm{out,D^+}}(\mathbf{x}_{\mathbf{b}}')\right]. \quad (71)$$

In addition to the projections of the boundary ion fluxes, $\Gamma_{\mathrm{out,D_2^+}}$ and $\Gamma_{\mathrm{out,D_2^+}}$, equations (70) and (71) take into account the projections along the direction normal to the boundary of the fluxes of D and D_2 outflowing to the limiter and walls, $\Gamma_{\mathrm{out,D}}$ and $\Gamma_{\mathrm{out,D_2}}$. These are defined based on the neutral fluxes directed towards the boundary (i.e. for $v_{\mathrm{p}} < 0$) as

$$\Gamma_{\mathrm{out,D}}(\mathbf{x}_{\mathbf{b}}') = -\int_{v_{\mathrm{p}}<0}\left(\mathbf{v}_{\mathbf{p}}\cdot\mathbf{n}\right)f_{\mathrm{D}}(\mathbf{x}_{\mathbf{b}}',\mathbf{v})\mathrm{d}\mathbf{v} \quad (72)$$

and

$$\Gamma_{\mathrm{out,D_2}}(\mathbf{x}_{\mathbf{b}}') = -\int_{v_{\mathrm{p}}<0}\left(\mathbf{v}_{\mathbf{p}}\cdot\mathbf{n}\right)f_{\mathrm{D_2}}(\mathbf{x}_{\mathbf{b}}',\mathbf{v})\mathrm{d}\mathbf{v}. \quad (73)$$

We assume that the velocity distribution of reemitted particles follows the Knudsen cosine law for a given wall temperature, T_{w}. This yields, for the D neutrals,

$$\chi_{\mathrm{in,D}}(\mathbf{x}_{\mathbf{b}}',\mathbf{v}) = \frac{3}{4\pi}\frac{m_{\mathrm{D}}^2}{T_{\mathrm{w}}^2}\cos(\theta)\exp\left(-\frac{m_{\mathrm{D}}v^2}{2T_{\mathrm{w}}}\right), \quad (74)$$

while the expression for D_2 molecules is analogously given by

$$\chi_{\mathrm{in,D_2}}(\mathbf{x}_{\mathbf{b}}',\mathbf{v}) = \frac{3}{4\pi}\frac{m_{\mathrm{D_2}}^2}{T_{\mathrm{w}}^2}\cos(\theta)\exp\left(-\frac{m_{\mathrm{D_2}}v^2}{2T_{\mathrm{w}}}\right). \quad (75)$$

We now follow the same approach described in reference [37] to obtain a set of time-independent two-dimensional integral equations for the D and D_2 densities, making the numerical implementation of the formal solution in equations (60) and (61) feasible. More precisely, we first make use of the fact that the neutral time of flight is typically shorter than the characteristic timescales of turbulence, $\tau_{\mathrm{n}} \ll \tau_{\mathrm{turb}}$, a condition that we denote as the neutral adiabatic regime. This allows us to approximate $t' = t$ in equations (60)–(67) or, equivalently, $\partial_t f_{\mathrm{D}} = 0$ and $\partial_t f_{\mathrm{D_2}} = 0$ in equations (58) and (59). Second, we note that the neutral mean free path is typically smaller than the characteristic elongation of turbulence structures along the magnetic field, $\lambda_{\mathrm{mfp,n}}k_{\parallel} \ll 1$. Therefore, our description of neutral motion is reduced to the analysis of a set of independent two-dimensional planes perpendicular to the magnetic field, approximately coincident with the poloidal planes. Then, integrating equations (60) and (61) over the velocity space, a system of two coupled equations for the densities of D and D_2 is obtained,

$$n_{\mathrm{D}}(\mathbf{x}_{\perp}) = \int_{\mathrm{D}}\mathrm{d}A'\frac{1}{r_{\perp}'}\int_0^{\infty}\mathrm{d}v_{\perp}\,v_{\perp}\int_0^{\infty}\mathrm{d}v_{\parallel}\left\{\frac{S_D(\mathbf{x}_{\perp}',\mathbf{v})}{v_{\perp}}\exp\left[-\frac{1}{v_{\perp}}\int_0^{r_{\perp}'}\nu_{\mathrm{eff,D}}(\mathbf{x}_{\perp}'')\mathrm{d}r_{\perp}''\right]\right\} + \int_{\partial\mathrm{D}}\mathrm{d}a_{\mathrm{b}}'\frac{\cos\theta'}{r_{\perp\mathrm{b}}'}\int_0^{\infty}\mathrm{d}v_{\perp}\,v_{\perp}\int_0^{\infty} \quad (76)$$

$$\times \mathrm{d}v_{\parallel}\left\{f_{\mathrm{D}}(\mathbf{x}'_{\perp\mathbf{b}},\mathbf{v})\exp\left[-\frac{1}{v_{\perp}}\int_0^{r'_{\perp}}\nu_{\mathrm{eff,D}}(\mathbf{x}''_{\perp})\mathrm{d}r''_{\perp}\right]\right\},$$

and

$$\begin{aligned}n_{\mathrm{D_2}}(\mathbf{x}_{\perp}) = &\int_{\mathrm{D}}\mathrm{d}A'\frac{1}{r'_{\perp}}\int_0^{\infty}\mathrm{d}v_{\perp}\,v_{\perp}\int_0^{\infty}\\ &\times\mathrm{d}v_{\parallel}\left\{\frac{S_{\mathrm{D_2}}(\mathbf{x}'_{\perp},\mathbf{v})}{v_{\perp}}\exp\left[-\frac{1}{v_{\perp}}\int_0^{r'_{\perp}}\nu_{\mathrm{eff,D_2}}(\mathbf{x}''_{\perp})\mathrm{d}r''_{\perp}\right]\right\}\\ &+\int_{\partial\mathrm{D}}\mathrm{d}a'_{\mathrm{b}}\frac{\cos\theta'}{r'_{\perp\mathrm{b}}}\int_0^{\infty}\mathrm{d}v_{\perp}\,v_{\perp}\int_0^{\infty}\\ &\times\mathrm{d}v_{\parallel}\left\{f_{\mathrm{D_2}}(\mathbf{x}'_{\perp\mathbf{b}},\mathbf{v})\exp\left[-\frac{1}{v_{\perp}}\int_0^{r'_{\perp}}\nu_{\mathrm{eff,D_2}}(\mathbf{x}''_{\perp})\mathrm{d}r''_{\perp}\right]\right\}\end{aligned}, \tag{77}$$

where the same geometrical arguments presented in reference [37] is used when considering the integral along the neutral path and the integral along the perpendicular velocity angle, that is

$$\int_0^{r_{\perp,\mathrm{b}}}\mathrm{d}r'_{\perp}\int_0^{2\pi}\mathrm{d}\vartheta\,F(\mathbf{x}_{\perp},\mathbf{x}'_{\perp}) = \int_{\mathrm{D}}\mathrm{d}A'\frac{1}{r'_{\perp}}F(\mathbf{x}_{\perp},\mathbf{x}'_{\perp}), \tag{78}$$

where $\mathrm{d}A'$ is the area element in the 2D poloidal plane and $F(\mathbf{x}_{\perp},\mathbf{x}'_{\perp})$ is a generic function. In addition, we use

$$\begin{aligned}&\int_0^{r_{\perp,\mathrm{b}}}\mathrm{d}r'_{\perp}\int_0^{2\pi}\mathrm{d}\vartheta\,\delta(r'_{\perp}-r'_{\perp\mathrm{b}})F(\mathbf{x}_{\perp},\mathbf{x}'_{\perp})\\ &\quad=\int_{\partial\mathrm{D}}\mathrm{d}a'_{\mathrm{b}}\frac{\cos\theta'}{r'_{\perp\mathrm{b}}}F(\mathbf{x}_{\perp},\mathbf{x}'_{\perp\mathrm{b}}),\end{aligned} \tag{79}$$

with $\mathrm{d}a'_{\mathrm{b}}$ being a line element along the boundary of D, denoted as $\partial\mathrm{D}$, and $\theta' = \arccos(\boldsymbol{\Omega}_{\perp}\cdot\hat{\mathbf{n}})$.

We now express the volumetric source terms appearing in equations (62) and (63), $S_{\mathrm{D}}(\mathbf{x}',\mathbf{v})$ and $S_{\mathrm{D_2}}(\mathbf{x}',\mathbf{v})$, in terms of n_{D} and $n_{\mathrm{D_2}}$, and the distribution functions of the neutral species at the boundary appearing in equations (63) and (66), f_{D} and $f_{\mathrm{D_2}}$, in terms of $\Gamma_{\mathrm{out,D^+}}$, $\Gamma_{\mathrm{out,D_2^+}}$, $\Gamma_{\mathrm{out,D}}$ and $\Gamma_{\mathrm{out,D_2}}$. For $n_{\mathrm{D_2}}$, this yields

$$\begin{aligned}n_{\mathrm{D_2}}(\mathbf{x}_{\perp}) = &\int_{\mathrm{D}}n_{\mathrm{D_2}}(\mathbf{x}'_{\perp})\nu_{\mathrm{cx,D_2}}(\mathbf{x}'_{\perp})K_{\mathrm{p\to p}}^{\mathrm{D_2,D_2^+}}(\mathbf{x}_{\perp},\mathbf{x}'_{\perp})\mathrm{d}A'\\ &+\int_{\partial\mathrm{D}}(1-\alpha_{\mathrm{refl}}(\mathbf{x}'_{\perp,\mathrm{b}}))\Gamma_{\mathrm{out,D_2}}(\mathbf{x}'_{\perp,\mathrm{b}})\\ &\times K_{\mathrm{b\to p}}^{\mathrm{D_2}}(\mathbf{x}_{\perp},\mathbf{x}'_{\perp,\mathrm{b}})\mathrm{d}a'_{\mathrm{b}}\\ &+\int_{\partial\mathrm{D}}(1-\alpha_{\mathrm{refl}}(\mathbf{x}'_{\perp,\mathrm{b}}))\frac{\beta_{\mathrm{assoc}}}{2}\Gamma_{\mathrm{out,D}}(\mathbf{x}'_{\perp,\mathrm{b}})\\ &\times K_{\mathrm{b\to p}}^{\mathrm{D_2}}(\mathbf{x}_{\perp},\mathbf{x}'_{\perp,\mathrm{b}})\mathrm{d}a'_{\mathrm{b}}\\ &+\int_{\mathrm{D}}n_{\mathrm{D}}(\mathbf{x}'_{\perp})\nu_{\mathrm{cx,D-D_2^+}}(\mathbf{x}'_{\perp})K_{\mathrm{p\to p}}^{\mathrm{D_2,D_2^+}}\\ &\times(\mathbf{x}_{\perp},\mathbf{x}'_{\perp})\mathrm{d}A' + n_{\mathrm{D_2[rec(D_2^+)]}}(\mathbf{x}_{\perp})\\ &+n_{\mathrm{D_2[out(D_2^+)]}}(\mathbf{x}_{\perp})+n_{\mathrm{D_2[out(D^+)]}}(\mathbf{x}_{\perp}),\end{aligned} \tag{80}$$

while for n_{D} one has

$$\begin{aligned}n_{\mathrm{D}}(\mathbf{x}_{\perp}) = &\int_{\mathrm{D}}n_{\mathrm{D}}(\mathbf{x}'_{\perp})\nu_{\mathrm{cx,D}}(\mathbf{x}'_{\perp})K_{\mathrm{p\to p}}^{\mathrm{D,D^+}}(\mathbf{x}_{\perp},\mathbf{x}'_{\perp})\mathrm{d}A'\\ &+\int_{\mathrm{D}}n_{\mathrm{D_2}}(\mathbf{x}'_{\perp})\nu_{\mathrm{cx,D_2-D^+}}(\mathbf{x}'_{\perp})\\ &\times K_{\mathrm{p\to p}}^{\mathrm{D,D^+}}(\mathbf{x}_{\perp},\mathbf{x}'_{\perp})\mathrm{d}A'\\ &+\int_{\mathrm{D}}2n_{\mathrm{D_2}}(\mathbf{x}'_{\perp})\nu_{\mathrm{diss,D_2^+}}(\mathbf{x}'_{\perp})\\ &\times K_{\mathrm{p\to p}}^{\mathrm{D,diss}\left(\mathrm{D_2^+}\right)}(\mathbf{x}_{\perp},\mathbf{x}'_{\perp})\mathrm{d}A'\\ &+\int_{\mathrm{D}}n_{\mathrm{D_2}}(\mathbf{x}'_{\perp})\nu_{\mathrm{diss-iz,D_2^+}}(\mathbf{x}'_{\perp})\\ &\times K_{\mathrm{p\to p}}^{\mathrm{D,diss-iz}\left(\mathrm{D_2^+}\right)}(\mathbf{x}_{\perp},\mathbf{x}'_{\perp})\mathrm{d}A'\\ &+\int_{\partial\mathrm{D}}(1-\alpha_{\mathrm{refl}}(\mathbf{x}'_{\perp,\mathrm{b}}))(1-\beta_{\mathrm{assoc}})\\ &\times\Gamma_{\mathrm{out,D}}(\mathbf{x}'_{\perp,\mathrm{b}})K_{\mathrm{b\to p}}^{\mathrm{D,reem}}(\mathbf{x}_{\perp},\mathbf{x}'_{\perp,\mathrm{b}})\mathrm{d}a'_{\mathrm{b}}\\ &+n_{\mathrm{D[rec(D^+)]}}(\mathbf{x}_{\perp})+n_{\mathrm{D[out(D^+)]}}(\mathbf{x}_{\perp})\\ &+n_{\mathrm{D[diss(D_2^+)]}}(\mathbf{x}_{\perp}).\end{aligned} \tag{81}$$

Replacing v_{p} in equations (72) and (73), the normal projections of the fluxes of $\mathrm{D_2}$ and D can be written respectively as $\Gamma_{\mathrm{out,D_2}}(\mathbf{x}'_{\perp,\mathrm{b}}) = -\int_{\cos(\theta)<0}v_{\perp}\cos\theta f_{\mathrm{D_2}}(\mathbf{x}'_{\perp,\mathrm{b}},\mathbf{v}_{\perp})\mathrm{d}\mathbf{v}_{\perp}$ and $\Gamma_{\mathrm{out,D}}(\mathbf{x}'_{\perp,\mathrm{b}}) = -\int_{\cos(\theta)<0}v_{\perp}\cos\theta f_{\mathrm{D}}(\mathbf{x}'_{\perp,\mathrm{b}},\mathbf{v}_{\perp})\mathrm{d}\mathbf{v}_{\perp}$. By replacing $f_{\mathrm{D_2}}(\mathbf{x}'_{\perp,\mathrm{b}},\mathbf{v}_{\perp})$ and $f_{\mathrm{D}}(\mathbf{x}'_{\perp,\mathrm{b}},\mathbf{v}_{\perp})$ by their expressions as given in equations (66) and (67), these fluxes can be rewritten in terms of n_{D}, $n_{\mathrm{D_2}}$, $\Gamma_{\mathrm{out,D^+}}$, $\Gamma_{\mathrm{out,D_2^+}}$, $\Gamma_{\mathrm{out,D}}$ and $\Gamma_{\mathrm{out,D_2}}$ as

$$\begin{aligned}\Gamma_{\mathrm{out,D_2}}(\mathbf{x}_{\perp,\mathrm{b}}) = &\int_{\mathrm{D}}n_{\mathrm{D_2}}(\mathbf{x}'_{\perp})\nu_{\mathrm{cx,D_2}}(\mathbf{x}'_{\perp})K_{\mathrm{p\to b}}^{\mathrm{D_2,D_2^+}}(\mathbf{x}_{\perp},\mathbf{x}'_{\perp})\mathrm{d}A'\\ &+\int_{\partial\mathrm{D}}(1-\alpha_{\mathrm{refl}}(\mathbf{x}'_{\perp,\mathrm{b}}))\Gamma_{\mathrm{out,D_2}}(\mathbf{x}'_{\perp,\mathrm{b}})K_{\mathrm{b\to b}}^{\mathrm{D_2}}\\ &\times(\mathbf{x}_{\perp},\mathbf{x}'_{\perp,\mathrm{b}})\mathrm{d}a'_{\mathrm{b}}\\ &+\int_{\partial\mathrm{D}}(1-\alpha_{\mathrm{refl}}(\mathbf{x}'_{\perp,\mathrm{b}}))\frac{\beta_{\mathrm{assoc}}}{2}\Gamma_{\mathrm{out,D}}(\mathbf{x}'_{\perp,\mathrm{b}})\\ &\times K_{\mathrm{b\to b}}^{\mathrm{D_2}}(\mathbf{x}_{\perp},\mathbf{x}'_{\perp,\mathrm{b}})\mathrm{d}a'_{\mathrm{b}}\\ &+\int_{\mathrm{D}}n_{\mathrm{D}}(\mathbf{x}'_{\perp})\nu_{\mathrm{cx,D-D_2^+}}(\mathbf{x}'_{\perp})K_{\mathrm{p\to b}}^{\mathrm{D_2,D_2^+}}(\mathbf{x}_{\perp},\mathbf{x}'_{\perp})\mathrm{d}A'\\ &+\Gamma_{\mathrm{out,D_2[rec(D_2^+)]}}(\mathbf{x}_{\perp})+\Gamma_{\mathrm{out,D_2[out(D_2^+)]}}(\mathbf{x}_{\perp})\\ &+\Gamma_{\mathrm{out,D_2[out(D^+)]}}(\mathbf{x}_{\perp}),\end{aligned} \tag{82}$$

and

$$\begin{aligned}\Gamma_{\mathrm{out,D}}(\mathbf{x}_{\perp,\mathrm{b}}) = &\int_{\mathrm{D}}n_{\mathrm{D}}(\mathbf{x}'_{\perp})\nu_{\mathrm{cx,D}}(\mathbf{x}'_{\perp})K_{\mathrm{p\to b}}^{\mathrm{D,D^+}}(\mathbf{x}_{\perp},\mathbf{x}'_{\perp})\mathrm{d}A'\\ &+\int_{\mathrm{D}}n_{\mathrm{D_2}}(\mathbf{x}'_{\perp})\nu_{\mathrm{cx,D_2-D^+}}(\mathbf{x}'_{\perp})\\ &\times K_{\mathrm{p\to b}}^{\mathrm{D,D^+}}(\mathbf{x}_{\perp},\mathbf{x}'_{\perp})\mathrm{d}A'\end{aligned}$$

$$
\begin{aligned}
&+ \int_{\mathrm{D}} 2 n_{\mathrm{D}_2}(\mathbf{x}'_{\perp}) \nu_{\mathrm{diss},\mathrm{D}_2^+}(\mathbf{x}'_{\perp}) \\
&\times K_{\mathrm{p}\to\mathrm{b}}^{\mathrm{D,diss}\left(\mathrm{D}_2^+\right)}(\mathbf{x}_{\perp},\mathbf{x}'_{\perp})\mathrm{d}A' \\
&+ \int_{\mathrm{D}} n_{\mathrm{D}_2}(\mathbf{x}'_{\perp}) \nu_{\mathrm{diss-iz},\mathrm{D}_2^+}(\mathbf{x}'_{\perp}) \\
&\times K_{\mathrm{p}\to\mathrm{b}}^{\mathrm{D,diss-iz}\left(\mathrm{D}_2^+\right)}(\mathbf{x}_{\perp},\mathbf{x}'_{\perp})\mathrm{d}A' \\
&+ \int_{\partial\mathrm{D}} (1-\alpha_{\mathrm{refl}}(\mathbf{x}'_{\perp,\mathrm{b}}))(1-\beta_{\mathrm{assoc}})\Gamma_{\mathrm{out,D}}(\mathbf{x}'_{\perp,\mathrm{b}}) \\
&\times K_{\mathrm{b}\to\mathrm{b}}^{\mathrm{D,reem}}(\mathbf{x}_{\perp},\mathbf{x}'_{\perp,\mathrm{b}})\mathrm{d}a'_{\mathrm{b}} \\
&+ \Gamma_{\mathrm{D[rec(D^+)]}}(\mathbf{x}_{\perp}) + \Gamma_{\mathrm{D[out(D^+)]}}(\mathbf{x}_{\perp}) \\
&+ \Gamma_{\mathrm{D[diss}(\mathrm{D}_2^+)]}(\mathbf{x}_{\perp}). \qquad (83)
\end{aligned}
$$

We note that that the neutral particle densities and fluxes in equations (80)–(83) are multiplied by a factor $1-\alpha_{\mathrm{refl}}(\mathbf{x}'_{\perp,\mathrm{b}})$ in order to account only for the contribution of particles that are reemitted at the boundary, hence excluding reflection. Neutral reflection is included, in the definition of the kernel functions that appear in equations (76) and (77).

We now turn to the definition of the kernel functions appearing in equations (80)–(83). These are defined as integrals over velocity space. For instance, $K_{\mathrm{p}\to\mathrm{p}}^{\mathrm{D}_2,\mathrm{D}_2^+}(\mathbf{x}_{\perp},\mathbf{x}'_{\perp})$ quantifies the amount of D_2 neutrals found at a location $\mathbf{x}_{\perp}$ in the plasma volume (p) being generated from collisions involving neutralization of D_2^+ ions at a location $\mathbf{x}'_{\perp}$ inside the plasma volume (p). Its expression is given by

$$
\begin{aligned}
K_{\mathrm{p}\to\mathrm{p}}^{\mathrm{D}_2,\mathrm{D}_2^+}(\mathbf{x}_{\perp},\mathbf{x}'_{\perp}) &= K_{\mathrm{p}\to\mathrm{p,dir}}^{\mathrm{D}_2,\mathrm{D}_2^+}(\mathbf{x}_{\perp},\mathbf{x}'_{\perp}) \\
&+ \alpha_{\mathrm{refl}} K_{\mathrm{p}\to\mathrm{p,refl}}^{\mathrm{D}_2,\mathrm{D}_2^+}(\mathbf{x}_{\perp},\mathbf{x}'_{\perp}) \qquad (84)
\end{aligned}
$$

which separates the contributions to n_{D_2} arising from the direct path of length $r'_{\perp,\mathrm{dir}}$ connecting $\mathbf{x}_{\perp}$ and $\mathbf{x}'_{\perp}$, $K_{\mathrm{p}\to\mathrm{p,dir}}^{\mathrm{D}_2,\mathrm{D}_2^+}(\mathbf{x}_{\perp},\mathbf{x}'_{\perp})$, and the path corresponding to the trajectory of neutrals that are reflected at the boundary, $K_{\mathrm{p}\to\mathrm{p,refl}}^{\mathrm{D}_2,\mathrm{D}_2^+}(\mathbf{x}_{\perp},\mathbf{x}'_{\perp})$. Both $K_{\mathrm{p}\to\mathrm{p,dir}}^{\mathrm{D}_2,\mathrm{D}_2^+}$ and $K_{\mathrm{p}\to\mathrm{p,refl}}^{\mathrm{D}_2,\mathrm{D}_2^+}$ have the same expression,

$$
\begin{aligned}
K_{\mathrm{p}\to\mathrm{p,path}}^{\mathrm{D}_2,\mathrm{D}_2^+}(\mathbf{x}_{\perp},\mathbf{x}'_{\perp}) = \int_0^{\infty} &\frac{1}{r'_{\perp,\mathrm{path}}} \Phi_{\perp\left[\mathbf{v}_{\perp\mathrm{D}_2^+},T_{\mathrm{D}_2^+}\right]}(\mathbf{x}'_{\perp},\mathbf{v}_{\perp}) \\
&\times \exp\left[-\frac{1}{v_{\perp}}\int_0^{r'_{\perp,\mathrm{path}}} \nu_{\mathrm{eff},\mathrm{D}_2}(\mathbf{x}''_{\perp})\mathrm{d}r''_{\perp}\right] \mathrm{d}v_{\perp}, \qquad (85)
\end{aligned}
$$

where path $=\{\mathrm{dir},\mathrm{refl}\}$ and $r'_{\perp,\mathrm{path}}$ is the distance between $\mathbf{x}_{\perp}$ and $\mathbf{x}'_{\perp}$ measured along the path (for the direct trajectory $r'_{\perp,\mathrm{dir}}$ is given by the distance between the two points along a straight line, while for the reflected trajectory $r'_{\perp,\mathrm{refl}}$ is the sum of the distances between $\mathbf{x}'_{\perp}$ and the boundary and the distance from the boundary to $\mathbf{x}_{\perp}$). We remark that $\Phi_{\perp\left[\mathbf{v}_{\perp\mathrm{D}_2^+},T_{\mathrm{D}_2^+}\right]}(\mathbf{x}'_{\perp},\mathbf{v}_{\perp})$ is the integral along the parallel velocity of the D_2^+ Maxwellian distribution function, $\Phi_{\perp\left[\mathbf{v}_{\perp\mathrm{D}_2^+},T_{\mathrm{D}_2^+}\right]}(\mathbf{x}'_{\perp},\mathbf{v}_{\perp}) = \int_{-\infty}^{\infty}\Phi_{\left[\mathbf{v}_{\perp\mathrm{D}_2^+},T_{\mathrm{D}_2^+}\right]}(\mathbf{x}',\mathbf{v}_{\perp})\mathrm{d}v_{\parallel}$. We also remark that $K_{\mathrm{p}\to\mathrm{p,dir}}^{\mathrm{D}_2,\mathrm{D}_2^+}$ in equation (85) is valid in case the points are optically connected, i.e. if the straight line connecting the two points does not cross the core region nor the limiter plates. Otherwise, if the points are not connected, one has $K_{\mathrm{p}\to\mathrm{p,dir}}^{\mathrm{D}_2,\mathrm{D}_2^+}=0$. As for $K_{\mathrm{p}\to\mathrm{p,refl}}^{\mathrm{D}_2,\mathrm{D}_2^+}$, in the present work we assume no reflection at the outer walls, while reflection of ions and neutrals may take place at the limiter plates. The other kernels appearing in equations (76) and (77) have the same structure as $K_{\mathrm{p}\to\mathrm{p}}^{\mathrm{D}_2,\mathrm{D}_2^+}$, and they take into account possible direct and reflected paths connecting the two points. These kernels are presented in detail in appendix C.

We now turn to the evaluation of the non-homogeneous terms appearing in equations (80)–(83), i.e. the terms that are not proportional to n_{D} nor n_{D_2}. For instance, these terms include the contribution of the ions recycled at the wall. In fact, the reflection and reemission of D^+ ions that outflow to the boundary and recombine with electrons contribute to the density of neutral D atoms, through the term

$$
\begin{aligned}
n_{\mathrm{D[out,D^+]}}(\mathbf{x}_{\perp}) = \int_{\partial\mathrm{D}} \Gamma_{\mathrm{out,D^+}}(\mathbf{x}'_{\perp,\mathrm{b}}) &\left[(1-\alpha_{\mathrm{refl}}(\mathbf{x}'_{\perp,\mathrm{b}}))\right. \\
&\times (1-\beta_{\mathrm{assoc}})\, K_{\mathrm{b}\to\mathrm{p}}^{\mathrm{D,reem}}(\mathbf{x}_{\perp},\mathbf{x}'_{\perp,\mathrm{b}}) \qquad (86) \\
&\left.+ \alpha_{\mathrm{refl}}(\mathbf{x}'_{\perp,\mathrm{b}}) K_{\mathrm{b}\to\mathrm{p}}^{\mathrm{D,refl}}(\mathbf{x}_{\perp},\mathbf{x}'_{\perp,\mathrm{b}})\right] \mathrm{d}a'_{\mathrm{b}},
\end{aligned}
$$

where $\Gamma_{\mathrm{out,D^+}}$ is defined in equation (68). Similarly, the recombination of D_2^+ ions with electrons at the walls that are then either reflected or reemitted as D_2, and the recombination of D^+ ions with electrons at the walls and the following association into D_2 molecules contribute to the density of the D_2 species. These contributions can be expressed as

$$
\begin{aligned}
n_{\mathrm{D_2[out,D_2^+]}}(\mathbf{x}_{\perp}) = \int_{\partial\mathrm{D}} \Gamma_{\mathrm{out},\mathrm{D}_2^+}(\mathbf{x}'_{\perp,\mathrm{b}}) &\qquad (87) \\
&\times \left[(1-\alpha_{\mathrm{refl}}(\mathbf{x}'_{\perp,\mathrm{b}}))K_{\mathrm{b}\to\mathrm{p}}^{\mathrm{D}_2,\mathrm{reem}}(\mathbf{x}_{\perp},\mathbf{x}'_{\perp,\mathrm{b}})\right. \\
&\left.+ \alpha_{\mathrm{refl}}(\mathbf{x}'_{\perp,\mathrm{b}})K_{\mathrm{b}\to\mathrm{p}}^{\mathrm{D}_2,\mathrm{refl}}(\mathbf{x}_{\perp},\mathbf{x}'_{\perp,\mathrm{b}})\right] \mathrm{d}a'_{\mathrm{b}},
\end{aligned}
$$

and

$$
\begin{aligned}
n_{\mathrm{D_2[out,D^+]}}(\mathbf{x}_{\perp}) = \int_{\partial\mathrm{D}} \Gamma_{\mathrm{out,D^+}}(\mathbf{x}'_{\perp,\mathrm{b}}) &\\
&\times \left[(1-\alpha_{\mathrm{refl}}(\mathbf{x}'_{\perp,\mathrm{b}}))\frac{\beta_{\mathrm{assoc}}}{2}\right. \\
&\left.\times K_{\mathrm{b}\to\mathrm{p}}^{\mathrm{D}_2,\mathrm{reem}}(\mathbf{x}_{\perp},\mathbf{x}'_{\perp,\mathrm{b}})\right] \mathrm{d}a'_{\mathrm{b}}. \qquad (88)
\end{aligned}
$$

We also define the non-homogeneous terms appearing in equations (82) and (83), that provide the contributions to the flux of neutrals at the boundary, $\Gamma_{\mathrm{out,D}}$ and $\Gamma_{\mathrm{out,D_2}}$, given by the ions outflowing to the wall. Following a similar approach to

the one presented above, this can be expressed as

$$\begin{aligned}\Gamma_{\mathrm{out,D_2[out,D_2^+]}}\left(\mathbf{x}_{\perp,\mathrm{b}}\right) &= \int_{\partial\mathrm{D}} \Gamma_{\mathrm{out,D_2^+}}(\mathbf{x}'_{\perp,\mathrm{b}}) \\ &\times \left[(1-\alpha_{\mathrm{refl}}(\mathbf{x}'_{\perp,\mathrm{b}}))K_{\mathrm{b}\to\mathrm{b}}^{\mathrm{D_2,reem}}(\mathbf{x}_{\perp,\mathrm{b}},\mathbf{x}'_{\perp,\mathrm{b}})\right. \\ &\left. + \alpha_{\mathrm{refl}}(\mathbf{x}'_{\perp,\mathrm{b}})K_{\mathrm{b}\to\mathrm{b}}^{\mathrm{D_2,refl}}(\mathbf{x}_{\perp,\mathrm{b}},\mathbf{x}'_{\perp,\mathrm{b}})\right]\mathrm{d}a'_{\mathrm{b}},\end{aligned} \tag{89}$$

$$\begin{aligned}\Gamma_{\mathrm{out,D_2[out,D^+]}}(\mathbf{x}_{\perp,\mathrm{b}}) &= \int_{\partial\mathrm{D}} \Gamma_{\mathrm{out,D^+}}(\mathbf{x}'_{\perp,\mathrm{b}}) \\ &\times \left[(1-\alpha_{\mathrm{refl}}(\mathbf{x}'_{\perp,\mathrm{b}}))\frac{\beta_{\mathrm{assoc}}}{2}\right. \\ &\left. \times K_{\mathrm{b}\to\mathrm{b}}^{\mathrm{D_2,reem}}(\mathbf{x}_{\perp,\mathrm{b}},\mathbf{x}'_{\perp,\mathrm{b}})\right]\mathrm{d}a'_{\mathrm{b}},\end{aligned} \tag{90}$$

and

$$\begin{aligned}\Gamma_{\mathrm{out,D[out,D^+]}}(\mathbf{x}_{\perp,\mathrm{b}}) &= \int_{\partial\mathrm{D}} \Gamma_{\mathrm{out,D^+}}(\mathbf{x}'_{\perp,\mathrm{b}}) \\ &\times \left[(1-\alpha_{\mathrm{refl}}(\mathbf{x}'_{\perp,\mathrm{b}}))\,(1-\beta_{\mathrm{assoc}})\,K_{\mathrm{b}\to\mathrm{b}}^{\mathrm{D,reem}}(\mathbf{x}_{\perp,\mathrm{b}},\mathbf{x}'_{\perp,\mathrm{b}})\right. \\ &\left. + \alpha_{\mathrm{refl}}(\mathbf{x}'_{\perp,\mathrm{b}})K_{\mathrm{b}\to\mathrm{b}}^{\mathrm{D,refl}}(\mathbf{x}_{\perp,\mathrm{b}},\mathbf{x}'_{\perp,\mathrm{b}})\right]\mathrm{d}a'_{\mathrm{b}}.\end{aligned} \tag{91}$$

We now turn to the evaluation of the contributions to the neutral particles appearing in equations (80)–(83) caused by volumetric processes that involve the ion species D^+ and D_2^+. The contribution to the D_2 density as a result of D_2^+ recombination processes is given by

$$\begin{aligned}n_{\mathrm{D_2[rec,D_2^+]}}(\mathbf{x}_\perp) &= \int_{\mathrm{D}} n_{\mathrm{D_2^+}}(\mathbf{x}'_\perp)\nu_{\mathrm{rec,D_2^+}}(\mathbf{x}'_\perp)K_{\mathrm{p}\to\mathrm{p}}^{\mathrm{D_2,D_2^+}} \\ &\times(\mathbf{x}_\perp,\mathbf{x}'_\perp)\mathrm{d}A',\end{aligned} \tag{92}$$

and the contribution to the flux of D_2 to the boundary, also associated to D_2^+ recombination events, is expressed as

$$\begin{aligned}\Gamma_{\mathrm{out,D_2[rec,D_2^+]}}(\mathbf{x}_\perp) &= \int_{\mathrm{D}} n_{\mathrm{D_2^+}}(\mathbf{x}'_\perp)\nu_{\mathrm{rec,D_2^+}}(\mathbf{x}'_\perp)K_{\mathrm{p}\to\mathrm{b}}^{\mathrm{D_2,D_2^+}} \\ &\times(\mathbf{x}_\perp,\mathbf{x}'_\perp)\mathrm{d}A'.\end{aligned} \tag{93}$$

Similar contributions from volumetric recombination processes are considered for the D neutral species. The contribution to the D density as a result of D^+ recombination yields

$$n_{\mathrm{D[rec,D^+]}}(\mathbf{x}_\perp) = \int_{\mathrm{D}} n_{\mathrm{D^+}}(\mathbf{x}'_\perp)\nu_{\mathrm{rec,D^+}}(\mathbf{x}'_\perp)K_{\mathrm{p}\to\mathrm{p}}^{\mathrm{D,D^+}}(\mathbf{x}_\perp,\mathbf{x}'_\perp)\mathrm{d}A', \tag{94}$$

while an analogous definition is used for the flux of D,

$$\begin{aligned}\Gamma_{\mathrm{out,D[rec,D^+]}}(\mathbf{x}_\perp) &= \int_{\mathrm{D}} n_{\mathrm{D^+}}(\mathbf{x}'_\perp)\nu_{\mathrm{rec,D^+}}(\mathbf{x}'_\perp)K_{\mathrm{p}\to\mathrm{b}}^{\mathrm{D,D^+}} \\ &\times(\mathbf{x}_\perp,\mathbf{x}'_\perp)\mathrm{d}A'.\end{aligned} \tag{95}$$

Finally, the contribution of the dissociation of D_2^+ ions to n_D appearing in equation (81) is evaluated as

$$\begin{aligned}n_{\mathrm{D[diss(D_2^+)]}}(\mathbf{x}_\perp) &= \int_{\mathrm{D}} n_{\mathrm{D_2^+}}(\mathbf{x}'_\perp)\nu_{\mathrm{diss,D_2^+}}(\mathbf{x}'_\perp) \\ &\times K_{\mathrm{p}\to\mathrm{p}}^{\mathrm{D,diss}\left(\mathrm{D_2^+}\right)}(\mathbf{x}_\perp,\mathbf{x}'_\perp)\mathrm{d}A' \\ &+ \int_{\mathrm{D}} 2n_{\mathrm{D_2^+}}(\mathbf{x}'_\perp)\nu_{\mathrm{diss-rec,D_2^+}}(\mathbf{x}'_\perp) \\ &\times K_{\mathrm{p}\to\mathrm{p}}^{\mathrm{D,diss-rec}\left(\mathrm{D_2^+}\right)}(\mathbf{x}_\perp,\mathbf{x}'_\perp)\mathrm{d}A'.\end{aligned} \tag{96}$$

Similarly, a dissociation process of D_2^+ ions results in a contribution to $\Gamma_{\mathrm{out,D}}$ in equation (83) given by

$$\begin{aligned}\Gamma_{\mathrm{out,D[diss(D_2^+)]}}(\mathbf{x}_\perp) &= \int_{\mathrm{D}} n_{\mathrm{D_2^+}}(\mathbf{x}'_\perp)\nu_{\mathrm{diss,D_2^+}}(\mathbf{x}'_\perp) \\ &\times K_{\mathrm{p}\to\mathrm{b}}^{\mathrm{D,diss}\left(\mathrm{D_2^+}\right)}(\mathbf{x}_{\perp,\mathbf{b}},\mathbf{x}'_\perp)\mathrm{d}A' \\ &+ \int_{\mathrm{D}} 2n_{\mathrm{D_2^+}}(\mathbf{x}'_\perp)\nu_{\mathrm{diss-rec,D_2^+}}(\mathbf{x}'_\perp) \\ &\times K_{\mathrm{p}\to\mathrm{b}}^{\mathrm{D,diss-rec}\left(\mathrm{D_2^+}\right)}(\mathbf{x}_{\perp,\mathbf{b}},\mathbf{x}'_\perp)\mathrm{d}A'.\end{aligned} \tag{97}$$

For their numerical solution, the system of kinetic equations for the neutral species is discretized on a regular Cartesian grid in the (R,Z) plasma and then written in matrix form. The details of the numerical implementation of the neutral model are discussed in appendix D.

6. First simulation of a multi-component plasma with the GBS code

We present the first results from simulations of turbulence in the tokamak boundary carried out by using the multi-component plasma model described in sections 2–4 and implemented in the GBS code. Similarly to [22, 37], we consider a tokamak with an infinitesimally thin toroidal limiter at the high-field side (HFS) equatorial midplane, with major radius $R_0/\rho_{\mathrm{s0}} = 500$, and we simulate a three-dimensional domain with an annular cross section that includes the edge and the open-field line region of the device. The radial size of the domain is $S_{\mathrm{rad}} = 150\rho_{\mathrm{s0}}$ and the poloidal size is $S_{\mathrm{pol}} = 800\rho_{\mathrm{s0}}$ at the core interface. Since the limiter has a radial width of $75\rho_{\mathrm{s0}}$), both the open and closed field-line regions have a radial extension of $75\rho_{\mathrm{s0}}$, corresponding to half the size along the radial direction. The parameters chosen for the present simulation are $q = 3.992$, $n_0 = 2\times10^{13}$ cm^{-3}, $T_0 = 20.0$ eV, $\Omega_{\mathrm{ci}} = 5.0\times10^7$ s^{-1}, $T_{\mathrm{w}} = 0.3$ eV, $\nu = 0.1$, $\eta_{0\mathrm{e}} = \eta_{0\mathrm{D^+}} = 1.0$, $\eta_{0\Omega} = 4.0$, $\chi_{\parallel0,\mathrm{e}} = 0.5$, $\chi_{\parallel0,\mathrm{D^+}} = 0.05$, $\chi_{\parallel0,\mathrm{D_2^+}} = 0.05$, $D_{\parallel n_\mathrm{e}} = 0.5$,

$D_{\|n_{D_2^+}} = 0.0$, $D_{\|v_{\|e}} = 0.5$, $D_{\|v_{\|D^+}} = 0.0$, $D_{\|v_{\|D_2^+}} = 0.5$, and $D_{\perp n_e} = 21.0$, $D_{\perp n_{D_2^+}} = D_{\perp\Omega} = D_{\perp v_{\|e}} = D_{\perp v_{\|D^+}} = D_{\perp v_{\|D_2^+}} = D_{\perp T_e} = D_{\perp T_{D^+}} = D_{\perp T_{D_2^+}} = 7.0$. We remark that, since the diffusion terms considered in equations (19)–(27) are introduced for numerical reasons, the diffusion coefficients are adjusted so as to ensure numerical stability, while having a negligible impact on the physical results of the simulation. We highlight that these simulation parameters correspond to the ones of a device with major radius $R_0 = 43.8$ cm, minor radius $a = 11.1$ cm, and on-axis magnetic field, $B_0 = 0.52$ T. Regarding the reflection probability at the limiter, we remark that it depends strongly on the particle energy and the wall material (see [1]). In this simulation, reflection of ions and neutrals takes place at the limiter plates with a given probability $\alpha_{\text{refl,lim}}$, constant along the limiter surface. The fraction of reflection at the boundary is therefore defined as

$$\alpha_{\text{refl}}(\mathbf{x}'_{\perp,\text{b}}) = \begin{cases} \alpha_{\text{refl,lim}} \neq 0 & \text{if } \mathbf{x}'_{\perp,\text{b}} \text{ is located at limiter walls} \\ 0 & \text{if } \mathbf{x}'_{\perp,\text{b}} \text{ is located at the outer and inner boundary.} \end{cases} \tag{98}$$

We choose to consider metallic boundaries and hence we assume $\alpha_{\text{refl,lim}} = 0.8$, a value similar to the one adopted in reference [37]. We also assume $\beta_{\text{assoc}} = 0.95$, which is consistent with the usual assumption that most D atoms associate into D_2 molecules at the boundary (see e.g. [3, 61]). On the other hand, we recall that, for the typical plasma conditions considered in this paper, the rate of electron–ion recombination is very low. Hence, we neglect volumetric recombination processes. These are expected to become important in detachment conditions, which will be the subject of future studies based on the GBS simulations of diverted configurations.

Regarding the numerical parameters, we note that the plasma grid resolution is $n_{x,\text{p}} \times n_{y,\text{p}} \times n_{z,\text{p}} = 255 \times 511 \times 64$ while neutral grid resolution is $n_{x,\text{n}} \times n_{y,\text{n}} \times n_{z,\text{n}} = 24 \times 138 \times 64$. The difference between the plasma and neutral grid resolution is due to the scale lengths the plasma and neutral models describe (ρ_s for the plasma and λ_{mfp} for the neutrals). In addition, the lower resolution neutral grid allows us to reduce the high computational cost associated with the solution of the neutral model. The difference between the neutral ans plasma grids results in the need for interpolations between them. On the other hand, the toroidal grid resolution is the same for both the plasma and neutral grids, since the neutrals are calculated on all poloidal planes where the plasma quantities are evolved. This is a similar approach to the one previously followed in the single-species neutral model implemented in GBS [37, 40]. The time step is $3.75 \times 10^{-5} R_0/c_s$ and the neutral quantities are evaluated every $\Delta t = 0.1 R_0/c_s$. Although we have not carried out convergence studies with the multispecies model presented in this paper, convergence on plasma and neutral grid refinement has been studied within the single component framework. The conclusions presented in reference [62], which we expect to remain valid in the multispecies model presented here, show that our results are converged with respect to the frequency of neutral calculation. We also note that the initial conditions of the simulation presented in this paper correspond to a snapshot from a single-component simulation carried out with the same parameters. The D_2 and D_2^+ molecular species are initialized with constant profiles. Our analysis focuses on the quasi-steady state that is established after a transient, when plasma sources, parallel and perpendicular transport, and losses to the wall balance each other. This quasi-steady-state is expected to be independent of the initial conditions.

For the description of the simulation results, we therefore focus on the quasi-steady-state regime, established after a transient, when the plasma and neutral profiles fluctuate around constant values. We take toroidal and time averages of the plasma quantities evolved by equations (19)–(28) over a time interval of $\Delta t \simeq 10 R_0/c_{s0}$. These quantities are shown in figure 2 on a poloidal cross section. In figure 3, we present the density of the neutral species, n_D and n_{D_2}, and the neutral–plasma collisional interaction terms taken into account in our model. The results of the multispecies simulations are compared with the one of a single-component plasma, with corresponding parameters. The time and toroidal averages of the plasma and neutral main quantities for the single species simulation are shown in figure 4.

We first focus on some general considerations on the plasma and neutral densities. The plots in figure 2 reveal that the density of the molecular ion species D_2^+ is three to four orders of magnitude smaller than the density of the main ion species D^+, a result in agreement with the assumption $n_{D_2^+}/n_{D^+} \ll 1$ used in equations (22)–(27) for the derivation of the parallel friction and heat flux terms and in equations (40)–(44) to obtain the boundary conditions at the limiter. We highlight that the density of D_2^+ peaks just inside the last closed flux surface (LCFS) next to the limiter, since most of the D_2 molecules cross the open-field line region without interacting and are then dissociated and/or ionized by the denser and warmer plasma inside the LCFS. As a matter of fact, $n_{D_2^+}$ exhibits a similar behavior to the profile of the molecular ionization source $n_{D_2}\nu_{\text{iz},D_2}$ presented in figure 3, which also peaks in the edge near the limiter. On the other hand, figure 2 shows that n_D and n_{D_2} are comparable to n_{D^+} near the limiter plates, while they are about one order of magnitude smaller than n_{D^+} in the rest of the scrape-off layer (SOL) and up to two orders of magnitude smaller inside the LCFS. Furthermore, regarding the relative

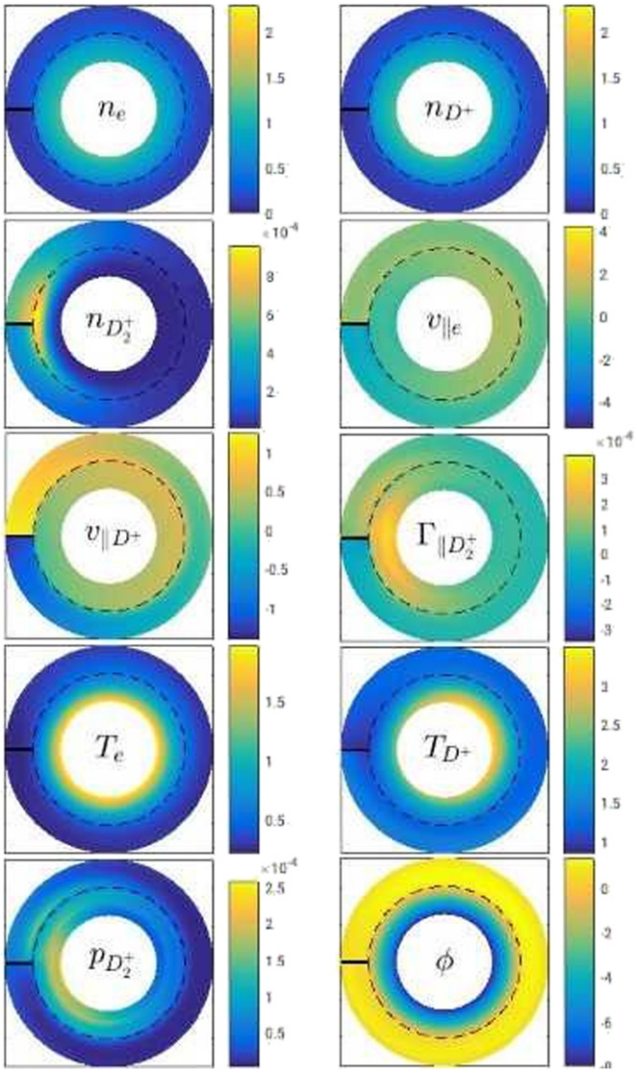

Figure 2. Cross section plots of the electron density (n_e), D^+ density (n_{D^+}), D_2^+ density ($n_{D_2^+}$), electron parallel velocity ($v_{\parallel e}$), D^+ parallel velocity ($v_{\parallel D^+}$), D_2^+ parallel velocity ($v_{\parallel D_2^+}$), electron temperature (T_e), D^+ temperature (T_{D^+}), D_2^+ temperature ($T_{D_2^+}$) and electrostatic potential (ϕ), toroidal and time-averaged over an interval of $\Delta t = 10.1 R_0/c_{s0}$ from the quasi-steady-state of the multi-component plasma simulation described in section 6.

importance of D and D_2, figure 3 shows that n_{D_2} is larger than n_D by a factor between two and three in the open-field line region around the limiter, while n_D is larger than n_{D_2} inside the LCFS at the HFS, as a consequence of the higher plasma densities and temperatures that lead to the dissociation of D_2 molecules in that region.

As a second set of observations, we focus on the asymmetry of the plasma density and flow. An up–down asymmetry in the edge region is shown by the profiles of n_e and n_{D^+}, which are noticeably larger below the equatorial midplane than above it. The underlying reason of this asymmetry can be inferred from the $v_{\parallel e}$, $v_{\parallel D^+}$ and $\Gamma_{\parallel D_2^+}$ profiles. In fact, the e^- and D^+ parallel flows are directed in the counterclockwise direction in the edge region. Therefore, the ionization of neutrals inside the LCFS, which occurs mostly in the proximity of the limiter at the HFS, leads to plasma particles subject to a downward flow. Albeit being small, this flow leads to a slightly larger density of e^- and D^+ below the equatorial midplane of the device. The parallel flux of D_2^+ ions is also directed counterclockwise in the edge at the HFS, which further enhances this mechanism, even though D_2^+ densities are small compared to the other species. We highlight that the n_{D^+} and $v_{\parallel D^+}$ profiles are slightly different when the single-component model of GBS is considered, as illustrated in figure 4. In this case, although it is also observed an up–down asymmetry in the n_{D^+} profile, this is related to the fact that the ionization source, $n_D \nu_{iz}$, is larger in the edge region below the limiter than above it, due to larger recycling rates at the lower limiter plate. In fact, contrary to the multi-species case, the $v_{\parallel D^+}$ is characterized by a counterclockwise parallel flow of D^+ ions in the edge below the midplane, while above it the parallel flow is directed clockwise.

In the multi-component plasma simulation we also observe a larger parallel flow of plasma in the open-field line region towards the upper side of the limiter when compared to the lower side. This can be observed in figure 2, that shows larger n_{D^+} and $v_{\parallel D^+}$ above the limiter plates than below it, ultimately leading to higher recycling rates and hence larger n_D and n_{D_2} densities in the region above the limiter, as shown in figure 3. The reason behind this behavior is again related to the $v_{\parallel D^+}$ profile. In fact, while the D^+ ions flow counterclockwise along the magnetic field lines in the edge, they undergo cross-field transport towards the SOL. As a result of the counterclockwise parallel flow and related asymmetry of n_{D^+} in the edge region, most ions cross the LCFS above the equatorial midplane, while flowing along the magnetic field lines towards the upper side of the limiter.

It is also observed that n_{D^+} is slightly larger in the HFS compared to the low-field side (LFS), which is due to the existence of D^+ sources in the HFS around the midplane. Similarly, also in the single-species simulation, n_{D^+} is larger in the HFS as a consequence of the ionization source, $n_D \nu_{iz}$.

Focusing on the temperature of the plasma components, we observe that the T_e profile presents a similar behavior to the one observed in single-component plasma simulations. A clear asymmetry between the HFS and the LFS is observed for T_{D^+}, which is qualitatively similar to the results for a single-component simulation in figure 4. As a matter of fact, the temperature is considerably lower on the HFS compared to the LFS, which is related to the generation of cold D^+ ions inside the LCFS due to ionization of D atoms, dissociative processes and charge-exchange interactions. This effect is particularly important above the limiter, where the recycling rates are larger. On the other hand, the profile of $p_{D_2^+}$ exhibits a maximum inside the LCFS at the HFS, where the majority of the D_2^+ ions are generated by ionization of D_2 molecules coming from the limiter. The up–down asymmetry of the D_2^+ pressure around the limiter is also due to the asymmetry of the recycling rates. As an aside note, we remark that, since it is strongly related to the T_e profile [63], the electrostatic potential profile revealed by the multi-component simulations is similar to the one observed in the single-component plasma model.

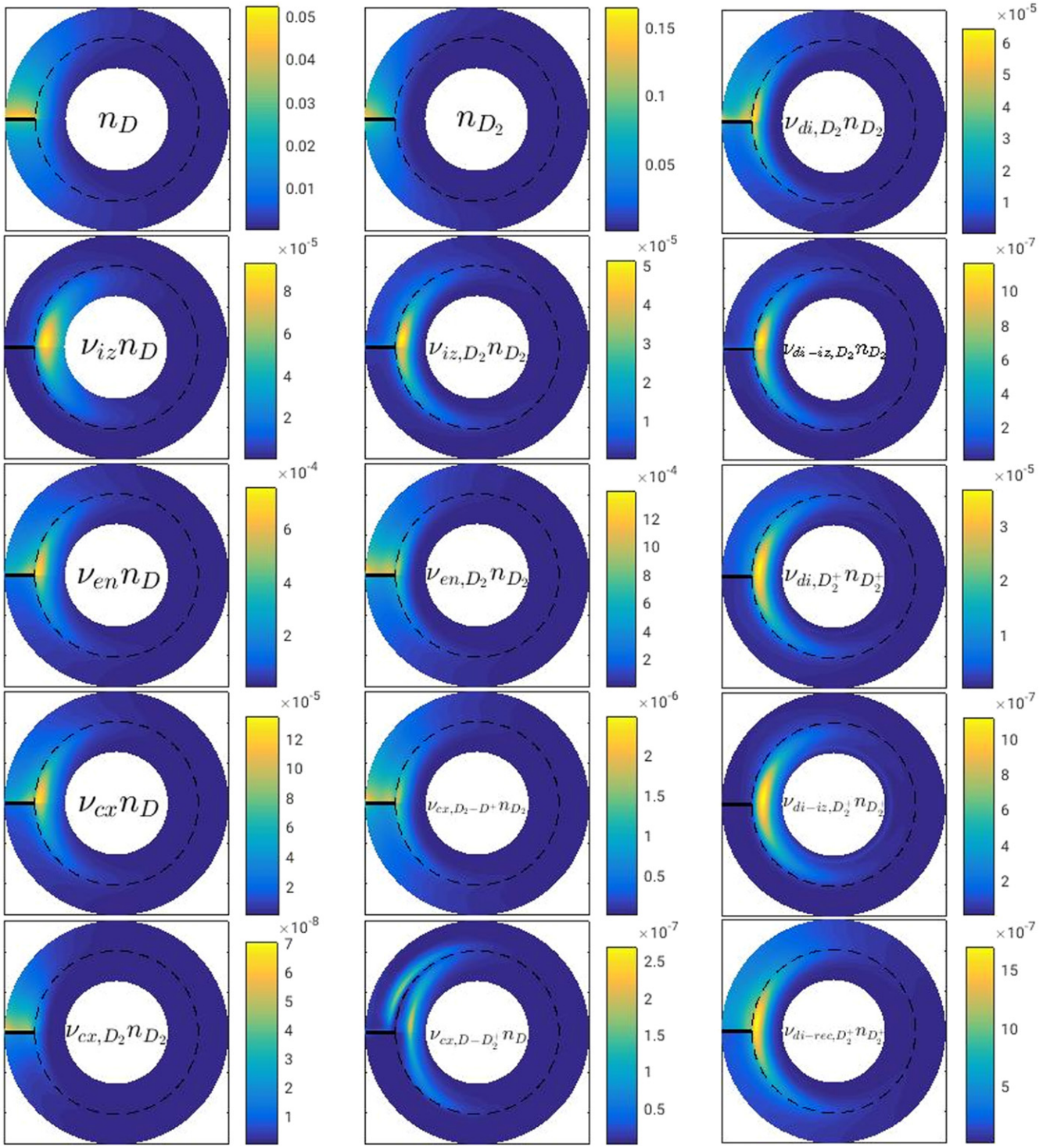

Figure 3. Cross section plots of the neutral species densities and source terms resulting from the neutral–plasma interaction, toroidal and time-averaged over an interval of $\Delta t = 10.1 R_0/c_{s0}$ from the quasi-steady-state of the multi-component plasma simulation described in section 6.

Analyzing the neutral–plasma interaction terms presented in figure 3, we first notice that ionization processes tend to be more important in the edge region at the HFS, with atomic and molecular ionization rates exhibiting similar profiles. However, $n_{D_2}\nu_{iz,D_2}$ peaks in the vicinity of the LCFS, while $n_D\nu_{iz,D}$ peaks further inside the LCFS and has a larger radial spread. In fact, D_2 molecules generated in the open-field line region and are dissociated and/or ionized in the proximity of the LCFS, where the plasma is warmer and denser. In contrast, although most D atoms are generated in the open-field line region, they are also created by dissociation of D_2 molecules in the edge. This shifts the maximum of $n_D\nu_{iz,D}$ radially inwards and makes

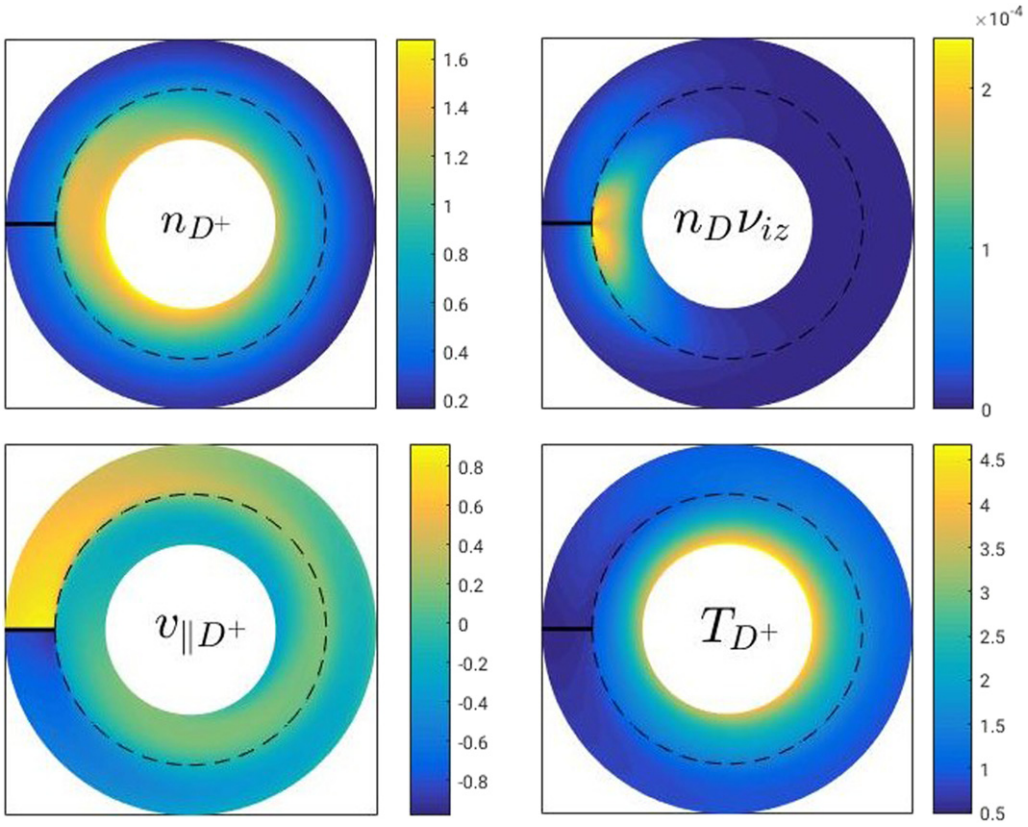

Figure 4. Cross section plots of plasma density $n = n_e = n_{D^+}$, ion parallel velocity $v_{\parallel D^+}$, ion temperature T_{D^+} and ionization source term $n_{D^+}\nu_{iz}$, toroidal and time-averaged over an interval of $\Delta t = 10.1 R_0/c_{s0}$ from a quasi-steady-state single-component plasma simulation. The grid sizes and simulation parameters are the same as the ones considered in the multi-component simulations, except for the wall re-emission temperature, which is set to $T_w = 3.0$ eV, to mimick Franck–Condon dissociation processes, and $D_{\perp n_e} = 7.0$.

the ionization source spread across a wider area. As a result of n_D being larger than n_{D_2} in the edge, the maximum of $n_D \nu_{iz,D}$ is also almost two times larger than $n_{D_2}\nu_{iz,D_2}$.

Focusing on the electron–neutral collisions, we note that the reactions involving D_2 occur more often in the open-field line region, mainly in the area surrounding the limiter plates where the majority of the neutral molecules are generated. Reactions with D_2 become less important in the edge, since most molecules are dissociated and/or ionized due to the higher densities and temperatures. On the other hand, electron–atom collision reactions involving the D species peak inside the LCFS, because the cross sections of these reactions are larger in the edge region due to the higher plasma density and temperature and because of the presence of D atom resulting from dissociative processes. We also highlight that elastic collisions and charge-exchange reactions are more frequent on the upper side of the limiter, in agreement with the strong up–down asymmetry discussed above. Regarding charge-exchange reactions, we observe that they are spatially localized similarly to the electron–neutral collisions. The reactions between the two molecular species (D_2–D_2^+ collisions) occur less often than the charge-exchange between monoatomic species (D–D^+ collisions) by three to four orders of magnitude, which is a result of the $n_{D_2^+}$ to n_{D^+} ratio. In addition, the terms arising from charge-exchange interactions between D_2 molecules and D^+ ions (D_2–D^+ collisions) are found to be two orders of magnitude smaller than the ones between the atomic species (D–D^+ collisions) in the region of the domain where these interactions are important. In turn, charge-exchange between D_2^+ ions and D atoms is three orders of magnitude smaller than D–D^+ charge-exchange, which is due to the fact that $n_D \nu_{cx,D-D_2^+}$ is proportional to $n_{D_2^+}$.

Finally, we analyze the dissociative processes, which represent a sink of molecular species D_2 and D_2^+ and sources of D atoms and D^+ ions. Simple dissociation of D_2 and D_2^+, described by the terms $n_{D_2}\nu_{diss,D_2}$ and $n_{D_2^+}\nu_{diss,D_2^+}$ respectively, which do not involve ionization nor recombination processes, are found to be dominant dissociation processes, and occur with a frequency similar to that of the ionization of D and D_2. We remark that dissociation of D_2 molecules peaks just above the limiter plate (where most D_2 molecules are generated) and in the edge region, in the vicinity of the LCFS, and then it is significantly smaller in the core, since n_{D_2} drops rapidly across the edge. In contrast, dissociation of D_2^+ ions is very small in the open-field line region, where the density of D_2^+ is negligible (at the typical electron temperature of the SOL, the D_2 ionization cross section is small), and is important only inside the LCFS, where D_2^+ ions are generated. The $n_{D_2^+}\nu_{diss,D_2^+}$ profile therefore closely follows the $n_{D_2^+}$ profile, with a larger radial spread when compared with the dissociation of D_2. As for dissociative ionization of D_2 and D_2^+,

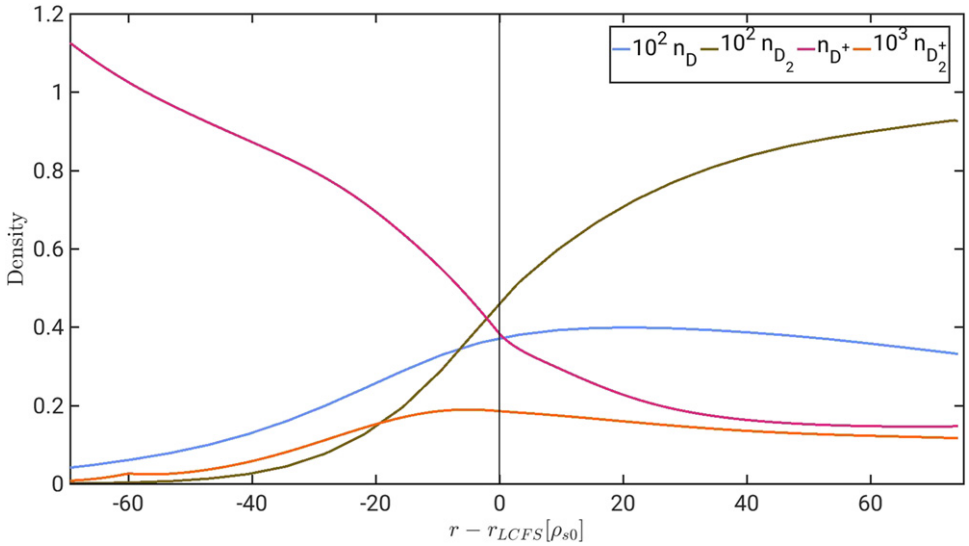

Figure 5. Radial profiles of the ions and neutrals species densities, averaged over the toroidal and poloidal directions, evaluated over an interval of $\Delta t = 10.1 R_0/c_{s0}$ from a quasi-steady-state simulation described in section 6.

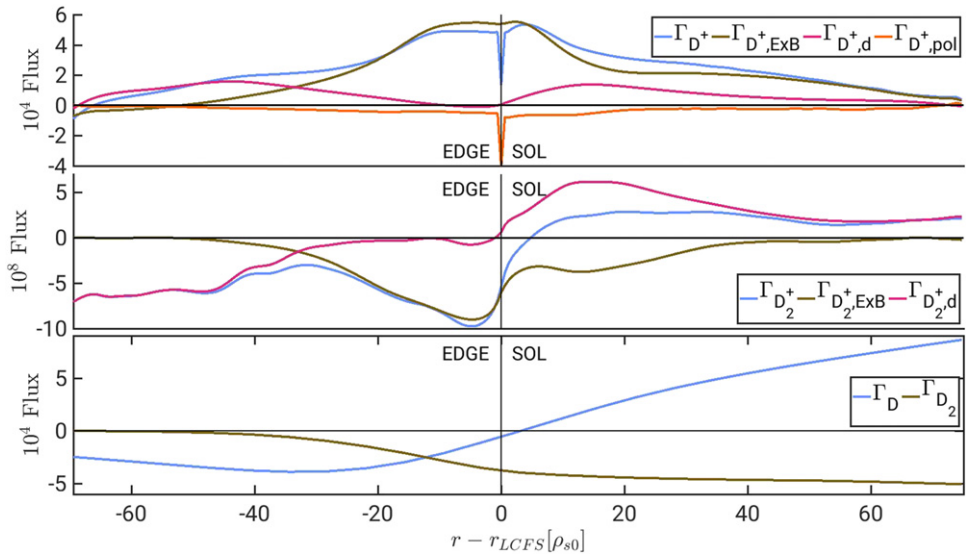

Figure 6. Radial profiles of the radial flux for D^+ ions (top), D_2^+ ions (middle) and neutral species D and D_2 (bottom), averaged over the toroidal and poloidal directions, evaluated over an interval of $\Delta t = 10.1 R_0/c_{s0}$ from the quasi-steady-state multi-component plasma simulation described in section 6. The components of the D^+ and D_2^+ radial flux are discriminated.

$n_{D_2}\nu_{\mathrm{diss-iz},D_2}$ and $n_{D_2^+}\nu_{\mathrm{diss-iz},D_2^+}$ respectively, we observe that the rates are smaller by one to two orders of magnitude with respect to the simple dissociation of D_2 and D_2^+ and peak in the edge region a bit further inside. This is due to the fact that the energy required to trigger dissociative ionization processes is considerably larger than the one needed to dissociate the particles without triggering an ionization process, as shown in table 2. Hence, these processes are only relevant in the edge region, where densities and temperatures are sufficiently high to make these cross sections significant. This is particularly the case of $n_{D_2^+}\nu_{\mathrm{diss-iz},D_2^+}$, since this term is also proportional to the density of D_2^+ ions, which is relevant only inside the LCFS. Nevertheless, we highlight that these reactions become considerably less important towards the core, as very few D_2 and D_2^+ cross the edge region without being dissociated. As for dissociative-recombination of D_2^+ particles, $n_{D_2^+}\nu_{\mathrm{diss-rec},D_2^+}$, its amplitude is also smaller than that of simple dissociation by one to two orders of magnitude and follows very closely the $n_{D_2^+}$ profile, since there is no energy threshold to trigger the reaction, unlike dissociative ionization processes.

These results allow us to draw a global picture of the main processes determining the dynamics of D_2 neutrals in the boundary. Although some D_2 molecules are dissociated in the SOL region, most of them cross the LCFS and are dissociated into D atoms within a short distance as they get in contact with the warmer and denser plasma of the edge. The remaining D_2 molecules penetrate further towards the core and are ionized by the increasingly warmer and denser plasma, giving rise to

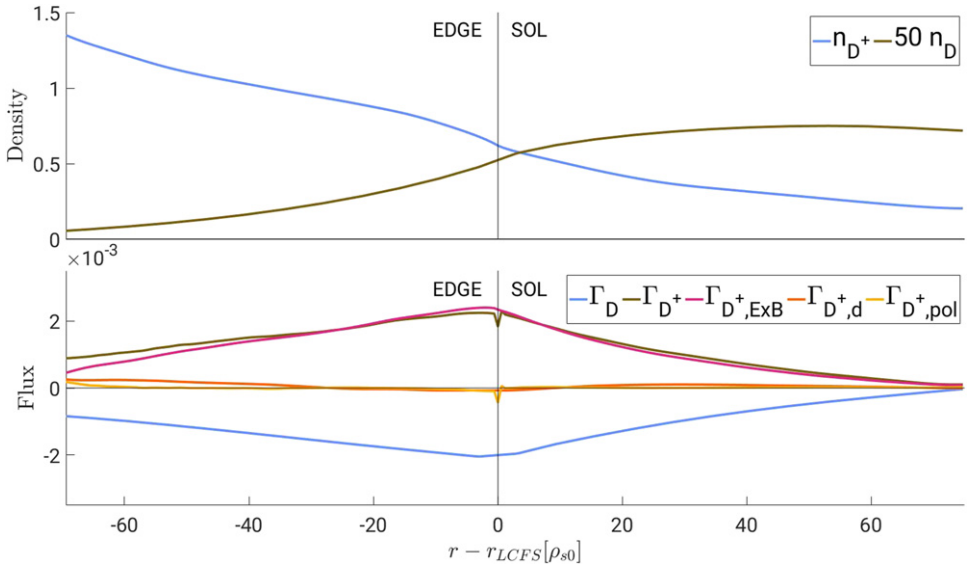

Figure 7. Radial profiles of density (top) and radial flux (bottom) for the D^+ and D species, averaged over the toroidal and poloidal directions, evaluated over an interval of $\Delta t = 10.1 R_0/c_{s0}$ from a quasi-steady-state single-component plasma situation. The components behind the radial ion flux are discriminated. Plasma and neutral grid resolution, as well as simulation parameters, are the same considered in figure 4.

D_2^+ ions, which in turn are quickly dissociated into D^+ ions and D atoms.

We remark that, in the multi-component as well as in the single-component simulations, given the low plasma density of the SOL, a significant amount of D atoms generated in the open-field line region (emitted at the limiter or created by dissociation of D_2 molecules) penetrate in the edge, where ionization takes place due to the higher plasma density and temperature. However, the presence of the D sources inside the LCFS in the multi-component simulations shifts the ionization processes, $n_D \nu_{iz}$, towards the core with respect to the results with respect to single-component simulations, as shown in figure 4.

To conclude, we present radial plots of the particle densities (figure 5) and radial fluxes (figure 6), obtained by evaluating the time, toroidal and poloidal average of these quantities. In figure 6, we discriminate the contributions of the $E \times B$, diamagnetic and polarization drifts to the flux of the plasma ion species, D^+ and D_2^+. The results from the single-component simulations are shown in figure 7. The n_{D^+} profile in figure 5 is similar to the one observed within the single-component plasma simulation in figure 7, with a large density gradient region near the LCFS and a density shoulder appearing in the far SOL. In turn, the density of D_2^+ is small in the whole domain and peaks in the edge, across the LCFS, where most D_2 molecules are ionized and decreases rapidly towards the core, due to the small penetration of D_2 molecules in the warmer and denser plasma of the region. On the other hand, the D_2^+ ions observed in the open-field line region result from charge-exchange interactions between D_2 and D^+ (see figure 3) and the ionization of D_2 molecules reemitted from the limiter and vessel wall.

Focusing on the neutral species, we note that n_D peaks in the open-field line region, in contrast to the single-component plasma simulation. This is the result of the D_2 molecules dissociated into D atoms in the edge and near SOL. On the other hand, we observe that n_{D_2} decreases monotonically from the outer wall to the core interface, since D_2 molecules are generated in the open-field line region as the result of recycling processes are lost due to dissociation and ionization processes which take place mostly in the edge and near SOL.

The dissociation of D_2 molecules also impacts Γ_D, the radial flux of D, presented in figure 6. In contrast with the single-component plasma simulation presented in figure 7, Γ_D points radially inwards in the edge, but reverses sign in the SOL region, a consequence of the release of D atoms because of the dissociation of D_2 molecules, particularly important close to the LCFS. In addition, the D atoms reaching the outer wall associate and are reemitted as D_2 molecules, thus contributing to the outward flux of D. The multi-component simulation shows that Γ_D peaks in the edge region, while for a single-component model Γ_D is maximum at the LCFS. This is due to the D atoms that are generated in the edge region close to the LCFS in a multi-component model, compensating their ionization. At the same time, we note that Γ_{D_2}, the radial flux of D_2 molecules, points radially inwards in the whole domain (see figure 6). More precisely, Γ_{D_2} is approximately constant in the SOL, because the loss of D_2 molecules due to dissociation is compensated by the D_2 molecules recycled at the limiter. Then, Γ_{D_2} decreases in the edge as a consequence of the molecules being dissociated and/or ionized because of the larger temperatures and densities in this region and becomes negligible towards the core.

Turning to the dynamics of the ion species, we note that the radial flux of D^+ ions points radially outwards across the whole domain and is mostly determined by the dominant $E \times B$ flux except near the core, where the diamagnetic flux,

dominates over the $E \times B$ flux. The polarization drift contribution is negligible in the whole domain. We also remark that the flux increases across the edge region from the core to the separatrix, having a maximum in the near SOL, and then decreases gradually across the open-field line region. This contrasts with the behavior of the ion flux in the single-component plasma simulation (see figure 7), where the flux peaks at the LCFS. This difference is related to the location of the ionization source $n_{\mathrm{D}}\nu_{\mathrm{iz}}$. Indeed, while the source has a smooth profile and peaks at the LCFS in the single-component model, the ionization source peaks further inside the edge in the multi-component model, accounting for a sharp increase of the D^+ flux in the edge close to the LCFS.

Figure 6 shows that the radial flux of D_2^+ ions points radially outwards in the SOL and radially inwards in the edge. This is a consequence of the fact that most D_2^+ are generated in the vicinity of the LCFS, where the D_2 molecules are ionized by the warmer and denser plasma. The D_2^+ radial flux is determined by the balance between the inward pointing $E \times B$ and outward pointing diamagnetic drift components in the SOL, by the $E \times B$ flux in the edge close to the LCFS, and by the diamagnetic component towards the core.

We also note that the inward pointing $\Gamma_{\mathrm{D}_2^+}$ is sharply peaked in the edge, close to the LCFS. This is because most D_2^+ ions are generated by ionization of D_2 molecules in that region and are then dissociated after traveling a short distance. Indeed, the location of the peak of $\Gamma_{\mathrm{D}_2^+}$ corresponds to the one of the $n_{\mathrm{D}_2^+}$ profile in figure 5. The flux of D_2^+ associated with the polarization drift is not represented in figure 6 because it is neglected in our model. We note that $\Gamma_{\mathrm{D}_2^+}$ is three to four orders of magnitude smaller than Γ_{D^+}, which is a consequence of the ratio $n_{\mathrm{D}_2^+}/n_{\mathrm{D}^+}$. Since the polarization drift component is expected to be small compared to the total molecular ion flux, $\Gamma_{\mathrm{D}_2^+}$, we conclude that neglecting the polarization drift terms in equations (19)–(27) has indeed a negligible impact on the simulation results.

7. Conclusions

In this work we present a multi-component model for the self-consistent description of the neutral and plasma dynamics in the tokamak boundary. This model is implemented in the GBS code, allowing for the simulation of a deuterium plasma in the edge and SOL regions of a tokamak, including electrons, D^+ and D_2^+ ions, D atoms and D_2 molecules. The neutral and the plasma models are coupled through a number of collisional processes, which give rise to neutral–plasma interaction terms in the plasma and neutral equations. The reactions considered include ionization, electron–neutral elastic collisions, charge-exchange and dissociative processes. The multi-component plasma model relies on the Braginskii fluid equations derived in the drift limit, being an extension of the single ion species model to account for D_2^+ ions and closed by following Zhdanov approach. As for the neutral species, we extend the approach considered in the single neutral species model of GBS [37] to include the molecular species, D_2. The neutrals are computed by solving two coupled kinetic equations for the D and D_2 species, which is carried out by using the method of characteristics. The resulting system of linear integral equations are then discretized and solved for the n_{D} and n_{D_2} densities.

The results from the first simulation carried out using the multi-component model are described in the sheath-limited regime in a toroidally limited plasma. The results exhibit some noticeable differences with respect to the single-ion component implemented in GBS. We observe an up–down asymmetry in the n_{e} and n_{D^+} density, which are larger below the equatorial midplane. This is related to the counterclockwise parallel flow of the plasma in the edge, observed in the profiles of $v_{\parallel \mathrm{e}}$, $v_{\parallel \mathrm{D}^+}$ and $v_{\parallel \mathrm{D}_2^+}$. This feature also leads to larger recycling rates and a higher density of neutral particles in the upper side of the limiter, compared to the lower side. Moreover, the simulation shows that the density of the neutral species, n_{D}, is about one order of magnitude smaller than n_{D^+} in the open-field line region and two orders of magnitude smaller in the edge, while $n_{\mathrm{D}_2^+}$ is about three to four orders of magnitude smaller than n_{D^+}, even in the edge close to the LCFS, where $n_{\mathrm{D}_2^+}$ peaks.

By taking into account the molecular dynamics, the first simulations based upon the multi-component model also shed some light on the role played by molecules on the plasma fueling. As a matter of fact, D_2 particles are generated close to the LCFS. A large fraction of D_2 molecules reach the closed field line region, where they are most often dissociated into atomic D by the warmer and denser plasma. The resulting D atoms and the remaining D_2 molecules are then ionized inside the edge, with the D_2^+ ions being quickly dissociated as a consequence of the high electron densities and temperatures. The simulation results therefore show that the peak of the ionization of D atoms is shifted radially inwards with respect to the results from the single-species simulations.

The radial profiles of the densities and radial fluxes are also impacted by the presence of molecular species. We observe that the radial flux of D^+ increases sharply in the edge close to the LCFS as a result of the peak of the ionization source observed in that region. The flux of D^+ then remains high in the vicinity of the LCFS, and decreases sharply again in the near SOL, where the sources of D^+ are outweighed by the sinks at the limiter. This is a major difference with respect to the D^+ flux observed in the single-ion species simulation, which is maximum at the LCFS. On the other hand, the D density peaks in the SOL due to the D_2^+ ions dissociated there. This also explains why the D radial flux reverses sign, pointing radially outwards in the far SOL. On the other hand, the inward flux of D atoms in the edge increases radially inwards in the vicinity of the LCFS, since D atoms are also generated in that region as a result of dissociation of D_2 molecules.

We highlight that adding the D_2^+ ion species does not affect the computational cost of our simulation significantly, while the generalisation from a single-species to a two-species neutral model by including D_2 molecules does increase the cost of the neutral calculation considerably. While the D_2 molecules

are observed to play an important role in the boundary dynamics, exhibiting a similar density to the D atom species, we notice that the density of D_2^+ ions is too small for this species to have a significant effect in the context of the simulation considered here. In fact, D_2^+ ions have very short lifetimes, since they are dissociated shortly after being generated by ionization of D_2 molecules, and they are not significantly transported. However, D_2^+ ions can play an important role in, e.g. GPI diagnostics, since dissociation of D_2^+ ions can contribute to the emission of light in the Balmer series that this diagnostics is based upon.

Ultimately, our results show that the multi-component model for the self-consistent description of the neutral–plasma interaction can provide a description of a deuterium plasma that captures the main features of the molecular dynamics and its overall impact. While describing the turbulent phenomena that lead to cross-field transport, it is possible to address a multi-component plasma and more than one neutral species at a kinetic level. The procedure described here can be extended to include additional plasma and neutral species, as well as additional collisional processes.

Future work with the multi-component model presented here will address the simulation of GPI diagnostics, extending the work performed in reference [39] to the case of a more realistic multi-component deuterium plasma. On the other hand, the multi-component model will be extended to diverted configurations in order to address the effect of molecular dynamics on physical phenomena, such as fueling or density shoulder formation [64], which involve the complex interplay between neutral and plasma, and will be considered in realistic geometries. Future projects include the simulation of plasma detachment, where recombination processes become important, and an extension of the present model to include more ion and neutral species is expected.

Acknowledgments

We would like to thank C. Theiler, C. Wersal, D. Mancini, J. Koerfer, K. Verhaegh and M. Wensing for useful discussions. The simulations presented herein were carried out in part at CSCS (Swiss National Supercomputing Center) under the project ID s882 and in part on the CINECA Marconi supercomputer under the GBSedge project. This work has been carried out within the framework of the EUROfusion Consortium and has received funding from the Fond National Suisse de la Recherche Scientifique and from the Euratom research and training programme 2014–2018 and 2019–2020 under Grant Agreement No. 633053. The views and opinions expressed herein do not necessarily reflect those of the European Commission.

Data availability statement

The data that support the findings of this study are available from the corresponding authors upon reasonable request.

Appendix A. Evaluation of average electron energy loss and reaction product energies in collisional processes

The Franck–Condon principle [65, 66] states that electronic excitation occurs over a timescale considerably shorter than the characteristic timescale associated with vibration or dissociation of the diatomic species. In turn, the vibration or dissociation timescales are much shorter than the electron deexcitation timescale. As a result, when an electron impacts a D_2 molecule or a D_2^+ ion, an electronic excitation is observed with no significant change in the inter-atomic distance (vertical transition). If the excited state is not stable, the molecule dissociates before deexcitation takes place. In this case, the difference between the excitation energy and the dissociation energy is converted into kinetic energy of the products (ionization and dissociative energies are discussed in reference [67]). We note that the exact energies of the products of dissociation reactions depend on the vibrational level of the D_2 molecule or D_2^+ ion. Considering the excitation of a D_2 molecule in a given initial state, the set of vibrational levels accessible for the molecule in the final state are the ones lying within the region of the potential energy surface accessed by that particular vertical transition, known as the Franck–Condon region. The mean energy of the reaction products is thus the average over the Franck–Condon region, taking into account all accessible vibrational states.

In the present work, we model the products of dissociative reactions by considering that they are reemitted isotropically in the reference frame of the incoming massive particle (D_2 or D_2^+), thus approximating their velocity distribution as a Maxwellian centered at the velocity of the incoming D_2 or D_2^+. The temperature of the Maxwellian, together with the average electron energy loss for each process, are obtained from the values presented in reference [47]. Since these energies depend on the intermediate excited state of the D_2 or D_2^+ particle, different values are found for different channels within the same dissociative process. This requires that an average is performed over all possible excited states, taking into account the respective cross section of each process. We present these calculations in detail for each process, following [47].

The energy loss and the energy of the reaction products may depend on the electronic levels (n) and sub-levels (l) of the reaction products, on the molecular orbital (MO) of the intermediate state, if bonding or antibonding, and on the energy of the incident electron. The energy values are experimentally determined for all relevant dissociation channels. These quantities are then averaged over all vibrational states v of the D_2 molecules or D_2^+ ion and over the Franck–Condon region, from [47].

We start by considering the dissociation of D_2 molecules, i.e.

$$e^- + D_2 \rightarrow e^- + D + D. \tag{99}$$

For this reaction, the values of the electron energy loss, $\langle \Delta E_e \rangle$, and reaction product energies, $\langle E_D \rangle$, depend significantly on the electronic state of the products. Hence, considering that

Table 3. $\langle \sigma v_e \rangle$ product, average electron energy loss and average energy of reaction products for each sub-process of D_2 dissociation.

Reaction	$\langle \sigma v_e \rangle_i$	$\langle \Delta E_e \rangle_i$	$\langle E_D \rangle_i$
$e^- + D_2 \rightarrow e^- + D(1s) + D(1s)$	3.8×10^{-9} cm^3 s^{-1}	10.5 eV	3 eV
$e^- + D_2 \rightarrow e^- + D(1s) + D^*(2s)$	5.3×10^{-9} cm^3 s^{-1}	15.3 eV	0.3 eV
$e^- + D_2 \rightarrow e^- + D^*(2p) + D^*(2s)$	9.2×10^{-10} cm^3 s^{-1}	34.6 eV	4.85 eV
$e^- + D_2 \rightarrow e^- + D(1s) + D^*(n = 3)$	5.7×10^{-10} cm^3 s^{-1}	21.5 eV	5.7 eV

Table 4. Average electron energy loss and average energy of reaction products for the two cases of dissociative-ionization of D_2.

Reaction	$\langle \Delta E_e \rangle$	$\langle E_D \rangle = \langle E_{D^+} \rangle$
$e^- + D_2 \rightarrow e^- + \left[D_2^+(\Sigma_g) + e^-\right] \rightarrow D + D^+ + 2e^-$	18.25 eV	0.25 eV
$e^- + D_2 \rightarrow e^- + \left[D_2^+(\Sigma_u) + e^-\right] \rightarrow D + D^+ + 2e^-$	33.6 eV	7.8 eV

Table 5. $\langle \sigma v_e \rangle$ product, average electron energy loss and average energy of reaction products for each sub-process of D_2^+ dissociation.

Reaction	$\langle \sigma v_e \rangle_i$	$\langle \Delta E_e \rangle_i$	$\langle E_D \rangle = \langle E_{D^+} \rangle_i$
$e^- + D_2^+ \rightarrow D^+ + D(1s) + e^-$	1.2×10^{-7} cm^3 s^{-1}	10.5 eV	4.3 eV
$e^- + D_2^+ \rightarrow D^+ + D^*(n = 2) + e^-$	1.0×10^{-7} cm^3 s^{-1}	17.5 eV	1.5 eV

there are $i = 1, \ldots, N$ electronic states of the reaction products and, associated, N different sub-processes contributing to the dissociation of D_2, the average electron energy loss $\langle \Delta E_e \rangle$ is obtained by performing a weighed average of $\langle \Delta E_e \rangle_i$, the energy loss for the sub-process i, based on the $\langle \sigma v \rangle_i$ reaction rate, yielding

$$\langle \Delta E_e \rangle = \frac{\Sigma_{i=1}^{N} \left[\langle \sigma v \rangle_i \langle \Delta E_e \rangle_i \right]}{\Sigma_{i=1}^{N} \left[\langle \sigma v \rangle_i \right]}. \tag{100}$$

For simplicity, we evaluate all quantities at the reference temperature, $T_e = 20$ eV. Similarly, the average value for the energy of the reaction products is obtained as

$$\langle E_D \rangle = \frac{\Sigma_{i=1}^{N} \left[\langle \sigma v \rangle_i \langle E_D \rangle_i \right]}{\Sigma_{i=1}^{N} \left[\langle \sigma v \rangle_i \right]}, \tag{101}$$

with $\langle E_D \rangle_i$ the average energy of the products for the sub-process i.

The values of $\langle \sigma v \rangle_i$, $\langle \Delta E_e \rangle_i$, $\langle E_D \rangle_i$ are presented in table 3 for all sub-processes. The additional information between brackets refers to the minimum and maximum of the range of energies accessible to $\langle \Delta E_e \rangle_i$ and $\langle E_D \rangle_i$, following the values listed in reference [47]. We highlight that D(1s) denotes a D atom in the fundamental state (electron at the lowest orbital 1s), while D*(2s) and D*(2p) denote an atom in the excited state $n = 2$ with the electron in an orbital of type s or p, respectively, and D$^*(n = 3)$ represents an atom in the excited state $n = 3$. Following [47], we assume that the energy is equally distributed over the reaction products, regardless of the fact that their electronic states are the same. Based on the values in table 3, from equations (100) and (101), we obtain $\langle \Delta E_e \rangle \simeq 14.3$ eV and $\langle E_D \rangle \simeq 1.95$ eV, respectively, at $T_e = 20$ eV. These are the values mentioned in table 2.

Focusing now on the dissociative-ionization of D_2,

$$e^- + D_2 \rightarrow D + D^+ + 2e^-, \tag{102}$$

we consider three cases. If the incoming electron has an energy $E_e < E_{th(g)}$, with $E_{th(g)} = 18$ eV, no dissociation takes place. If $E_{th(g)} < E_e < E_{th(u)}$, with $E_{th(u)} = 26$ eV, the electron can ionize the molecule, resulting in an unstable D_2^+ ion, which then dissociates into a D atom and a D^+ ion. The short-lived D_2^+ has the electron in a bonding MO with σ-symmetry, thus exhibiting *gerade* (g) symmetry (German for even) state, denoted as $D_2^+(\Sigma_g)$. If $E_e > E_{th(u)}$, the intermediate D_2^+ ion has the electron in a higher-energy antibonding MO with σ-symmetry, which exhibits *ungerade* (u) symmetry (German for odd), thus denoted as $D_2^+(\Sigma_u)$. As a result of the different energy levels of the intermediate D_2^+ ion, the energy of the final products will also be different, as well as the average electron energy loss. According to the results presented in reference [47], these energies still depend on the energy of the incoming electron within each sub-process. To simplify the evaluation of the $\langle \Delta E_e \rangle$ and the energy of the products, we consider the energy to be evenly distributed by the reaction products (D and D^+) and we consider the two cases separately. For $E_{th(g)} < E_e < E_{th(u)}$, all dissociative-ionization events originate an intermediate state $D_2^+(\Sigma_g)$, while for $E_e > E_{th(u)}$ all events generate an intermediate state $D_2^+(\Sigma_u)$. The values for the electron energy loss and reaction product energies being considered for each case are evaluated for [47] and listed in table 4. We note that this is just an approximation, as even with $T_e < E_{th(u)}$ there are electrons with energies superior to the threshold that will generate a D_2^+ ion in a $D_2^+(\Sigma_u)$ state, and vice versa. Nevertheless, this approximation avoids us to evaluate $\langle \Delta E_e \rangle$ and $\langle E_D \rangle$ at every single value of T_e.

For the dissociation of D_2^+, i.e.

$$e^- + D_2^+ \rightarrow D^+ + D + e^-, \tag{103}$$

different sub-processes are taken into account, following an approach similar to the one adopted to treat the dissociation of D_2. We perform a weighed average of the electron energy loss and the reaction products energy by using equations (100) and (101), respectively. The values of $\langle \sigma v_e \rangle_i$, $\langle \Delta E_e \rangle_i$ and $\langle E_D \rangle = \langle E_{D^+} \rangle_i$ for each sub-process are presented in table 5. The weighed averaged values for the electron energy loss and reaction products energy at the reference temperature, $T_e = 20$ eV, yield $\langle \Delta E_e \rangle = 13.7$ eV and $\langle E_D \rangle = \langle E_{D^+} \rangle = 3.0$ eV, as listed in table 5.

Regarding the dissociative-ionization of D_2^+, i.e.

$$e^- + D_2^+ \rightarrow D^+ + D^+ + 2e^-, \tag{104}$$

we follow [47], where the average energy of the resulting D^+ ions is obtained from an average performed over all vibrational states ($v = 0$–9) of the D_2^+ ion and over the Franck–Condon region. This yields $\langle E_{D^+} \rangle = 0.4$ eV, while the average electron energy loss is $\langle \Delta E_e \rangle = 15.5$ eV.

We finally focus on the dissociative-recombination of D_2^+, which generates a D atom in the fundamental state (electron in orbital 1s) and a D atom in an excited state (electron with principal quantum number $n \geqslant 2$), i.e.

$$e^- + D_2^+ \rightarrow D(1s) + D^*(n \geqslant 2). \tag{105}$$

We assume that the energy of the products is evenly distributed among the two D atoms and is given by

$$\langle E_{D(1s)} \rangle \simeq \langle E_{D^*(n \geqslant 2)} \rangle \simeq \frac{1}{2} \left(E_e + \frac{Ry}{n^2} \right), \tag{106}$$

with $Ry = 13.6$ eV the Rydberg unit of energy (corresponding to the electron binding energy in a hydrogen atom in the fundamental state). Since this expression depends on the energy of the incoming electron, E_e, and the electronic level n of the excited atom, D^*, we assume an energy of the incident electron of $E_e \simeq 20$ eV, the typical value in the region around the LCFS at the HFS, and consider that these atoms are most likely in the accessible state of lowest energy $n = 2$ (considering a higher excited state would not change the value of the energy of the products by a significant amount). Under these assumptions, we get $\langle E_{D(1s)} \rangle \simeq \langle E_{D^*(n \geqslant 2)} \rangle \simeq 11.7$ eV.

Appendix B. Zhdanov collisional closure

We focus on the derivation of the parallel friction forces and the parallel heat fluxes, denoted respectively by $R_{\parallel\alpha} = \mathbf{R_\alpha} \cdot \mathbf{b}$ and $q_{\parallel\alpha} = \mathbf{q_\alpha} \cdot \mathbf{b}$ for a given species α, with $\mathbf{R_\alpha} = \int m_\alpha \mathbf{v}' C_\alpha \, d\mathbf{v}$ and $\mathbf{q_\alpha} = \int (m_\alpha v'^2)/2 \mathbf{v}' \, f_\alpha \, d\mathbf{v}$, where we introduce the thermal component of the velocity, $\mathbf{v}' = \mathbf{v} - \mathbf{v}_\alpha$, with $\mathbf{v}_\alpha = \int \mathbf{v} f_\alpha \, d\mathbf{v}$ the fluid velocity of the α species, and the collision operator $C_\alpha = \Sigma_\beta C_{\alpha\beta}(f_\alpha, f_\beta)$, with $C_{\alpha\beta}$ describing collisions of species α with species β. We consider the collisional closure derived by Zhdanov in reference [43], relying on the approach proposed in reference [32] and discussed in reference [54] for its numerical implementation.

Following [43], the parallel component of the friction forces and heat fluxes of the species α is related to the parallel gradients of the temperature and parallel velocity of all species through

$$\begin{bmatrix} q_{\parallel\alpha} \\ R_{\parallel\alpha} \end{bmatrix} = \sum_\beta Z_{\alpha\beta} \begin{bmatrix} \nabla_\parallel T_\beta \\ w_{\parallel\beta} \end{bmatrix}, \tag{107}$$

where T_β denotes the temperature of plasma species β and $w_{\parallel\beta}$ is the parallel component of the fluid velocity of species β with respect to the center of mass of the plasma, $\mathbf{w_\beta} = \mathbf{v_\beta} - \mathbf{v_{CM}}$, with $\mathbf{v_{CM}} = \left(\sum_\beta n_\beta m_\beta \mathbf{v_\beta} \right) / \left(\sum_\beta n_\beta m_\beta \right)$. The matrix $Z_{\alpha\beta}$ relates the parallel heat fluxes and friction forces with the parallel gradients of temperature and parallel velocity. We remark that equation (107) simplifies the general result obtained by Zhdanov [43] to the case of singly-ionized states, neglecting possible multiplicity of charge states for the chemical species present in the plasma.

In order to compute the matrix $Z_{\alpha\beta}$, we consider the $21N$-moment approximation of the distribution function [43], thus including the moments up to the fifth order moment. We first express $\mathbf{R}_\alpha$ and $\mathbf{q}_\alpha$ in terms of these moments of the distribution function, namely the first order moment, $\mathbf{w}_\alpha$, the third order moment, $\mathbf{h}_\alpha = q_{\parallel\alpha}$, and the fifth order moment, $\mathbf{r}_\alpha = m_\alpha/4 \int (c^4 - 14c^2/\gamma_\alpha + 35\gamma_\alpha) \mathbf{c} f_\alpha \, d\mathbf{c}$, where we introduce the velocity with respect to the center of mass of the plasma, $\mathbf{c} = \mathbf{v} - \mathbf{v_{CM}}$, and the parameter $\gamma_\alpha = m_\alpha/(kT_\alpha)$, with $T_\alpha = \int (m_\alpha v'^2/2) f_\alpha \, d\mathbf{v}$. Since only the expressions for the parallel component of the friction forces and heat fluxes are needed, we consider only the parallel component of these equations. The heat flux, $q_{\parallel\alpha}$, simply corresponds to the third order moment, $h_{\parallel\alpha}$, while the friction forces, $R_{\parallel\alpha}$, are obtained in terms of $w_{\parallel\alpha}$, $h_{\parallel\alpha}$ and $r_{\parallel\alpha}$ [68], yielding

$$q_{\parallel\alpha} = h_{\parallel\alpha}, \tag{108}$$

$$R_{\parallel\alpha} = \sum_\beta \left[G^{(1)}_{\alpha\beta} \left(w_{\parallel\alpha} - w_{\parallel\beta} \right) + \frac{\mu_{\alpha\beta}}{kT} G^{(2)}_{\alpha\beta} \left(\frac{h_{\parallel\alpha}}{m_\alpha n_\alpha} - \frac{h_{\parallel\beta}}{m_\beta n_\beta} \right) + \left(\frac{\mu_{\alpha\beta}}{kT} \right)^2 G^{(8)}_{\alpha\beta} \left(\frac{r_\alpha}{m_\alpha n_\alpha} - \frac{r_\beta}{m_\beta n_\beta} \right) \right], \tag{109}$$

where m_α and n_α are respectively the mass and density of species α, $\mu_{\alpha\beta} = (m_\alpha m_\beta)/(m_\alpha + m_\beta)$ is the reduced mass, and $G^{(n)}_{\alpha\beta}$ are polynomial functions of the local plasma density and temperature, their exact expressions being presented in reference [43] (chapter 8.1, pp 163–164). Equations (108) and (109) can then be written in matrix form as

$$\begin{bmatrix} q_{\parallel\alpha} \\ R_{\parallel\alpha} \end{bmatrix} = \sum_\beta A_{\alpha\beta} \begin{bmatrix} h_{\parallel\beta} \\ r_{\parallel\beta} \end{bmatrix} + \sum_\beta B_{\alpha\beta} \begin{bmatrix} \nabla_\parallel T_\beta \\ w_{\parallel\beta} \end{bmatrix}, \tag{110}$$

where the matrices A and B are defined to satisfy equations (108) and (109). We now aim at expressing the moments $\mathbf{h}_\alpha$ and ∇r_α in terms of $\mathbf{w}_\alpha$ and ∇T_α. This can be achieved by solving a system of moment equations similar to the one presented in reference [43] (chapter 8.1, pp 162–163),

including the time evolution of the moments ($\mathbf{w}_\alpha$, $\mathbf{h}_\alpha$ and ∇r_α) and the time evolution of basic thermodynamic variables (ρ, $\mathbf{v}_{\mathbf{CM}}$ and T). We neglect time derivatives and nonlinear terms. For simplicity, we also assume that, for two massive particle species D^+ and D_2^+, the condition $|T_{D_2^+} - T_{D^+}| \ll T_{D_2^+}$ is fulfilled, which allows us to write $T_{D_2^+} = T_{D^+} = T$. Moreover, as long as $T_e/T_{D^+} \gg m_e/m_{D^+}$ is verified, T can also be replaced by T_e, following [43] (the simulation results shown in figure 2 meet these conditions). We therefore impose $T_{D_2^+} = T_{D^+} = T_e = T$, while no assumption is made on the temperature and pressure gradients, i.e. temperature gradients can be different from species to species [43].

The parallel projection of the system of moment equations can then be written as (see [68])

$$\frac{5}{2} n_{\parallel\alpha} k \nabla T_\alpha = \sum_\beta \left[\frac{5}{2} \frac{\mu_{\alpha\beta}}{m_\alpha} G^{(2)}_{\alpha\beta} \left(w_{\parallel\alpha} - w_{\parallel\beta} \right) + G^{(5)}_{\alpha\beta} \frac{h_{\parallel\alpha}}{p_\alpha} + G^{(6)}_{\alpha\beta} \frac{h_{\parallel\beta}}{p_\beta} + \frac{\mu_{\alpha\beta}}{kT} \left(G^{(9)}_{\alpha\beta} \frac{r_{\parallel\alpha}}{p_\alpha} + G^{(10)}_{\alpha\beta} \frac{r_{\parallel\beta}}{p_\beta} \right) \right], \tag{111}$$

$$0 = \sum_\beta \left[\frac{35}{2} \left(\frac{\mu_{\alpha\beta}}{m_\alpha} \right)^2 G^{(8)}_{\alpha\beta} \left(w_{\parallel\alpha} - w_{\parallel\beta} \right) + 7 \frac{\mu_{\alpha\beta}}{m_\alpha} \left(G^{(9)}_{\alpha\beta} \frac{h_{\parallel\alpha}}{p_\alpha} + G^{(10)}_{\alpha\beta} \frac{h_\beta}{p_\beta} \right) + \frac{m_\alpha}{kT} G^{(11)}_{\alpha\beta} \frac{r_{\parallel\alpha}}{p_\alpha} + \frac{m_\beta}{kT} G^{(12)}_{\alpha\beta} \frac{r_{\parallel\beta}}{p_\beta} \right], \tag{112}$$

where p_α is the pressure of species α. Rewriting equations (111) and (112) in matrix form, one obtains

$$\sum_\gamma P_{\alpha\gamma} \begin{bmatrix} \nabla_\parallel T_\gamma \\ w_{\parallel\gamma} \end{bmatrix} = \sum_\beta M_{\alpha\beta} \begin{bmatrix} h_{\parallel\beta} \\ r_{\parallel\beta} \end{bmatrix}, \tag{113}$$

which can be inverted to express the parallel third and fourth order fluid moments in terms of the parallel gradient of temperature and relative parallel velocity as

$$\begin{bmatrix} h_{\parallel\beta} \\ r_{\parallel\beta} \end{bmatrix} = \sum_\alpha \sum_\gamma M^{-1}_{\alpha\beta} P_{\alpha\gamma} \begin{bmatrix} \nabla_\parallel T_\gamma \\ w_{\parallel\gamma} \end{bmatrix}. \tag{114}$$

Finally, making use of equation (114) to express $h_{\parallel\alpha}$ and $r_{\parallel\alpha}$ in equation (110) in terms of the parallel temperature gradients and relative velocities, one obtains the expressions for the parallel heat flux and friction forces in the matrix form presented in equation (107), that is

$$\begin{bmatrix} q_{\parallel\alpha} \\ R_{\parallel\alpha} \end{bmatrix} = \left(A_{\alpha\lambda} M^{-1}_{\gamma\lambda} P_{\gamma\beta} + B_{\alpha\beta} \right) \begin{bmatrix} \nabla_\parallel T_\beta \\ w_{\parallel\beta} \end{bmatrix}. \tag{115}$$

Since the matrices A, B, P and M are fully determined by equations (108), (109), (111) and (112), the expressions of the parallel heat flux and friction forces can be found. Following Zhdanov [43], these matrices can be expressed in terms of the local values of plasma quantities, namely densities n_e, n_{D^+} and $n_{D_2^+}$ and temperatures T_e and T_{D^+} (we again assume $T_{D_2^+} = T_{D^+}$, mass ratios and characteristic time scales τ_{eD} and τ_{DD}, with τ_{eD} defined as the inverse of the collision frequency for momentum transfer between electrons and D^+ ions, and τ_{DD} the ion timescale defined as the inverse of the collision frequency for momentum transfer between D^+ ions). We retain only terms of leading order in $\sqrt{m_e/m_D}$, while terms proportional to the fast electron timescale τ_{eD} are neglected when compared to terms proportional to τ_{DD}, which considerably simplifies the final expressions. We also highlight that, besides imposing the quasi-neutrality relation $n_e = n_{D^+} + n_{D_2^+}$, we take into account the fact that the density of the molecular ion species is much smaller than the density of the main ion species D^+ for typical tokamak boundary conditions, i.e. $n_{D_2^+}/n_{D^+} \ll 1$, keeping therefore only leading order terms in $n_{D_2^+}/n_{D^+}$. As a result, the friction forces between molecular ions and other species are neglected, as well as molecular ion temperature gradient terms, while friction and thermal force contributions involving D^+ and e^- species are kept in the expressions of the parallel components of the heat fluxes and friction forces. The expressions obtained for the friction forces and heat fluxes finally yield

$$\begin{aligned} q_{\parallel e} &= -\frac{3.16 n_e T_e \tau_{eD}}{m_e} \nabla_\parallel T_e + 0.71 n_e T_e (v_{\parallel e} - v_{\parallel D^+}), \\ q_{\parallel D^+} &= -\frac{4.52 n_e T_{D^+} \tau_{DD}}{m_D} \nabla_\parallel T_{D^+}, \\ q_{\parallel D_2^+} &= -\frac{1.80 n_e T_{D^+} \tau_{DD}}{m_D} \nabla_\parallel T_{D^+}, \\ R_{\parallel e} &= -0.71 n_e \nabla_\parallel T_e - \frac{0.51 m_e n_e}{\tau_{eD}} (v_{\parallel e} - v_{\parallel D^+}), \\ R_{\parallel D^+} &= 0.71 n_e \nabla_\parallel T_e - \frac{0.51 m_e n_e}{\tau_{eD}} (v_{\parallel D^+} - v_{\parallel e}), \\ R_{\parallel D_2^+} &= 0. \end{aligned} \tag{116}$$

The expressions in equation (116) can be simplified by applying the relation between the electron and ion characteristic times,

$$\frac{\tau_{DD}}{\tau_{eD}} = \frac{1}{\sqrt{2}} \sqrt{\frac{m_D}{m_e}} \left(\frac{T_e}{T_{D^+}} \right) \sim \frac{1}{\sqrt{2}} \sqrt{\frac{m_D}{m_e}}, \tag{117}$$

having again assumed $T_{D^+} \sim T_e$. This enables one to write τ_{DD} appearing in equation (116) in terms of τ_{eD}. Following Braginskii's approach [69] and considering that the electron characteristic time is $\tau_e = \tau_{eD}$, we then write equation (116) in terms of the resistivity, defined as [22, 23]

$$\nu = 0.51 \frac{m_e}{m_D} \frac{R_0}{c_{s0}} \frac{1}{n_e \tau_{eD}}, \tag{118}$$

The parallel friction forces and heat fluxes, as they appear in equations (22)–(24) and equations (25)–(27), respectively, are

therefore written in normalized units as

$$
\begin{aligned}
R_{\parallel \mathrm{e}} &= -0.71 n_\mathrm{e} \nabla_\parallel T_\mathrm{e} - \nu n_\mathrm{e}(v_{\parallel \mathrm{e}} - v_{\parallel \mathrm{D}^+}),\\
R_{\parallel \mathrm{D}^+} &= 0.71 n_\mathrm{e} \nabla_\parallel T_\mathrm{e} - \nu n_\mathrm{e}(v_{\parallel \mathrm{D}^+} - v_{\parallel \mathrm{e}}),\\
R_{\parallel \mathrm{D}_2^+} &= 0,\\
q_{\parallel \mathrm{e}} &= -\frac{1.62}{\nu} n_\mathrm{e} T_\mathrm{e} \nabla_\parallel T_\mathrm{e} + 0.71 n_\mathrm{e} T_\mathrm{e}(v_{\parallel \mathrm{e}} - v_{\parallel \mathrm{D}^+}),\\
q_{\parallel \mathrm{D}^+} &= -\frac{2.32}{\sqrt{2}\nu}\sqrt{\frac{m_\mathrm{e}}{m_\mathrm{D}}} n_\mathrm{e} T_{\mathrm{D}^+} \nabla_\parallel T_{\mathrm{D}^+},\\
q_{\parallel \mathrm{D}_2^+} &= -\frac{0.92}{\sqrt{2}\nu}\sqrt{\frac{m_\mathrm{e}}{m_\mathrm{D}}} n_\mathrm{e} T_{\mathrm{D}^+} \nabla_\parallel T_{\mathrm{D}^+}.
\end{aligned}
\tag{119}
$$

We note that, similarly to the single-ion species model implemented in GBS [22], the ohmic heating terms are neglected.

Appendix C. List of kernel functions

The kernels used in equations (80)–(83) for n_{D_2}, $\Gamma_{\mathrm{out},\mathrm{D}_2}$, n_D and Γ_D are defined as

$$
K_{\mathrm{p}\to\mathrm{p}}^{\mathrm{D}_2,\mathrm{D}_2^+}(\mathbf{x}_\perp,\mathbf{x}'_\perp) = K_{\mathrm{p}\to\mathrm{p},\mathrm{dir}}^{\mathrm{D}_2,\mathrm{D}_2^+}(\mathbf{x}_\perp,\mathbf{x}'_\perp) + \alpha_\mathrm{refl} K_{\mathrm{p}\to\mathrm{p},\mathrm{refl}}^{\mathrm{D}_2,\mathrm{D}_2^+}(\mathbf{x}_\perp,\mathbf{x}'_\perp), \tag{120}
$$

$$
K_{\mathrm{b}\to\mathrm{p}}^{\mathrm{D}_2,\mathrm{reem}}(\mathbf{x}_\perp,\mathbf{x}'_{\perp\mathbf{b}}) = K_{\mathrm{b}\to\mathrm{p},\mathrm{dir}}^{\mathrm{D}_2,\mathrm{reem}}(\mathbf{x}_\perp,\mathbf{x}'_{\perp\mathbf{b}}) + \alpha_\mathrm{refl} K_{\mathrm{b}\to\mathrm{p},\mathrm{refl}}^{\mathrm{D}_2,\mathrm{reem}}(\mathbf{x}_\perp,\mathbf{x}'_{\perp\mathbf{b}}), \tag{121}
$$

$$
K_{\mathrm{b}\to\mathrm{p}}^{\mathrm{D}_2,\mathrm{refl}}(\mathbf{x}_\perp,\mathbf{x}'_{\perp\mathbf{b}}) = K_{\mathrm{b}\to\mathrm{p},\mathrm{dir}}^{\mathrm{D}_2,\mathrm{refl}}(\mathbf{x}_\perp,\mathbf{x}'_{\perp\mathbf{b}}) + \alpha_\mathrm{refl} K_{\mathrm{b}\to\mathrm{p},\mathrm{refl}}^{\mathrm{D}_2,\mathrm{refl}}(\mathbf{x}_\perp,\mathbf{x}'_{\perp\mathbf{b}}), \tag{122}
$$

$$
K_{\mathrm{p}\to\mathrm{b}}^{\mathrm{D}_2,\mathrm{D}_2^+}(\mathbf{x}_{\perp\mathbf{b}},\mathbf{x}'_\perp) = K_{\mathrm{p}\to\mathrm{b},\mathrm{dir}}^{\mathrm{D}_2,\mathrm{D}_2^+}(\mathbf{x}_{\perp\mathbf{b}},\mathbf{x}'_\perp) + \alpha_\mathrm{refl} K_{\mathrm{p}\to\mathrm{b},\mathrm{refl}}^{\mathrm{D}_2,\mathrm{D}_2^+}(\mathbf{x}_{\perp\mathbf{b}},\mathbf{x}'_\perp), \tag{123}
$$

$$
K_{\mathrm{b}\to\mathrm{b}}^{\mathrm{D}_2,\mathrm{reem}}(\mathbf{x}_{\perp\mathbf{b}},\mathbf{x}'_{\perp\mathbf{b}}) = K_{\mathrm{b}\to\mathrm{b},\mathrm{dir}}^{\mathrm{D}_2,\mathrm{reem}}(\mathbf{x}_{\perp\mathbf{b}},\mathbf{x}'_{\perp\mathbf{b}}) + \alpha_\mathrm{refl} K_{\mathrm{b}\to\mathrm{b},\mathrm{refl}}^{\mathrm{D}_2,\mathrm{reem}}(\mathbf{x}_{\perp\mathbf{b}},\mathbf{x}'_{\perp\mathbf{b}}), \tag{124}
$$

$$
K_{\mathrm{b}\to\mathrm{b}}^{\mathrm{D}_2,\mathrm{refl}}(\mathbf{x}_{\perp\mathbf{b}},\mathbf{x}'_{\perp\mathbf{b}}) = K_{\mathrm{b}\to\mathrm{b},\mathrm{dir}}^{\mathrm{D}_2,\mathrm{refl}}(\mathbf{x}_{\perp\mathbf{b}},\mathbf{x}'_{\perp\mathbf{b}}) + \alpha_\mathrm{refl} K_{\mathrm{b}\to\mathrm{b},\mathrm{refl}}^{\mathrm{D}_2,\mathrm{refl}}(\mathbf{x}_{\perp\mathbf{b}},\mathbf{x}'_{\perp\mathbf{b}}), \tag{125}
$$

$$
K_{\mathrm{p}\to\mathrm{p}}^{\mathrm{D},\mathrm{D}^+}(\mathbf{x}_\perp,\mathbf{x}'_\perp) = K_{\mathrm{p}\to\mathrm{p},\mathrm{dir}}^{\mathrm{D},\mathrm{D}^+}(\mathbf{x}_\perp,\mathbf{x}'_\perp) + \alpha_\mathrm{refl} K_{\mathrm{p}\to\mathrm{p},\mathrm{refl}}^{\mathrm{D},\mathrm{D}^+}(\mathbf{x}_\perp,\mathbf{x}'_\perp), \tag{126}
$$

$$
K_{\mathrm{p}\to\mathrm{p}}^{\mathrm{D},\mathrm{D}_2^+}(\mathbf{x}_\perp,\mathbf{x}'_\perp) = K_{\mathrm{p}\to\mathrm{p},\mathrm{dir}}^{\mathrm{D},\mathrm{D}_2^+}(\mathbf{x}_\perp,\mathbf{x}'_\perp) + \alpha_\mathrm{refl} K_{\mathrm{p}\to\mathrm{p},\mathrm{refl}}^{\mathrm{D},\mathrm{D}_2^+}(\mathbf{x}_\perp,\mathbf{x}'_\perp), \tag{127}
$$

$$
K_{\mathrm{p}\to\mathrm{p}}^{\mathrm{D},\mathrm{diss}\left(\mathrm{D}_2^+\right)}(\mathbf{x}_\perp,\mathbf{x}'_\perp) = K_{\mathrm{b}\to\mathrm{b},\mathrm{dir}}^{\mathrm{D},\mathrm{reem}}(\mathbf{x}_{\perp\mathbf{b}},\mathbf{x}'_{\perp\mathbf{b}}) + \alpha_\mathrm{refl} K_{\mathrm{b}\to\mathrm{b},\mathrm{refl}}^{\mathrm{D},\mathrm{reem}}(\mathbf{x}_{\perp\mathbf{b}},\mathbf{x}'_{\perp\mathbf{b}}), \tag{128}
$$

$$
K_{\mathrm{p}\to\mathrm{p}}^{\mathrm{D},\mathrm{diss}-\mathrm{rec}\left(\mathrm{D}_2^+\right)}(\mathbf{x}_\perp,\mathbf{x}'_\perp) = K_{\mathrm{b}\to\mathrm{b},\mathrm{dir}}^{\mathrm{D},\mathrm{reem}}(\mathbf{x}_{\perp\mathbf{b}},\mathbf{x}'_{\perp\mathbf{b}}) + \alpha_\mathrm{refl} K_{\mathrm{b}\to\mathrm{b},\mathrm{refl}}^{\mathrm{D},\mathrm{reem}}(\mathbf{x}_{\perp\mathbf{b}},\mathbf{x}'_{\perp\mathbf{b}}), \tag{129}
$$

$$
K_{\mathrm{p}\to\mathrm{p}}^{\mathrm{D},\mathrm{diss}(\mathrm{D}_2)}(\mathbf{x}_\perp,\mathbf{x}'_\perp) = K_{\mathrm{b}\to\mathrm{b},\mathrm{dir}}^{\mathrm{D},\mathrm{reem}}(\mathbf{x}_{\perp\mathbf{b}},\mathbf{x}'_{\perp\mathbf{b}}) + \alpha_\mathrm{refl} K_{\mathrm{b}\to\mathrm{b},\mathrm{refl}}^{\mathrm{D},\mathrm{reem}}(\mathbf{x}_{\perp\mathbf{b}},\mathbf{x}'_{\perp\mathbf{b}}), \tag{130}
$$

$$
K_{\mathrm{p}\to\mathrm{p}}^{\mathrm{D},\mathrm{diss}-\mathrm{iz}(\mathrm{D}_2)}(\mathbf{x}_\perp,\mathbf{x}'_\perp) = K_{\mathrm{b}\to\mathrm{b},\mathrm{dir}}^{\mathrm{D},\mathrm{reem}}(\mathbf{x}_{\perp\mathbf{b}},\mathbf{x}'_{\perp\mathbf{b}}) + \alpha_\mathrm{refl} K_{\mathrm{b}\to\mathrm{b},\mathrm{refl}}^{\mathrm{D},\mathrm{reem}}(\mathbf{x}_{\perp\mathbf{b}},\mathbf{x}'_{\perp\mathbf{b}}), \tag{131}
$$

$$
K_{\mathrm{b}\to\mathrm{p}}^{\mathrm{D},\mathrm{reem}}(\mathbf{x}_\perp,\mathbf{x}'_{\perp\mathbf{b}}) = K_{\mathrm{b}\to\mathrm{b},\mathrm{dir}}^{\mathrm{D},\mathrm{reem}}(\mathbf{x}_{\perp\mathbf{b}},\mathbf{x}'_{\perp\mathbf{b}}) + \alpha_\mathrm{refl} K_{\mathrm{b}\to\mathrm{b},\mathrm{refl}}^{\mathrm{D},\mathrm{reem}}(\mathbf{x}_{\perp\mathbf{b}},\mathbf{x}'_{\perp\mathbf{b}}), \tag{132}
$$

$$
K_{\mathrm{b}\to\mathrm{p}}^{\mathrm{D},\mathrm{refl}}(\mathbf{x}_\perp,\mathbf{x}'_{\perp\mathbf{b}}) = K_{\mathrm{b}\to\mathrm{b},\mathrm{dir}}^{\mathrm{D},\mathrm{reem}}(\mathbf{x}_{\perp\mathbf{b}},\mathbf{x}'_{\perp\mathbf{b}}) + \alpha_\mathrm{refl} K_{\mathrm{b}\to\mathrm{b},\mathrm{refl}}^{\mathrm{D},\mathrm{reem}}(\mathbf{x}_{\perp\mathbf{b}},\mathbf{x}'_{\perp\mathbf{b}}), \tag{133}
$$

$$
K_{\mathrm{p}\to\mathrm{b}}^{\mathrm{D},\mathrm{D}^+}(\mathbf{x}_{\perp\mathbf{b}},\mathbf{x}'_\perp) = K_{\mathrm{b}\to\mathrm{b},\mathrm{dir}}^{\mathrm{D},\mathrm{reem}}(\mathbf{x}_{\perp\mathbf{b}},\mathbf{x}'_{\perp\mathbf{b}}) + \alpha_\mathrm{refl} K_{\mathrm{b}\to\mathrm{b},\mathrm{refl}}^{\mathrm{D},\mathrm{reem}}(\mathbf{x}_{\perp\mathbf{b}},\mathbf{x}'_{\perp\mathbf{b}}), \tag{134}
$$

$$
K_{\mathrm{p}\to\mathrm{b}}^{\mathrm{D},\mathrm{D}_2^+}(\mathbf{x}_{\perp\mathbf{b}},\mathbf{x}'_\perp) = K_{\mathrm{b}\to\mathrm{b},\mathrm{dir}}^{\mathrm{D},\mathrm{reem}}(\mathbf{x}_{\perp\mathbf{b}},\mathbf{x}'_{\perp\mathbf{b}}) + \alpha_\mathrm{refl} K_{\mathrm{b}\to\mathrm{b},\mathrm{refl}}^{\mathrm{D},\mathrm{reem}}(\mathbf{x}_{\perp\mathbf{b}},\mathbf{x}'_{\perp\mathbf{b}}), \tag{135}
$$

$$
K_{\mathrm{p}\to\mathrm{b}}^{\mathrm{D},\mathrm{diss}\left(\mathrm{D}_2^+\right)}(\mathbf{x}_{\perp\mathbf{b}},\mathbf{x}'_\perp) = K_{\mathrm{b}\to\mathrm{b},\mathrm{dir}}^{\mathrm{D},\mathrm{reem}}(\mathbf{x}_{\perp\mathbf{b}},\mathbf{x}'_{\perp\mathbf{b}}) + \alpha_\mathrm{refl} K_{\mathrm{b}\to\mathrm{b},\mathrm{refl}}^{\mathrm{D},\mathrm{reem}}(\mathbf{x}_{\perp\mathbf{b}},\mathbf{x}'_{\perp\mathbf{b}}), \tag{136}
$$

$$
K_{\mathrm{p}\to\mathrm{b}}^{\mathrm{D},\mathrm{diss}-\mathrm{rec}\left(\mathrm{D}_2^+\right)}(\mathbf{x}_{\perp\mathbf{b}},\mathbf{x}'_\perp) = K_{\mathrm{b}\to\mathrm{b},\mathrm{dir}}^{\mathrm{D},\mathrm{reem}}(\mathbf{x}_{\perp\mathbf{b}},\mathbf{x}'_{\perp\mathbf{b}}) + \alpha_\mathrm{refl} K_{\mathrm{b}\to\mathrm{b},\mathrm{refl}}^{\mathrm{D},\mathrm{reem}}(\mathbf{x}_{\perp\mathbf{b}},\mathbf{x}'_{\perp\mathbf{b}}), \tag{137}
$$

$$
K_{\mathrm{p}\to\mathrm{b}}^{\mathrm{D},\mathrm{diss}(\mathrm{D}_2)}(\mathbf{x}_{\perp\mathbf{b}},\mathbf{x}'_\perp) = K_{\mathrm{b}\to\mathrm{b},\mathrm{dir}}^{\mathrm{D},\mathrm{reem}}(\mathbf{x}_{\perp\mathbf{b}},\mathbf{x}'_{\perp\mathbf{b}}) + \alpha_\mathrm{refl} K_{\mathrm{b}\to\mathrm{b},\mathrm{refl}}^{\mathrm{D},\mathrm{reem}}(\mathbf{x}_{\perp\mathbf{b}},\mathbf{x}'_{\perp\mathbf{b}}), \tag{138}
$$

$$
K_{\mathrm{p}\to\mathrm{b}}^{\mathrm{D},\mathrm{diss}-\mathrm{iz}(\mathrm{D}_2)}(\mathbf{x}_{\perp\mathbf{b}},\mathbf{x}'_\perp) = K_{\mathrm{b}\to\mathrm{b},\mathrm{dir}}^{\mathrm{D},\mathrm{reem}}(\mathbf{x}_{\perp\mathbf{b}},\mathbf{x}'_{\perp\mathbf{b}}) + \alpha_\mathrm{refl} K_{\mathrm{b}\to\mathrm{b},\mathrm{refl}}^{\mathrm{D},\mathrm{reem}}(\mathbf{x}_{\perp\mathbf{b}},\mathbf{x}'_{\perp\mathbf{b}}), \tag{139}
$$

$$
K_{\mathrm{b}\to\mathrm{b}}^{\mathrm{D},\mathrm{reem}}(\mathbf{x}_{\perp\mathbf{b}},\mathbf{x}'_{\perp\mathbf{b}}) = K_{\mathrm{b}\to\mathrm{b},\mathrm{dir}}^{\mathrm{D},\mathrm{reem}}(\mathbf{x}_{\perp\mathbf{b}},\mathbf{x}'_{\perp\mathbf{b}}) + \alpha_\mathrm{refl} K_{\mathrm{b}\to\mathrm{b},\mathrm{refl}}^{\mathrm{D},\mathrm{reem}}(\mathbf{x}_{\perp\mathbf{b}},\mathbf{x}'_{\perp\mathbf{b}}), \tag{140}
$$

$$K^{\mathrm{D,refl}}_{\mathrm{b}\to\mathrm{b}}(\mathbf{x}_{\perp\mathbf{b}},\mathbf{x}'_{\perp\mathbf{b}}) = K^{\mathrm{D,refl}}_{\mathrm{b}\to\mathrm{b,dir}}(\mathbf{x}_{\perp\mathbf{b}},\mathbf{x}'_{\perp\mathbf{b}}) + \alpha_{\mathrm{refl}} K^{\mathrm{D,reem}}_{\mathrm{b}\to\mathrm{b,refl}}(\mathbf{x}_{\perp\mathbf{b}},\mathbf{x}'_{\perp\mathbf{b}}), \quad (141)$$

where the kernel functions for a given path $= \{\mathrm{dir}, \mathrm{refl}\}$ are defined as

$$K^{\mathrm{D_2,D_2^+}}_{\mathrm{p}\to\mathrm{p,path}}(\mathbf{x}_\perp,\mathbf{x}'_\perp) = \int_0^\infty \frac{1}{r'_\perp}\Phi_{\perp\left[\mathbf{v}_{\perp,\mathrm{D_2^+}},T_{\mathrm{D_2^+}}\right]}(\mathbf{x}'_\perp,\mathbf{v}_\perp) \times \exp\left[-\frac{1}{v_\perp}\int_0^{r'_\perp}\nu_{\mathrm{eff,D_2}}(\mathbf{x}''_\perp)\mathrm{d}r''_\perp\right]\mathrm{d}v_\perp, \quad (142)$$

$$K^{\mathrm{D_2,reem}}_{\mathrm{b}\to\mathrm{p,path}}(\mathbf{x}_\perp,\mathbf{x}'_{\perp\mathbf{b}}) = \int_0^\infty \frac{v_\perp}{r'_\perp}\cos\,\theta'\chi_{\perp,\mathrm{in,D_2}}(\mathbf{x}'_{\perp\mathbf{b}},\mathbf{v}_\perp) \times \exp\left[-\frac{1}{v_\perp}\int_0^{r'_\perp}\nu_{\mathrm{eff,D_2}}(\mathbf{x}''_\perp)\mathrm{d}r''_\perp\right]\mathrm{d}v_\perp, \quad (143)$$

$$K^{\mathrm{D_2,refl}}_{\mathrm{b}\to\mathrm{p,path}}(\mathbf{x}_\perp,\mathbf{x}'_{\perp\mathbf{b}}) = \int_0^\infty \frac{1}{r'_\perp}\Phi_{\perp\left[\mathbf{v}_{\mathrm{refl}\left(\mathrm{D_2^+}\right)},T_{\mathrm{D_2^+}}\right]}(\mathbf{x}',\mathbf{v}) \times \exp\left[-\frac{1}{v_\perp}\int_0^{r'_\perp}\nu_{\mathrm{eff,D_2}}(\mathbf{x}''_\perp)\mathrm{d}r''_\perp\right]\mathrm{d}v_\perp, \quad (144)$$

$$K^{\mathrm{D_2,D_2^+}}_{\mathrm{p}\to\mathrm{b,path}}(\mathbf{x}_{\perp\mathbf{b}},\mathbf{x}'_\perp) = \int_0^\infty \frac{v_\perp}{r'_\perp}\cos\,\theta\Phi_{\perp\left[\mathbf{v}_{\perp,\mathrm{D_2^+}},T_{\mathrm{D_2^+}}\right]}(\mathbf{x}'_\perp,\mathbf{v}_\perp) \times \exp\left[-\frac{1}{v_\perp}\int_0^{r'_\perp}\nu_{\mathrm{eff,D_2}}(\mathbf{x}''_\perp)\mathrm{d}r''_\perp\right]\mathrm{d}v_\perp, \quad (145)$$

$$K^{\mathrm{D_2,reem}}_{\mathrm{b}\to\mathrm{b,path}}(\mathbf{x}_{\perp\mathbf{b}},\mathbf{x}'_{\perp\mathbf{b}}) = \int_0^\infty \frac{v_\perp^2}{r'_\perp}\cos\,\theta\,\cos\,\theta'\chi_{\perp,\mathrm{in,D_2}}(\mathbf{x}'_{\perp\mathbf{b}},\mathbf{v}_\perp) \times \exp\left[-\frac{1}{v_\perp}\int_0^{r'_\perp}\nu_{\mathrm{eff,D_2}}(\mathbf{x}''_\perp)\mathrm{d}r''_\perp\right]\mathrm{d}v_\perp, \quad (146)$$

$$K^{\mathrm{D_2,refl}}_{\mathrm{b}\to\mathrm{b,path}}(\mathbf{x}_{\perp\mathbf{b}},\mathbf{x}'_{\perp\mathbf{b}}) = \int_0^\infty \frac{v_\perp}{r'_\perp}\cos\,\theta\Phi_{\perp\left[\mathbf{v}_{\mathrm{refl}\left(\mathrm{D_2^+}\right)},T_{\mathrm{D_2^+}}\right]}(\mathbf{x}',\mathbf{v}) \times \exp\left[-\frac{1}{v_\perp}\int_0^{r'_\perp}\nu_{\mathrm{eff,D_2}}(\mathbf{x}''_\perp)\mathrm{d}r''_\perp\right]\mathrm{d}v_\perp, \quad (147)$$

$$K^{\mathrm{D,D^+}}_{\mathrm{p}\to\mathrm{p,path}}(\mathbf{x}_\perp,\mathbf{x}'_\perp) = \int_0^\infty \frac{1}{r'_\perp}\Phi_{\perp\left[\mathbf{v}_{\perp,\mathrm{D^+}},T_{\mathrm{D^+}}\right]}(\mathbf{x}'_\perp,\mathbf{v}_\perp) \times \exp\left[-\frac{1}{v_\perp}\int_0^{r'_\perp}\nu_{\mathrm{eff,D}}(\mathbf{x}''_\perp)\mathrm{d}r''_\perp\right]\mathrm{d}v_\perp, \quad (148)$$

$$K^{\mathrm{D,D_2^+}}_{\mathrm{p}\to\mathrm{p,path}}(\mathbf{x}_\perp,\mathbf{x}'_\perp) = \int_0^\infty \frac{1}{r'_\perp}\Phi_{\perp\left[\mathbf{v}_{\perp,\mathrm{D_2^+}},T_{\mathrm{D_2^+}}\right]}(\mathbf{x}'_\perp,\mathbf{v}_\perp) \times \exp\left[-\frac{1}{v_\perp}\int_0^{r'_\perp}\nu_{\mathrm{eff,D}}(\mathbf{x}''_\perp)\mathrm{d}r''_\perp\right]\mathrm{d}v_\perp, \quad (149)$$

$$K^{\mathrm{D,diss}\left(\mathrm{D_2^+}\right)}_{\mathrm{p}\to\mathrm{p,path}}(\mathbf{x}_\perp,\mathbf{x}'_\perp) = \int_0^\infty \frac{1}{r'_{\perp,}}\Phi_{\perp\left[\mathbf{v}_{\perp,\mathrm{D_2^+}},T_{\mathrm{D,diss}\left(\mathrm{D_2^+}\right)}\right]}(\mathbf{x}'_\perp,\mathbf{v}_\perp) \times \exp\left[-\frac{1}{v_\perp}\int_0^{r'_\perp}\nu_{\mathrm{eff,D}}(\mathbf{x}''_\perp)\mathrm{d}r''_\perp\right]\mathrm{d}v_\perp, \quad (150)$$

$$K^{\mathrm{D,diss-rec}\left(\mathrm{D_2^+}\right)}_{\mathrm{p}\to\mathrm{p,path}}(\mathbf{x}_\perp,\mathbf{x}'_\perp) = \int_0^\infty \frac{1}{r'_\perp}\Phi_{\perp\left[\mathbf{v}_{\perp,\mathrm{D_2^+}},T_{\mathrm{D,diss-rec}\left(\mathrm{D_2^+}\right)}\right]}(\mathbf{x}'_\perp,\mathbf{v}_\perp) \times \exp\left[-\frac{1}{v_\perp}\int_0^{r'_\perp}\nu_{\mathrm{eff,D}}(\mathbf{x}''_\perp)\mathrm{d}r''_\perp\right]\mathrm{d}v_\perp, \quad (151)$$

$$K^{\mathrm{D,diss(D_2)}}_{\mathrm{p}\to\mathrm{p,path}}(\mathbf{x}_\perp,\mathbf{x}'_\perp) = \int_0^\infty \frac{1}{r'_\perp}\Phi_{\perp\left[\mathbf{v}_{\perp,\mathrm{D_2}},T_{\mathrm{D,diss}\left(D_2\right)}\right]}(\mathbf{x}'_\perp,\mathbf{v}_\perp) \times \exp\left[-\frac{1}{v_\perp}\int_0^{r'_\perp}\nu_{\mathrm{eff,D}}(\mathbf{x}''_\perp)\mathrm{d}r''_\perp\right]\mathrm{d}v_\perp, \quad (152)$$

$$K^{\mathrm{D,diss-iz(D_2)}}_{\mathrm{p}\to\mathrm{p,path}}(\mathbf{x}_\perp,\mathbf{x}'_\perp) = \int_0^\infty \frac{1}{r'_\perp}\Phi_{\perp\left[\mathbf{v}_{\perp,\mathrm{D_2}},T_{\mathrm{D,diss-iz}\left(D_2\right)}\right]}(\mathbf{x}'_\perp,\mathbf{v}_\perp) \times \exp\left[-\frac{1}{v_\perp}\int_0^{r'_\perp}\nu_{\mathrm{eff,D}}(\mathbf{x}''_\perp)\mathrm{d}r''_\perp\right]\mathrm{d}v_\perp, \quad (153)$$

$$K^{\mathrm{D,reem}}_{\mathrm{b}\to\mathrm{p,path}}(\mathbf{x}_\perp,\mathbf{x}'_{\perp\mathbf{b}}) = \int_0^\infty \frac{v_\perp}{r'_\perp}\cos\,\theta'\chi_{\perp,\mathrm{in,D}}(\mathbf{x}'_{\perp\mathbf{b}},\mathbf{v}_\perp) \times \exp\left[-\frac{1}{v_\perp}\int_0^{r'_\perp}\nu_{\mathrm{eff,D}}(\mathbf{x}''_\perp)\mathrm{d}r''_\perp\right]\mathrm{d}v_\perp, \quad (154)$$

$$K^{\mathrm{D,refl}}_{\mathrm{b}\to\mathrm{p,path}}(\mathbf{x}_\perp,\mathbf{x}'_{\perp\mathbf{b}}) = \int_0^\infty \frac{1}{r'_\perp}\Phi_{\perp\left[\mathbf{v}_{\mathrm{refl}(\mathrm{D}^+)},T_{\mathrm{D}^+}\right]}(\mathbf{x}',\mathbf{v}) \times \exp\left[-\frac{1}{v_\perp}\int_0^{r'_\perp}\nu_{\mathrm{eff,D}}(\mathbf{x}''_\perp)\mathrm{d}r''_\perp\right]\mathrm{d}v_\perp, \quad (155)$$

$$K^{\mathrm{D,D}^+}_{\mathrm{p}\to\mathrm{b,path}}(\mathbf{x}_{\perp\mathbf{b}},\mathbf{x}'_\perp) = \int_0^\infty \frac{v_\perp}{r'_\perp}\cos\,\theta\Phi_{\perp\left[\mathbf{v}_{\perp,\mathrm{D}^+},T_{\mathrm{D}^+}\right]}(\mathbf{x}'_\perp,\mathbf{v}_\perp) \times \exp\left[-\frac{1}{v_\perp}\int_0^{r'_\perp}\nu_{\mathrm{eff,D}}(\mathbf{x}''_\perp)\mathrm{d}r''_\perp\right]\mathrm{d}v_\perp, \quad (156)$$

$$K^{\mathrm{D,D}_2^+}_{\mathrm{p}\to\mathrm{b,path}}(\mathbf{x}_{\perp\mathbf{b}},\mathbf{x}'_\perp) = \int_0^\infty \frac{v_\perp}{r'_\perp}\cos\,\theta\Phi_{\perp\left[\mathbf{v}_{\perp,\mathrm{D}_2^+},T_{\mathrm{D}_2^+}\right]}(\mathbf{x}'_\perp,\mathbf{v}_\perp) \times \exp\left[-\frac{1}{v_\perp}\int_0^{r'_\perp}\nu_{\mathrm{eff,D}}(\mathbf{x}''_\perp)\mathrm{d}r''_\perp\right]\mathrm{d}v_\perp, \quad (157)$$

$$K^{\mathrm{D,diss}\left(\mathrm{D}_2^+\right)}_{\mathrm{p}\to\mathrm{b,path}}(\mathbf{x}_{\perp\mathbf{b}},\mathbf{x}'_\perp) = \int_0^\infty \frac{v_\perp}{r'_\perp}\cos\,\theta\Phi_{\perp\left[\mathbf{v}_{\perp,\mathrm{D}_2^+},T_{\mathrm{D,diss}\left(D_2^+\right)}\right]}(\mathbf{x}'_\perp,\mathbf{v}_\perp) \times \exp\left[-\frac{1}{v_\perp}\int_0^{r'_\perp}\nu_{\mathrm{eff,D}}(\mathbf{x}''_\perp)\mathrm{d}r''_\perp\right]\mathrm{d}v_\perp, \quad (158)$$

$$K^{\mathrm{D,diss-rec}\left(\mathrm{D}_2^+\right)}_{\mathrm{p}\to\mathrm{b,path}}(\mathbf{x}_{\perp\mathbf{b}},\mathbf{x}'_\perp) = \int_0^\infty \frac{v_\perp}{r'_\perp}\cos\,\theta\Phi_{\perp\left[\mathbf{v}_{\perp,\mathrm{D}_2^+},T_{\mathrm{D,diss-rec}\left(D_2^+\right)}\right]}(\mathbf{x}'_\perp,\mathbf{v}_\perp) \times \exp\left[-\frac{1}{v_\perp}\int_0^{r'_\perp}\nu_{\mathrm{eff,D}}(\mathbf{x}''_\perp)\mathrm{d}r''_\perp\right]\mathrm{d}v_\perp, \quad (159)$$

$$K^{\mathrm{D,diss(D_2)}}_{\mathrm{p}\to\mathrm{b,path}}(\mathbf{x}_{\perp\mathbf{b}},\mathbf{x}'_\perp) = \int_0^\infty \frac{v_\perp}{r'_\perp}\cos\,\theta\Phi_{\perp\left[\mathbf{v}_{\perp,\mathrm{D}_2},T_{\mathrm{D,diss}\left(D_2\right)}\right]}(\mathbf{x}'_\perp,\mathbf{v}_\perp) \times \exp\left[-\frac{1}{v_\perp}\int_0^{r'_\perp}\nu_{\mathrm{eff,D}}(\mathbf{x}''_\perp)\mathrm{d}r''_\perp\right]\mathrm{d}v_\perp, \quad (160)$$

$$K^{\mathrm{D,diss-iz(D_2)}}_{\mathrm{p}\to\mathrm{b,path}}(\mathbf{x}_{\perp\mathbf{b}},\mathbf{x}'_\perp) = \int_0^\infty \frac{v_\perp}{r'_\perp}\cos\,\theta\Phi_{\perp\left[\mathbf{v}_{\perp,\mathrm{D}_2},T_{\mathrm{D,diss-iz}\left(D_2\right)}\right]}(\mathbf{x}'_\perp,\mathbf{v}_\perp) \times \exp\left[-\frac{1}{v_\perp}\int_0^{r'_\perp}\nu_{\mathrm{eff,D}}(\mathbf{x}''_\perp)\mathrm{d}r''_\perp\right]\mathrm{d}v_\perp, \quad (161)$$

$$K^{\mathrm{D,reem}}_{\mathrm{b}\to\mathrm{b,path}}(\mathbf{x}_{\perp\mathbf{b}},\mathbf{x}'_{\perp\mathbf{b}}) = \int_0^\infty \frac{v_\perp^2}{r'_\perp}\cos\,\theta\,\cos\,\theta'\chi_{\perp,\mathrm{in,D}}(\mathbf{x}'_{\perp\mathbf{b}},\mathbf{v}_\perp) \times \exp\left[-\frac{1}{v_\perp}\int_0^{r'_\perp}\nu_{\mathrm{eff,D}}(\mathbf{x}''_\perp)\mathrm{d}r''_\perp\right]\mathrm{d}v_\perp, \quad (162)$$

$$K^{\mathrm{D,refl}}_{\mathrm{b}\to\mathrm{b,path}}(\mathbf{x}_{\perp\mathbf{b}},\mathbf{x}'_{\perp\mathbf{b}}) = \int_0^\infty \frac{v_\perp}{r'_\perp}\cos\,\theta\Phi_{\perp\left[\mathbf{v}_{\mathrm{refl}(\mathrm{D}^+)},T_{\mathrm{D}^+}\right]}(\mathbf{x}',\mathbf{v}) \times \exp\left[-\frac{1}{v_\perp}\int_0^{r'_\perp}\nu_{\mathrm{eff,D}}(\mathbf{x}''_\perp)\mathrm{d}r''_\perp\right]\mathrm{d}v_\perp. \quad (163)$$

We remark that all velocity distributions given by a Maxwellian or a Knudsen cosine law are integrated along the parallel velocity, that is

$$\Phi_{\perp\left[\mathbf{v}_{\perp,\mathrm{D}_2^+},T_{\mathrm{D}_2^+}\right]}(\mathbf{x}'_\perp,\mathbf{v}_\perp) = \int_0^\infty \Phi_{\left[\mathbf{v}_{\perp,\mathrm{D}_2^+},T_{\mathrm{D}_2^+}\right]}(\mathbf{x}'_\perp,\mathbf{v}_\perp)\mathrm{d}v_\parallel, \quad (164)$$

$$\Phi_{\perp\left[\mathbf{v}_{\perp,\mathrm{D}^+},T_{\mathrm{D}^+}\right]}(\mathbf{x}'_\perp,\mathbf{v}_\perp) = \int_0^\infty \Phi_{\left[\mathbf{v}_{\perp,\mathrm{D}^+},T_{\mathrm{D}^+}\right]}(\mathbf{x}'_\perp,\mathbf{v}_\perp)\mathrm{d}v_\parallel, \quad (165)$$

$$\Phi_{\perp\left[\mathbf{v}_{\perp,\mathrm{D}_2},T_{\mathrm{D,diss}\left(\mathrm{D}_2\right)}\right]}(\mathbf{x}'_\perp,\mathbf{v}_\perp) = \int_0^\infty \Phi_{\mathbf{v}_{\perp,\mathrm{D}_2},T_{\mathrm{D,diss}\left(\mathrm{D}_2\right)}}(\mathbf{x}'_\perp,\mathbf{v}_\perp)\mathrm{d}v_\parallel, \quad (166)$$

$$\Phi_{\perp\left[\mathbf{v}_{\perp,\mathrm{D}_2},T_{\mathrm{D,diss-iz}\left(\mathrm{D}_2\right)}\right]}(\mathbf{x}'_\perp,\mathbf{v}_\perp) = \int_0^\infty \Phi_{\left[\mathbf{v}_{\perp,\mathrm{D}_2},T_{\mathrm{D,diss-iz}\left(\mathrm{D}_2\right)}\right]}(\mathbf{x}'_\perp,\mathbf{v}_\perp)\mathrm{d}v_\parallel, \quad (167)$$

$$\Phi_{\perp\left[\mathbf{v}_{\perp,\mathrm{D}_2^+},T_{\mathrm{D,diss}\left(D_2^+\right)}\right]}(\mathbf{x}'_\perp,\mathbf{v}_\perp) = \int_0^\infty \Phi_{\left[\mathbf{v}_{\perp,\mathrm{D}_2^+},T_{\mathrm{D,diss}\left(D_2^+\right)}\right]}(\mathbf{x}'_\perp,\mathbf{v}_\perp)\mathrm{d}v_\parallel, \quad (168)$$

$$\Phi_{\perp\left[\mathbf{v}_{\perp,\mathrm{D}_2^+},T_{\mathrm{D,diss-rec}\left(D_2^+\right)}\right]}(\mathbf{x}'_\perp,\mathbf{v}_\perp) = \int_0^\infty \Phi_{\left[\mathbf{v}_{\perp,\mathrm{D}_2^+},T_{\mathrm{D,diss-rec}\left(D_2^+\right)}\right]}(\mathbf{x}'_\perp,\mathbf{v}_\perp)\mathrm{d}v_\parallel, \quad (169)$$

$$\Phi_{\perp\left[\mathbf{v}_{\mathrm{refl}(\mathrm{D}^+)},T_{\mathrm{D}^+}\right]}(\mathbf{x}',\mathbf{v}) = \int_0^\infty \Phi_{\left[\mathbf{v}_{\mathrm{refl}(\mathrm{D}^+)},T_{\mathrm{D}^+}\right]}(\mathbf{x}',\mathbf{v})\mathrm{d}v_\parallel, \quad (170)$$

$$\Phi_{\perp\left[\mathbf{v}_{\mathrm{refl}\left(\mathrm{D}_2^+\right)},T_{\mathrm{D}_2^+}\right]}(\mathbf{x}',\mathbf{v}) = \int_0^\infty \Phi_{\left[\mathbf{v}_{\mathrm{refl}\left(\mathrm{D}_2^+\right)},T_{\mathrm{D}_2^+}\right]}(\mathbf{x}',\mathbf{v})\mathrm{d}v_\parallel, \tag{171}$$

$$\chi_{\perp,\mathrm{in},\mathrm{D}_2}(\mathbf{x}'_{\perp,\mathrm{b}},\mathbf{v}_\perp) = \int_0^\infty \chi_{\mathrm{in},\mathrm{D}_2}(\mathbf{x}'_{\perp,\mathrm{b}},\mathbf{v}_\perp)\mathrm{d}v_\parallel, \tag{172}$$

$$\chi_{\perp,\mathrm{in},\mathrm{D}}(\mathbf{x}'_{\perp,\mathrm{b}},\mathbf{v}_\perp) = \int_0^\infty \chi_{\mathrm{in},\mathrm{D}}(\mathbf{x}'_{\perp,\mathrm{b}},\mathbf{v}_\perp)\mathrm{d}v_\parallel. \tag{173}$$

Appendix D. Numerical solution of the neutral equations

The coupled neutral equations for D_2 and D, equations (80)–(83), may be discretized as a linear matrix system, $\mathbf{x} = A\mathbf{x} + \mathbf{b}$, with the unknown $\mathbf{x}$ representing the density and boundary flux of the D_2 and D species. Indicating with N_P the number of points that discretize the poloidal plane and N_B the number of points discretizing the boundary, $\mathbf{x}$ is a vector of size $2(N_\mathrm{P}+N_\mathrm{B})$, A is a $2(N_\mathrm{P}+N_\mathrm{B})\times 2(N_\mathrm{P}+N_\mathrm{B})$ matrix and $\mathbf{b}$ is a $2(N_\mathrm{P}+N_\mathrm{B})$ vector that includes all contributions not proportional to the neutral density or flux, namely the effect of recombination of D^+ and D_2^+ with electrons, the effect of dissociative processes to which D_2^+ ions are subject and the contributions from the flux of D^+ and D_2^+ ions to the boundary.

The matrix M, and the vectors $\mathbf{x}$ and $\mathbf{b}$ can then be written as

$$\mathbf{x} = \begin{bmatrix} n_\mathrm{D} \\ \Gamma_{\mathrm{out,D}} \\ n_{\mathrm{D}_2} \\ \Gamma_{\mathrm{out},\mathrm{D}_2} \end{bmatrix}, M = \begin{bmatrix} M_{11} & M_{12} & M_{13} & M_{14} \\ M_{21} & M_{22} & M_{23} & M_{24} \\ M_{31} & M_{32} & M_{33} & M_{34} \\ M_{41} & M_{42} & M_{43} & M_{44} \end{bmatrix}, \mathbf{b} = \begin{bmatrix} b_1 \\ b_2 \\ b_3 \\ b_4 \end{bmatrix}, \tag{174}$$

where M_{11} is a matrix of size $N_\mathrm{P}\times N_\mathrm{P}$,

$$M_{11} = \nu_{\mathrm{cx,D}} K_{\mathrm{p}\to\mathrm{p}}^{\mathrm{D,D}^+}, \tag{175}$$

that discretizes the kernel $K_{\mathrm{p}\to\mathrm{p}}^{\mathrm{D,D}^+}$ defined in equation (84) at the spatial points where n_D is evaluated. The matrix

$$M_{21} = \nu_{\mathrm{cx,D}} K_{\mathrm{p}\to\mathrm{b}}^{\mathrm{D,D}^+}, \tag{176}$$

has size $N_\mathrm{B}\times N_\mathrm{P}$ and discretizes the kernel $K_{\mathrm{p}\to\mathrm{b}}^{\mathrm{D,D}^+}$ defined in equation (134) at the points where Γ_D is evaluated. The other matrices appearing in the definition of M are defined similarly,

$$M_{31} = \left[\frac{n_{\mathrm{D}_2^+}}{n_\mathrm{D}}\nu_{\mathrm{cx},\mathrm{D}_2^+-\mathrm{D}}\right] K_{\mathrm{p}\to\mathrm{p}}^{\mathrm{D}_2,\mathrm{D}_2^+}, \tag{177}$$

$$M_{41} = \left[\frac{n_{\mathrm{D}_2^+}}{n_\mathrm{D}}\nu_{\mathrm{cx},\mathrm{D}_2^+-\mathrm{D}}\right] K_{\mathrm{p}\to\mathrm{b}}^{\mathrm{D}_2,\mathrm{D}_2^+}, \tag{178}$$

$$M_{12} = (1-\alpha_\mathrm{refl})(1-\beta_\mathrm{assoc}) K_{\mathrm{b}\to\mathrm{p}}^{\mathrm{D,reem}}, \tag{179}$$

$$M_{22} = (1-\alpha_\mathrm{refl})(1-\beta_\mathrm{assoc}) K_{\mathrm{b}\to\mathrm{b}}^{\mathrm{D,reem}}, \tag{180}$$

$$M_{32} = (1-\alpha_\mathrm{refl})\frac{\beta_\mathrm{assoc}}{2} K_{\mathrm{b}\to\mathrm{p}}^{\mathrm{D}_2,\mathrm{reem}}, \tag{181}$$

$$M_{42} = (1-\alpha_\mathrm{refl})\frac{\beta_\mathrm{assoc}}{2} K_{\mathrm{b}\to\mathrm{b}}^{\mathrm{D}_2,\mathrm{reem}}, \tag{182}$$

$$M_{13} = \nu_{\mathrm{cx},\mathrm{D}_2-\mathrm{D}^+} K_{\mathrm{p}\to\mathrm{p}}^{\mathrm{D,D}^+} + \nu_{\mathrm{diss},\mathrm{D}_2} K_{\mathrm{p}\to\mathrm{p}}^{\mathrm{D,diss}(\mathrm{D}_2)} + \nu_{\mathrm{diss-iz},\mathrm{D}_2} K_{\mathrm{p}\to\mathrm{p}}^{\mathrm{D,diss-iz}(\mathrm{D}_2)}, \tag{183}$$

$$M_{23} = \nu_{\mathrm{cx},\mathrm{D}_2-\mathrm{D}^+} K_{\mathrm{p}\to\mathrm{b}}^{\mathrm{D,D}^+} + \nu_{\mathrm{diss},\mathrm{D}_2} K_{\mathrm{p}\to\mathrm{b}}^{\mathrm{D,diss}(\mathrm{D}_2)} + \nu_{\mathrm{diss-iz},\mathrm{D}_2} K_{\mathrm{p}\to\mathrm{b}}^{\mathrm{D,diss-iz}(\mathrm{D}_2)}, \tag{184}$$

$$M_{33} = \nu_{\mathrm{cx},\mathrm{D}_2} K_{\mathrm{p}\to\mathrm{p}}^{\mathrm{D}_2,\mathrm{D}_2^+}, \tag{185}$$

$$M_{43} = \nu_{\mathrm{cx},\mathrm{D}_2} K_{\mathrm{p}\to\mathrm{b}}^{\mathrm{D}_2,\mathrm{D}_2^+}, \tag{186}$$

$$M_{14} = 0, \tag{187}$$

$$M_{24} = 0, \tag{188}$$

$$M_{34} = (1-\alpha_\mathrm{refl}) K_{\mathrm{b}\to\mathrm{p}}^{\mathrm{D}_2}, \tag{189}$$

$$M_{44} = (1-\alpha_\mathrm{refl}) K_{\mathrm{b}\to\mathrm{b}}^{\mathrm{D}_2}. \tag{190}$$

The vector $\mathbf{b}$ is defined through the vectors b_1 and b_3 of size N_P,

$$b_1 = n_{\mathrm{D}[\mathrm{rec}(\mathrm{D}^+)]}(\mathbf{x}_\perp) + n_{\mathrm{D}[\mathrm{diss}(\mathrm{D}_2^+)]}(\mathbf{x}_\perp) + n_{\mathrm{D}[\mathrm{out}(\mathrm{D}^+)]}(\mathbf{x}_\perp), \tag{191}$$

$$b_3 = n_{\mathrm{D}_2[\mathrm{rec}(\mathrm{D}_2^+)]}(\mathbf{x}_\perp) + n_{\mathrm{D}_2[\mathrm{out}(\mathrm{D}_2^+)]}(\mathbf{x}_\perp) + n_{\mathrm{D}_2[\mathrm{out}(\mathrm{D}^+)]}(\mathbf{x}_\perp), \tag{192}$$

and the vector b_2 and b_4 of size N_B,

$$b_2 = \Gamma_{\mathrm{out,D}[\mathrm{rec}(\mathrm{D}^+)]}(\mathbf{x}_\perp) + \Gamma_{\mathrm{out,D}[\mathrm{diss}(\mathrm{D}_2^+)]}(\mathbf{x}_\perp) + \Gamma_{\mathrm{out,D}[\mathrm{out}(\mathrm{D}^+)]}(\mathbf{x}_\perp), \tag{193}$$

$$b_4 = \Gamma_{\mathrm{out},\mathrm{D}_2[\mathrm{rec}(\mathrm{D}_2^+)]}(\mathbf{x}_\perp) + \Gamma_{\mathrm{out},\mathrm{D}_2[\mathrm{out}(\mathrm{D}_2^+)]}(\mathbf{x}_\perp) + \Gamma_{\mathrm{out},\mathrm{D}_2[\mathrm{out}(\mathrm{D}^+)]}(\mathbf{x}_\perp). \tag{194}$$

It is remarked that the vector $\mathbf{b}$ can also be written as $\mathbf{b} = N\mathbf{x}_\mathrm{i}$, where $\mathbf{x}_\mathrm{i}$ refers to the densities and boundary fluxes of the D^+ and D_2^+ ion species,

$$\mathbf{x}_\mathrm{i} = \begin{bmatrix} n_{\mathrm{D}^+} \\ \Gamma_{\mathrm{out,D}^+} \\ n_{\mathrm{D}_2^+} \\ \Gamma_{\mathrm{out},\mathrm{D}_2^+} \end{bmatrix}, \tag{195}$$

and the matrix N can be expressed as

$$N = \begin{bmatrix} N_{11} & N_{12} & N_{13} & N_{14} \\ N_{21} & N_{22} & N_{23} & N_{24} \\ N_{31} & N_{32} & N_{33} & N_{34} \\ N_{41} & N_{42} & N_{43} & N_{44} \end{bmatrix}, \tag{196}$$

with entries

$$N_{11} = \nu_{\mathrm{rec,D}^+} K^{\mathrm{D,D}^+}_{\mathrm{p}\to\mathrm{p}}, \tag{197}$$

$$N_{21} = \nu_{\mathrm{rec,D}^+} K^{\mathrm{D,D}^+}_{\mathrm{p}\to\mathrm{b}}, \tag{198}$$

$$N_{31} = \nu_{\mathrm{rec,D}_2^+} K^{\mathrm{D}_2,\mathrm{D}_2^+}_{\mathrm{p}\to\mathrm{p}}, \tag{199}$$

$$N_{41} = \nu_{\mathrm{rec,D}_2^+} K^{\mathrm{D}_2,\mathrm{D}_2^+}_{\mathrm{p}\to\mathrm{b}}, \tag{200}$$

$$N_{12} = (1-\alpha_{\mathrm{refl}})(1-\beta_{\mathrm{assoc}}) K^{\mathrm{D,reem}}_{\mathrm{b}\to\mathrm{p}} + \alpha_{\mathrm{refl}} K^{\mathrm{D,refl}}_{\mathrm{b}\to\mathrm{p}}, \tag{201}$$

$$N_{22} = (1-\alpha_{\mathrm{refl}})(1-\beta_{\mathrm{assoc}}) K^{\mathrm{D,reem}}_{\mathrm{b}\to\mathrm{b}} + \alpha_{\mathrm{refl}} K^{\mathrm{D,refl}}_{\mathrm{b}\to\mathrm{b}}, \tag{202}$$

$$N_{32} = (1-\alpha_{\mathrm{refl}})\frac{\beta_{\mathrm{assoc}}}{2} K^{\mathrm{D}_2,\mathrm{reem}}_{\mathrm{b}\to\mathrm{p}}, \tag{203}$$

$$N_{42} = (1-\alpha_{\mathrm{refl}})\frac{\beta_{\mathrm{assoc}}}{2} K^{\mathrm{D}_2,\mathrm{reem}}_{\mathrm{b}\to\mathrm{b}}, \tag{204}$$

$$N_{13} = \nu_{\mathrm{diss,D}_2^+} K^{\mathrm{D,diss}\left(\mathrm{D}_2^+\right)}_{\mathrm{p}\to\mathrm{p}} + 2\nu_{\mathrm{diss-rec,D}_2^+} K^{\mathrm{D,diss-rec}\left(\mathrm{D}_2^+\right)}_{\mathrm{p}\to\mathrm{p}}, \tag{205}$$

$$N_{23} = \nu_{\mathrm{diss,D}_2^+} K^{\mathrm{D,diss}\left(\mathrm{D}_2^+\right)}_{\mathrm{p}\to\mathrm{b}} + 2\nu_{\mathrm{diss-rec,D}_2^+} K^{\mathrm{D,diss-rec}\left(\mathrm{D}_2^+\right)}_{\mathrm{p}\to\mathrm{b}}, \tag{206}$$

$$N_{33} = \nu_{\mathrm{rec,D}_2^+} K^{\mathrm{D}_2,\mathrm{D}_2^+}_{\mathrm{p}\to\mathrm{p}}, \tag{207}$$

$$N_{43} = \nu_{\mathrm{rec,D}_2^+} K^{\mathrm{D}_2,\mathrm{D}_2^+}_{\mathrm{p}\to\mathrm{b}}, \tag{208}$$

$$N_{14} = 0, \tag{209}$$

$$N_{24} = 0, \tag{210}$$

$$N_{34} = (1-\alpha_{\mathrm{refl}}) K^{\mathrm{D}_2,\mathrm{reem}}_{\mathrm{b}\to\mathrm{p}}, \tag{211}$$

$$N_{44} = (1-\alpha_{\mathrm{refl}}) K^{\mathrm{D}_2,\mathrm{reem}}_{\mathrm{b}\to\mathrm{b}} + \alpha_{\mathrm{refl}} K^{\mathrm{D}_2,\mathrm{refl}}_{\mathrm{b}\to\mathrm{b}}. \tag{212}$$

We remark that a convergence study to estimate the error introduced by the discretization of the neutral equation was carried out for a single neutral species model and it is reported in reference [62].

ORCID iDs

A. Coroado https://orcid.org/0000-0001-9619-4265

References

[1] Stangeby P.C. 2000 *The Plasma Boundary of Magnetic Fusion Devices* (Bristol: Institute of Physics Publishing)

[2] Pitcher C.S. 1988 Tokamak plasma interaction with limiters *PhD Thesis* University of Toronto

[3] Zhang C., Sang C., Wang L., Chang M., Liu D. and Wang D. 2019 Effect of carbon and tungsten plasma-facing materials on the divertor and pedestal plasma in EAST *Plasma Phys. Control. Fusion* **61** 115013

[4] Stotler D. and Karney C. 1994 Neutral gas transport modeling with DEGAS 2 *Contrib. Plasma Phys.* **34** 392–7

[5] Braams B.J. 1996 Radiative divertor modelling for ITER and TPX *Contrib. Plasma Phys.* **36** 276

[6] Baelmans M., Reiter D. and Weynants R.R. 1996 New developments in plasma edge modeling with particular emphasis on drift flows and electric fields *Contrib. Plasma Phys.* **36** 117

[7] Simonini R., Corrigan G., Radford G., Spence J. and Taroni A. 1994 Models and numerics in the multi-fluid 2-D edge plasma code EDGE2D/U *Contrib. Plasma.Phys.* **34** 368

[8] Feng Y., Sardei F. and Kisslinger J. 1999 3D fluid modelling of the edge plasma by means of a Monte Carlo technique *J. Nucl. Mater.* **266–269** 812–8

[9] Bufferand H., Ciraolo G., Isoardi L., Chiavassa G., Schwander F., Serre E., Fedorczak N., Ghendrih P. and Tamain P. 2011 Applications of SOLEDGE-2D code to complex SOL configurations and analysis of Mach probe measurements *J. Nucl. Mater.* **415** S589–92

[10] Zagórski R., Gerhauser H. and Claaßen H. A. 1998 Numerical simulation of the TEXTOR edge plasma including drifts and impurities *Contrib. Plasma. Phys.* **38** 61

[11] Sawada K. and Fujimoto T. 1995 Effective ionization and dissociation rate coefficients of molecular hydrogen in plasma *J. Appl. Phys.* **78** 2913

[12] Pigarov A.Y. *et al* 2003 DIII-D edge plasma simulations with UEDGE code including non-diffusive anomalous cross-field transport *J. Nucl. Mater.* **313–316** 1076–80

[13] Reiter D., Baelmans M. and Börner P. 2005 The EIRENE and B2-EIRENE codes *Fusion Sci. Technol.* **47** 172–86

[14] Mandrekas J. 2004 GTNEUT: a code for the calculation of neutral particle transport in plasmas based on the transmission and escape probability method *Comput. Phys. Commun.* **161** 36–64

[15] Shimizu K., Takizuka T., Sakurai S., Tamai H., Takenaga H., Kubo H. and Miura Y. 2003 Simulation of divertor detachment characteristics in JT-60 with superconducting coils *J. Nucl. Mater.* **313–316** 1277–81

[16] Lawson K.D. *et al* 2017 A study of the atomic and molecular power loss terms in EDGE2D-EIRENE simulations of JET ITER-like wall L-mode discharges *Nucl. Mater. Energy* **12** 924–30

[17] Lore J.D., Canik J.M., Feng Y., Ahn J.-W., Maingi R. and Soukhanovskii V. 2012 Implementation of the 3D edge plasma code EMC3-EIRENE on NSTX *Nucl. Fusion* **52** 054012

[18] Schneider R., Bonnin X., Borrass K., Coster D.P., Kastelewicz H., Reiter D., Rozhansky V.A. and Braams B.J. 2006 Plasma edge physics with B2-Eirene *Contrib. Plasma Phys.* **46** 3–191

[19] Dudson B.D., Umansky M.V., Xu X.Q., Snyder P.B. and Wilson H.R. 2009 BOUT++: a framework for parallel plasma fluid simulations *Comput. Phys. Commun.* **180** 1467–80

[20] Dudson B.D. and Hermes J.L. 2017 Global plasma edge fluid turbulence simulations *Plasma Phys. Control. Fusion* **59** 054010

[21] Wiesenberger M., Einkemmer L., Held M., Gutierrez-Milla A., Sáez X. and Iakymchuk R. 2019 Reproducibility, accuracy and performance of the FELTOR code and library on parallel computer architectures *Comput. Phys. Commun.* **238** 145–56

[22] Ricci P., Halpern F.D., Jolliet S., Loizu J., Mosetto A., Fasoli A., Furno I. and Theiler C. 2012 Simulation of plasma turbulence in scrape-off layer conditions: the GBS code, simulation results and code validation *Plasma Phys. Control. Fusion* **54** 124047

[23] Halpern F.D. *et al* 2016 The GBS code for tokamak scrape-off layer simulations *J. Comput. Phys.* **315** 388–408

[24] Francisquez M., Zhu B. and Rogers B.N. 2017 Global 3D Braginskii simulations of the tokamak edge region of IWL discharges *Nucl. Fusion* **57** 116049

[25] Stegmeir A., Coster D., Ross A., Maj O., Lackner K. and Poli E. 2018 GRILLIX: a 3D turbulence code based on the flux-coordinate independent approach *Plasma Phys. Control. Fusion* **60** 035005
[26] Thrysøe A.S., Løiten M., Madsen J., Naulin V., Nielsen A.H. and Rasmussen J.J. 2018 Plasma particle sources due to interactions with neutrals in a turbulent scrape-off layer of a toroidally confined plasma *Phys. Plasmas* **25** 032307
[27] Baudoin C., Tamain P., Bufferand H., Ciraolo G., Fedorczak N., Galassi D., Ghendrih P. and Nace N. 2018 Turbulent heat transport in TOKAM3X edge plasma simulations *Contrib. Plasma Phys.* **58** 484–9
[28] Shi E.L., Hammett G.W., Stoltzfus-Dueck T. and Hakim A. 2017 Gyrokinetic continuum simulation of turbulence in a straight open-field-line plasma *J. Plasma Phys.* **83** 905830304
[29] Chang C.S. and Ku S. 2008 Spontaneous rotation sources in a quiescent tokamak edge plasma *Phys. Plasmas* **15** 062510
[30] Ku S., Chang C.S. and Diamond P.H. 2009 Full-f gyrokinetic particle simulation of centrally heated global ITG turbulence from magnetic axis to edge pedestal top in a realistic tokamak geometry *Nucl. Fusion* **49** 115021
[31] Bufferand H. *et al* 2017 Implementation of drift velocities and currents in SOLEDGE2D-EIRENE *Nucl. Mater. Energy* **12** 852–7
[32] Bufferand H. *et al* 2019 Three-dimensional modelling of edge multi-component plasma taking into account realistic wall geometry *Nucl. Mater. Energy* **18** 82–6
[33] Thrysøe A.S., Tophøj L.E.H., Naulin V., Rasmussen J.J., Madsen J. and Nielsen A.H. 2016 The influence of blobs on neutral particles in the scrape-off layer *Plasma Phys. Control. Fusion* **58** 044010
[34] Thrysøe A.S., Madsen J., Naulin V. and Rasmussen J.J. 2018 Influence of molecular dissociation on blob-induced atom density perturbations *Nucl. Fusion* **58** 096005
[35] Bisai N., Jha R. and Kaw P.K. 2015 Role of neutral gas in scrape-off layer tokamak plasma *Phys. Plasmas* **22** 022517
[36] Bisai N. and Kaw P.K. 2016 Role of neutral gas in scrape-off layer of tokamak plasma in the presence of finite electron temperature and its gradient *Phys. Plasmas* **23** 092509
[37] Wersal C. and Ricci P. 2015 A first-principles self-consistent model of plasma turbulence and kinetic neutral dynamics in the tokamak scrape-off layer *Nucl. Fusion* **55** 123014
[38] Wersal C., Ricci P. and Loizu J. 2017 A comparison between a refined two-point model for the limited tokamak SOL and self-consistent plasma turbulence simulations *Plasma Phys. Control. Fusion* **59** 044011
[39] Wersal C. and Ricci P. 2017 Impact of neutral density fluctuations on gas puff imaging diagnostics *Nucl. Fusion* **57** 116018
[40] Coroado A. and Ricci P. 2021 Moving toward mass-conserving simulations of plasma turbulence and kinetic neutrals in the tokamak boundary with the GBS code *Phys. Plasmas* **28** 022310
[41] Baelmans M., Börner P., Ghoos K. and Samaey G. 2017 Efficient code simulation strategies for B2-EIRENE *Nucl. Mater. Energy* **12** 858–63
[42] Marandet Y., Bufferand H., Ciraolo G., Genesio P., Meliga P., Rosato J., Serre E. and Tamain P. 2016 Effect of statistical noise on simulation results with a plasma fluid code coupled to a Monte Carlo kinetic neutral code *Contrib. Plasma Phys.* **56** 604–9
[43] Zhdanov V.M. 2002 Transport processes in multicomponent plasma *Plasma Phys. Control. Fusion* **44** 2283
[44] Stotler D.P., Skinner C.H., Budny R.V., Ramsey A.T., Ruzic D.N. and Turkot R.B. 1996 Modeling of neutral hydrogen velocities in the tokamak fusion test reactor *Phys. Plasmas* **3** 4084
[45] Wensing M. *et al* 2019 SOLPS-ITER simulations of the TCV divertor upgrade *Plasma Phys. Control. Fusion* **61** 085029
[46] Reiter D. 2011 The data file AMJUEL: additional atomic and molecular data for EIRENE *Technical Report* FZ, Forschungszentrum Julich GmbH FRG
[47] Janev R.K. and Langer W.D. 1987 *The Janev–Langer Hydrogen–Helium Database* (Berlin: Springer)
[48] Janev R.K. 1995 *Atomic and Molecular Processes in Fusion Edge Plasmas* (New York: Plenum)
[49] Yoon J.-S., Song M.-Y., Han J.-M., Hwang S.H., Chang W.-S., Lee B. and Itikawa Y. 2008 Cross sections for electron collisions with hydrogen molecules *J. Phys. Chem. Ref. Data* **37** 913
[50] Chung H.K. 2017 Data for atomic processes of neutral beams in fusion plasma *Summary Report of the First Research Coordination Meeting. Technical Report* IAEA Nuclear Data Section
[51] Krstić P.S. 2002 Inelastic processes from vibrationally excited states in slow $H^+ + H_2$ and $H + H_2^+$ collisions: excitations and charge transfer *Phys. Rev.* A **66** 042717
[52] Krstić P.S. 2005 Vibrationally resolved collisions in cold hydrogen plasma *Nucl. Instrum. Methods Phys. Res.* B **241** 58–62
[53] Zeiler A., Drake J.F. and Rogers B. 1997 Nonlinear reduced Braginskii equations with ion thermal dynamics in toroidal plasma *Phys. Plasmas* **4** 2134–8
[54] Raghunathan M., Marandet Y., Bufferand H., Guido C., Ghendrih P., Tamain P. and Serre E. 2021 Generalized collisional fluid theory for multi-component, multi-temperature plasma using the linearized Boltzmann collision operator for scrape-off layer/edge applications *Plasma Phys. Control. Fusion* **29** 064005
[55] Ricci P. and Rogers B.N. 2010 Turbulence phase space in simple magnetized toroidal plasmas *Phys. Rev. Lett.* **104** 145001
[56] Poulsen A., Rasmussen J.J., Wiesenberger M. and Naulin V. 2020 Collisional multispecies drift fluid model *Phys. Plasmas* **27** 032305
[57] Loizu J., Ricci P., Halpern F.D. and Jolliet S. 2012 Boundary conditions for plasma fluid models at the magnetic presheath entrance *Phys. Plasmas* **19** 122307
[58] Mosetto A., Halpern F.D., Jolliet S., Loizu J. and Ricci P. 2015 Finite ion temperature effects on scrape-off layer turbulence *Phys. Plasmas* **22** 012308
[59] Tskhakaya D., Kuhn S. and Tomita Y. 2006 Formulation of boundary conditions for the unmagnetized multi-ion-component plasma sheath *Contrib. Plasma Phys.* **46** 649–54
[60] Paruta P., Ricci P., Riva F., Wersal C., Beadle C. and Frei B. 2018 Simulation of plasma turbulence in the periphery of diverted tokamak by using the GBS code *Phys. Plasmas* **25** 112301
[61] Galassi D., Reimerdes H., Theiler C., Wensing M., Bufferand H., Ciraolo G., Innocente P., Marandet Y. and Tamain P. 2020 Numerical investigation of optimal divertor gas baffle closure on TCV *Plasma Phys. Control. Fusion* **62** 115009
[62] Giacomin M., Ricci P., Coroado A., Fourestey G., Galassi D., Lanti E. and Mancini D. 2021 The GBS code for the self-consistent simulation of plasma turbulence and kinetic neutral dynamics in the tokamak boundary *Comput. Phys. Commun.* submitted
[63] Loizu J., Ricci P., Halpern F.D., Jolliet S. and Mosetto A. 2013 On the electrostatic potential in the scrape-off layer of magnetic confinement devices *Plasma Phys. Control. Fusion* **55** 124019
[64] Mancini D., Ricci P., Vianello N., Giacomin M. and Coroado A. 2021 Investigation of the density shoulder formation by using self-consistent simulations of plasma turbulence and neutral kinetic dynamics *Nucl. Fusion* **61** 126029
[65] Franck J. and Dymond E.G. 1926 Elementary processes of photochemical reactions *Trans. Faraday Soc.* **21** 536–42

[66] Condon E.U. 1928 Nuclear motions associated with electron transitions in diatomic molecules *Phys. Rev.* **32** 858–72
[67] Liu J., Salumbides E.J., Hollenstein U., Koelemeij J.C.J., Eikema K.S.E., Ubachs W. and Merkt F. 2009 Determination of the ionization and dissociation energies of the hydrogen molecule *J. Chem. Phys.* **130** 174306
[68] Zhdanov V.M. and Yushmanov P.N. 1981 Diffusion and heat transfer in a multicomponent completely ionized plasma *J. Appl. Mech. Tech. Phys.* **21** 453
[69] Braginskii S.I. 1965 Transport processes in a plasma *Reviews of Plasma Physics* vol 1 (New York: Consultants Bureau)